Deuterium labelling of membrane and soluble proteins for neutron crystallography

Swati Aggarwal

THÈSE

Pour obtenir le grade de

DOCTEUR DE L'UNIVERSITÉ GRENOBLE ALPES

Spécialité : Physique pour les Sciences du Vivant

Arrêté ministériel : 25 mai 2016

Présentée par

Swati AGGARWAL

Thèse dirigée par **Monika SPANO**,Maître de Conférence, Université Grenoble Alpes
et codirigée par **Esko Oksanen**, European Spallation Source

préparée au sein du **Laboratoire Institut de Biologie Structurale** dans **l'École Doctorale Physique**

Marquage au deutérium des protéines membranaires et solubles pour la cristallographie neutronique

Deuterium labelling of membrane and soluble proteins for neutron crystallography

Thèse soutenue publiquement le **28 septembre 2021**, devant le jury composé de :

Madame FLORA MEILLEUR
PROFESSEUR ASSOCIE, North Carolina State University, Rapporteure
Monsieur JENS PREBEN MORTH
PROFESSEUR, Danmarks Tekniske Universitet, Rapporteur
Monsieur JOSEPH LYONS
PROFESSEUR ASSOCIE, Aarhus Universitet, Examinateur
Monsieur PETRI KURSULA
PROFESSEUR, Universitetet I Bergen, Examinateur
Monsieur MARC JAMIN
PROFESSEUR DES UNIVERSITES, UNIVERSITE GRENOBLE ALPES, Président

Table of Contents

Chapter I. Introduction

I.1. Types of proteins

Proteins are the macromolecules that comprise more than half the solid matter of all organisms. They are the ultimate players in the cells responsible for occurrence of almost ever reaction. They are involved in enzymatic reactions, hormonal regulation, transporters and receptor of molecules inside-outside cells of living organisms. Each protein is unique to the species it is derived from, although quite similar in structure and function, they still have slight differences in composition. They are composed of amino acids joined by peptide bonds to form a long unbranched polypeptide chain [1]. Proteins are distinguished on basis of the sequence of amino acids and their interaction in different ways to form a three-dimensional conformation. Structure of proteins is very complex and divided into four categories. 1) *Primary structure* is the sequence of amino acids; 2) *Secondary structure* is the spatial arrangement of amino acids due to numerous forces such as hydrogen bonds, hydrophilic or hydrophobic interactions, disulfide or salt bridges. All these interactions cause protein to self-fold by bending or coiling into α-helix and β-pleated sheet; 3) *Tertiary structure* refers to the three-dimensional (3-D) arrangement of secondary structure to cause more compactness and a specific shape; 4) *Quaternary structure* designates the overall arrangement of different subunits of a protein [2]. The overall 3-D structure of proteins are very distinct and range from globular to very complex membrane-bound proteins that will be discussed further in this section. Understanding the structures of these proteins is very important for assessing their functions and usually determined at atomic level by crystallography techniques such as X-ray and neutron diffraction. There are numerous proteins whose structures are to be solved but requirement of large quantities of pure protein still remains a major constraint.

I.1.1. Soluble proteins

There are numerous soluble proteins each of which has a specific function. They are in globular shape and have characteristic conformations that bring together or move apart particular reactive species. To do this, molecules are folded in a complex manner to produce a specific shape with a charged pattern [2]. Usually, the large proteins are composed of two polypeptide chains that may or may not be identical. Such proteins are referred as *oligomeric* with their constituent chains designated as subunits or monomers. The folded chains of soluble proteins are very flexible and can easily undergo changes required for their biological function [3]. The most commonly found soluble proteins divided on basis of shape and solubility are globular and fibrous proteins, however, in this section focus will be on globular proteins.

Globular proteins are named according to their spherical-like shape and these are the most abundant proteins in nature. Nearly all such proteins are composed of α-helices and β-sheets that fold into a compact structure stabilized by polar and nonpolar interactions between side chains of amino acids. Usually, in globular protein structure, hydrophobic side chains are buried in the interior region while hydrophilic side chains reside on the surface exposed to water. Due to their compact folded structure, globular proteins are very stable and soluble in aqueous solutions. This makes their isolation and characterization easy unlike other proteins. Due to their diverse structure, they perform various functions such as catalysis, transport, signaling, binding and many more. Globular proteins are sensitive to physiological conditions such as pH and temperature. The most known examples are hemoglobin, protein kinase A, triose phosphate isomerase and immunoglobulins.

I.1.2. Membrane proteins (MPs)

Membrane proteins are known to be ~30% of proteins in eukaryotic cells and vital in many biological processes. They have various important functions such as transportation of substance in and out of the cell, acting as receptors for transfer of signals or pumping of protons in and out of the cell and most importantly as drug targets. Approximately, 60% of currently available drugs target membrane proteins such as G protein-coupled receptors (GPCRs) and ion channels [4]. Membrane proteins reside in association with the membrane of cells. For their interaction with lipid-containing non-polar part of membranes, their hydrophobic side chains are oriented outwards while hydrophilic side chains in the interior region unlike globular proteins. Membrane proteins are anchored to the lipid bilayer in two different ways: as integral proteins embedded within the layer or as peripheral proteins residing on the surface. Integral proteins are totally insoluble in aqueous solutions and require detergent to be solubilized. On the contrary, peripheral proteins are only bound to the charged groups of lipid bilayer, thus easy to remove by just increasing the ionic strength of solution [2]. The interior of membrane proteins is composed of internally hydrogen bonded α-helix and β-pleated sheets with major area buried within the lipid bilayer. Even though average hydrophobicity of interiors is as same as soluble proteins, outer surface membrane protein is composed of more hydrophobic amino acids.

For extraction of membrane proteins from native membranes, amphipathic compounds such as detergents are necessary to solubilize and maintain their stability in solutions. Detergents act as a membrane mimetic system with hydrophobic core and a hydrophilic exterior. They form micelles around the protein above its critical micelle concentration (CMC) [5]. Detergent concentration is very crucial to protein stability in micelles. Although, lack of enough detergent often leads to protein aggregation, excess amount of detergent may lead to protein inactivation due to removal essential native lipids. Due to their importance in protein solubilization and purification. Although various detergents are available, selection of an optimal detergent is one of the most challenging tasks. Unfortunately, due to very less information available on detergent-protein relationships, there is no perfect guideline so far on optimum detergent selection [6]. This little understanding of detergent-MP structure interaction and their efficiency for MP stabilization hampers the advances in this area.

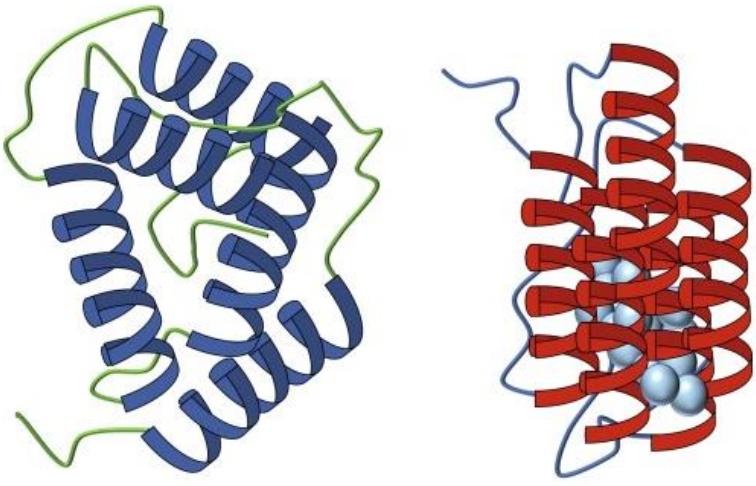

Figure 1.

I.2. Structural determination techniques of proteins

Biomacromolecules are crucial to all living organisms and their function relies on their unique structures. The major classes of biomacromolecules are: proteins, carbohydrates, nucleic acids and lipids. They are mostly formed by joining simpler biomolecules like amino acids and nucleotides that arrange in a specific order to form large biological macromolecules like proteins and nucleic acids. The most abundant and diverse biomacromolecules are proteins. Understanding their structure is central to recognize their role and functions in various biological activities like metabolism, chemical reactions, reproduction and stress responses. They are, however, highly susceptible to denaturation and difficulties in their extraction from source organism brings in great difficulties to study their structure.

Structure determination of biological macromolecules is a complex and multi-step procedure by which one can determine three-dimensional (3D) coordinates of a biomolecule using various analytical and modelling techniques (Figure 1). The process begins from determining the molecular structure of a protein based on genetic code to characterizing its structural space by using a combination of experimental and modelling techniques. The most commonly used and high-throughput methods for structure determination such as X-ray crystallography (MX), along with complementary techniques such as neutron macromolecular crystallography will be further discussed in this section.

I.2.1. X-Ray Crystallography

Until 19th century, researchers were struggling with understanding the chemical composition, properties and methods to extract complex biomacromolecules. It is only in 1934 that John Bernal and Dorothy Crowfoot postulated the structural organization of biomolecules with their first X-Ray diffraction image on pepsin crystals. This led to the breakthrough in development of crystallography techniques with first biological macromolecule structure of sperm whale myoglobin and bovine hemoglobin by John Kendrew and Max F. Perutz [7].
X-rays have short wavelengths suitable to determine the relative position of atoms in a molecule. However, the amount of radiation that is scattered by one molecule is way too small to measure making it necessary to make many copies of molecules for enhanced diffraction signal. This can be achieved by using a crystal – an ordered arrangement of numerous molecules – as the sample. Crystals are mounted on a goniometer diffracting X-rays into different directions to generate a 3D-image with unique diffraction pattern of spots by measuring the angle and density of diffracted rays [8]. Each spot corresponds to the reflection of X-rays by atoms. A crystallographer processes this image by using various software to generate an electron density map. From this map, one can determine the positions of atoms in a crystal [9].

With recent advances in molecular biology tools and high-energy radiation X-ray sources, speedy structural determination of several biomacromolecules has become routine. However, sample preparation for crystallography techniques has never been easy with a general challenge of insufficient amount of crystallizable protein. This is a major challenge in case of membrane proteins due to their amphiphilic nature. Purifying homogeneous membrane proteins without significant batch to batch variation is the major hurdle. Another limiting factor is the size of repeating unit cell. With the increasing size, crystallography becomes less resolved with a smeared and blobby appearance of atoms and chemical bonds in the crystal structures. Moreover, the problems do not end with obtaining diffracting crystals rather end with labor-intensive data processing to interpret the structural models. Ultimately, these models provide

the information of structural arrangement of atoms in macromolecular complex that suggests its functional role.
Nonetheless, even with many shortcomings, protein X-ray crystallography has been the major workhorse of protein structure determination. Currently, 90% of the total deposited structures in RCSB Protein Data Bank (PDB) are resolved using MX and remaining 10% structures are resolved using various other techniques discussed further in this section.

I.2.2. Neutron Diffraction

The neutron diffraction was first demonstrated by Halban and Preiswerk (1936) and Mitchell and Powers (1936) using radium-beryllium neutron sources [10, 11]. With the advent of chain-reacting atomic piles, neutrons were established as probes for diffraction techniques analogous to X-rays. Neutrons are subatomic particles with neutral charge that interact weakly with matter and penetrates in a non-destructive way. While X-rays interact with the electron cloud of atoms, neutrons interact only with nuclei. This means that the scattering factor of X-rays is dependent on atomic Z number, so light atoms like hydrogen are not easily visible. Determination of hydrogen positions by X-rays is only possible at ultra-high resolution which is not achievable for all proteins. Since neutron scattering is independent of the number of electrons, this property is exploited in locating hydrogens in a protein structure and used as a complementary technique to MX for determination of 3D structures of proteins.

Neutron scattering lengths for most commonly found atoms in proteins are shown in Table 1. Protium (^{1}H) has a comparable scattering length to of other common atoms such as carbon, oxygen and nitrogen. However, ^{1}H has a negative scattering length and large incoherent cross-section giving rise to a significant background noise in data collection. Due to the negative scattering length, ^{1}H complicates the data analysis by cancellation of positive peaks of surrounding atoms. To solve this issue, ^{1}H can be substituted by the heavier isotope, deuterium (^{2}H or D). Deuteration leads to much better nuclear scattering length density maps due to its positive scattering length and smaller incoherent cross-section [12-14]. Replacement of ^{1}H to D maximizes the signal-to-noise ratio and enhanced scattering signal can give insights of location and dynamics of hydrogen atoms in a protein structure [15-17]. Sample preparation for NMX is further discussed in **Section 3.**

Even though deuteration can solve one problem, deuterated sample preparation is an expensive process and requires lot of optimization. There are several other problems associated with this technique like limited number of neutron sources as compared to X-ray sources worldwide. Due to lower flux of currently available neutron sources, large crystal volume (<0.5 mm^3) and long exposure time (at least 2 weeks) is a prerequisite [13]. This is clearly visible with only 176 neutron structures deposited in PDB relative to 153564 X-ray structures (accessed on 17/04/2021) (Figure 2). Considering the problems with sample preparation and requirement of large volume of sample has lead to no membrane protein neutron structure so far. However, neutron data collection of a potassium channel has been attempted previously [18].
In recent years, there has been an increasing interest in neutron macromolecular crystallography (NMX) benefitted from high-performance computing techniques and shared resources and associated expertise from co-location of neutron sources with other advanced research facilities [19]. For example, the Institut Laue-Langevin (ILL) with European Synchrotron Radiation Facility (ESRF) in Grenoble, France, ISIS Neutron and Muon Source with the Diamond Light Source in the UK, the Japan Proton Accelerator Research Complex (J-PARC) spallation neutron source with the Japan Atomic Energy Research Institute (JAERI) reactor neutron source in Tokai-mura, Japan, Spallation Neutron Source (SNS) and High-flux

Isotope Reactor (HFIR) at Oak ridge national laboratory in USA and the MAX-IV synchrotron-radiation source with the future European Spallation Source (ESS) in Lund, Sweden. NMX has been recognized as a powerful complementary tool with the rapid progress in improved detectors and establishment of high-throughput deuteration laboratories for sample preparation.

Table 1. Neutron scattering length and cross sections of commonly found atoms in proteins. Adapted from [20]

Isotope	**Atomic Number**	**Incoherent Cross-section(barn)**	**Neutron Scattering Length (fm)**
Hydrogen (^{1}H)	1	80.27	-3.74
Deuterium (^{2}H)	1	2.05	6.67
Carbon (^{12}C)	6	0.0	6.65
Nitrogen (^{14}N)	7	0.5	9.37
Oxygen (^{16}O)	8	0.0	5.80

I.3. Deuterium labelling for NMX

Incorporation of deuterium into proteins can be achieved in three different ways: 1) H/D exchange where only labile hydrogens are replaced with deuterium and performed after protein production ('H/D exchanged'); 2) deuteration by expression of protein in D_2O-containing media using a protiated carbon source ('deuterated'); 3) deuteration by expression of protein in fully deuterated conditions where carbon source is deuterated ('perdeuterated'). In the first condition, only solvent accessible H atoms approximately 25% of the protein is incorporated with deuterium. Use of hydrogenated carbon source can lead to ~70-80% incorporation of D in protein unlike perdeuteration where ~99% is achieved including peptide backbone chain carbon atoms. For H/D exchanged, protiated crystallization buffer is replaced with deuterated counterpart either while setting up the drops or after appearance of crystals. Due to ease of sample preparation and lower cost, most of the neutron structures deposited in PDB followed this approach (Figure 1). The second most commonly approach was use of protiated carbon source with least perdeuterated protein structures deposited so far.

Hydrogen and its isotope deuterium are similar but have few distinguishable physical properties. Deuterium is almost twice as heavy as hydrogen and this is the reason deuterium-rich water is called as heavy water. H_2O and D_2O have different densities (1 and 1.108 g cm^{-3}, respectively), melting points (0 and 3.8 °C, respectively) and boiling points (100 and 101.4 °C, respectively) [21]. Solubility of different compounds in D_2O is also affected, for instance, carbon dioxide solubility is 10% less soluble in D_2O as compared to H_2O. Substitution of ^{1}H with ^{2}H results in kinetic isotope effect (k_H/k_D) defined as the change in the ratio of rate constant when a hydrogen atom is replaced with its isotope deuterium in a particular reaction. While kinetic isotope effect has an effect on enzymatic mechanism, its effect on biological systems is not very well understood. It has been reported previously that eukaryotes (animals and plants) are less tolerant to heavy water unlike bacteria and algae that can bear high concentration of heavy water [22-24]. However, it causes an imbalance between ^{1}H and ^{2}H atoms which is due to high kinetic isotope effect [22]. Previous studies have reported that kinetic isotope effect can even cause stress response in yeast mutant cell lines leading to increased expression of heat

shock protein Hsp70 [25]. Deuterium also has significant effects on central carbon metabolism and growth of *E. coli* fed on different carbon sources in deuterated media showed apparent differences in growth rate and cell size [26, 27]. All these subtle differences between growth in H_2O and D_2O make production of deuterated recombinant proteins technically challenging. and adaptation of host organism becomes quintessential. Since, *E. coli* readily ad apts with an advantage of easy genetic manipulation has become the preferred organism for producing deuterium-labelled proteins. This is clearly reflected with ~60% of perdeuterated protein neutron structures deposited in PDB are produced in *E. coli.* However, due to the requirement of post-translational modifications in eukaryotic proteins, yeast is selected instead of *E. coli* [28].

The most commonly used *E. coli* strain for recombinant protein production is BL21. In general, bacteria require adaptation in deuterated conditions which is achieved by repeated plating of the strain on deuterated media and subsequently several cycles of sub-culturing in deuterated minimal media. Even though consistent growth is achieved, this method is time consuming and adds extra cost of labelled material to the procedure. However, in this study we will use a deuterium adapted strain which was originally obtained from *E. coli* strain K-12 [29]. This ease of bacterial cultivation often relies upon the choice of deuterated medium and carbon source. The most commonly used economic media is defined minimal medium (M9) with varying carbon source such as succinate, protiated glycerol or d_8-glycerol, acetate and pyruvate. By varying salt and carbon source concentration in M9 media, protein expression level and yield can be improved [30]. So far, For production of protein in deuterated rich media, deuterated algal extract has been used as a supplement of carbon source. Growing deuterated algae is fairly simple as nutrient solution is made up of organic salts dissolved in D_2O instead of water. Moreover, the heavy water is almost entirely recoverable. However, the cost of algae production in D_2O is prohibitive due to the requirement of special setup for growing algae, its slower growth in heavy water and batch-to-batch variations within the commercial extracts [31]. This is evident with only one neutron structure deposited so far in PDB where BioExpress deuterated medium was used to produce T4 phage lysozyme [32].

I.4. Model systems

I.4.1. Triose phosphate isomerase (TIM) as a potential candidate for NMX studies

TIM (TIM, EC 5.3.1.1) is a ubiquitous glycolytic enzyme that plays a key role in glycolysis cycle of all organisms by controlling the inter-conversion of dihydroxyacetone phosphate (DHAP) into glyceraldehyde-3-phosphate (GAP) [33]. GAP is further used as a substrate in glycolysis to produce ATP and also pyruvate for Tricarboxylic acid cycle. TIM is found in cytosol of most organisms, but it is also present in glycosome of *Leishmania* and trypanosomes [34]. There is only one gene that encodes for TIM enzyme in all organisms. The decreased activity of TIM in organisms can cause severe diseases due to accumulation of dihydroxyacetone phosphate (DHAP). The glycolysis pathway is also interconnected to other metabolic pathways and lipid metabolism in a biological organism [35]. Thus, TIM deficiency also accounts for metabolic related disease symptoms and making it vital enzyme for proper functioning of the cells [36].

TIM has a high catalytic efficiency of controlling the isomerization reaction of DHAP into D-GAP by diffusion control at the maximum value of k_{cat}/K_m (10^9 M^{-1} s^{-1}) [37]. This reaction involves a proton transfer between the carbonyl group of the substrate (DHAP) and product (GAP). The carbonyl group is keto group in forward reaction (DHAP as substrate) and the aldehyde group in reverse reaction (GAP is substrate). It has been proposed that rate limiting

step in forward reaction is a proton abstraction step from DHAP leading to formation of an enediolate intermediate and conformational changes (loop opening) in GAP in the reverse reaction. Thus, TIM is also an enolising enzyme with high affinity for C3- sugar phosphates. Knowles and coworkers determined the free energy profile of TIM where the predominant complex in the reaction was predicted to be the enzyme-DHAP complex along with GAP and intermediates [38]. However, with NMR studies at steady state showed no presence of intermediates suggesting the fast turn over time of TIM [39]. With free energy profile it was measured previously that TIM-catalyzed deprotonation reaction is 10^9 times faster than the solution general-base catalysis [40].

I.4.1.1. TIM-barrel topology and structural studies

Corran and coworkers reported the first crystal structure of TIM where they revealed the closed TIM-barrel topology [41]. Each subunit of TIM is composed of alternating repeating segments of α-helix and β-sheets folding onto each other to form $(\beta\alpha)_8$-fold. This fold is commonly found enzyme fold shaping the active site located at the C-terminal end [42]. Usually, loops at C-terminal end (catalytic end) are longer than the N-terminal end (stability end). TIM-barrel domain has 250 residues wherein four layers point outwards (towards α-helix) and four inwards (towards β-sheets) giving a fourfold symmetry to barrel. The βα-loops corresponds to active site and αβ-loops at the backside are responsible for stability of protein [43]. Previously it has been reported that backbone atoms generate positive potential at the C-terminal end correlating the preferred binding of TIM-barrels with negatively charged phosphate containing molecules [40].
The catalytic site residue and geometry is conserved in TIM-barrels in all organisms (Figure 1). In this study, residue numbering in TIM will be used from the organism *Leishmania mexicana.* TIM catalytic residues are present in three βα-loops connected by loop-1 (Asn11, Lys13), loop-4 (His95) and loop-6 (Glu167) along with a flexible loop that is part of loop-6-8. The active site is shaped by all these loops and together they provide the fully active TIM-dimer interface. However, all the active site residues come from the same subunit. The key steps of TIM catalysis are (1) abstraction of proton by Glu167 residue in active site (2) oxyanion stabilization and (3) burying active site by exclusion of bulk solvent. The importance of loop-6 has been highlighted in substrate-binding and the catalytic mechanism. It is known to move 7 Å from an open to closed form on substrate-binding. Loop-6 interacts with loop-5 in the unliganded (open) conformation and with loop-7 in the liganded (closed) conformation. The closed form generates a phosphate-dianion pocket leading to the formation of four hydrogen bonds with main chain -NH groups in the loops and surrounding water molecules keeping the substrate intact. It has also been established that formation of the phosphate-dianion pocket prevents the transformation of reaction intermediates into toxic methylglyoxal [44]. All these factors make TIM-barrel fold a very good framework for studying different enzymatic active sites and even designing non-natural enzymes [45].

Figure 1.

I.4.1.2. Proposed reaction mechanisms

The catalytic conversion of DHAP to GAP is a stereospecific reaction where Glu 167 is proposed as the catalytic base in the rate limiting step to generate an enediolate intermediate. The intermediates in the reaction are further stabilized by electrostatic stabilization provided by Asn11 and Lys13 together with His95 to form an oxyanion-hole-like environment [33]. For efficient catalysis, pK_a value of the catalytic base and substrate should be in the same range. It

is established that pK_a value is modified during the reaction bringing the two moieties close to each other facilitated by buried active site geometry in presence of ligand (closed form). The transition and intermediate states have also been suggested to be stabilized by low-barrier hydrogen bonds (LBHBs) [46]. However, their importance in catalytic rate enhancement is to be investigated further. Previous studies have proposed two mechanism for proton transfer pathways (Figure 2). In the classical mechanism Glu167 and His95 are both involved in a proton shuttling process. His95 is suggested to donate a proton to enediolate intermediate and then abstract a proton from another hydroxyl group of the enediolate intermediate. This results in a negatively charged histidine residue with no further movement. In the criss-cross mechanism, only Glu167 carries forward all proton transfer reaction with His95 being involved in stabilizing the negative charge by forming hydrogen bonds. Glu167 first abstracts the proton from a hydroxyl group and then reprotonates the charged enediolate oxygen resulting in product formation.

Extensive studies have been done on the understanding the catalytic mechanism of TIM by using two competitive inhibitors 2-Phosphoglycolate (2PG) and phosphoglycohydroxamate (PGH). Three atomic resolution structures in complex with substrate and inhibitors have been reported in PDB [47-49]. In previously published structures, a complex with PGA and Glu167 showed pK_a changes from ~ 4 to ~10, mimicking the substrate binding on protonation of Glu167 [50]. Another structure with PGH was reported mimicking PGH as an uncharged enediol intermediate [51]. Using high-resolution structures with these molecules it was possible to determine the protonation states of some TIM active site residues. Each of these structures pointed out tight interactions between the catalytic carboxylate group of glutamate and reactive side of substrate. For instance, TIM-2PG structures (0.82 Å) revealed a Glu167-Pro168 planar strained conformation and it is speculated to have a major role in loop opening and product release after reaction completion [48]. TIM-PGH atomic resolution structure provided the information on movement of Glu167 by 1 Å above cis-enediolate intermediate plane which was due to small changes in main chain residues geometry (Gly211 and Pro168). This movement plays a key role in shuttling of protons between C1-O1 and C2-O2 moiety of cis-enediolate intermediate. This also shows the high affinity of carboxylate for proton and its abstraction from C1 in classical mechanism [52]

I.4.1 3. TIM variants Glu97Q (E97Q)

Even though, TIM is a well-studied enzyme, there are still many open questions on its catalytic mechanism. While the chemical role of all residues in active site is thoroughly investigated, the importance of residues in catalytic mechanism adjacent to active site is not well understood. All the structures of TIM show E97 situated adjacent to active site residue Lys13. There have been contradictory views in literature on role of E97 on catalytic efficiency of TIM. Knowles et al. reported no change in catalytic activity in a TIM mutant bearing E97D mutation in chicken muscle [53]. Later, Samantha et al. reported 100-fold decrease in k_{cat} with E97D mutation in Plasmodium falciparum. Another mutation E97Q lead to even lower k_{cat} activity with 4000-fold decrease than wild-type [54]. This suggests a direct role of E97 in TIM reaction mechanism. However, Richard et al. also suggested no role of E97 in proton transfer, instead just involved in stabilizing K13 [55]. In the E97Q variant TIM X-ray structure, movement of K13 away from substrate was observed. According to Richard and coworkers, this movement is due to loss of ion pair between residues K13 and E97 contributing to reduction in activity. Ion pair between K13 and E97 immobilize the side chain of K13 preventing undesirable formation of flexible ion pair with the intermediates in catalytic isomerization reaction. It was

speculated that these ion pairs may somehow affect the activity of TIM enzyme but significant reduction was just because of mutation from ionizable form (E97) to neutral form (Q97).
Effect on catalytic rate of an enzyme is often evaluated by site-directed mutagenesis studies. These studies not only give insights into the role of individual amino acids but also any unfavorable interactions between side chains in or around active site. To deepen the understanding of function of non-active site residues a TIM variant E97Q was generated and structurally characterized in this study.

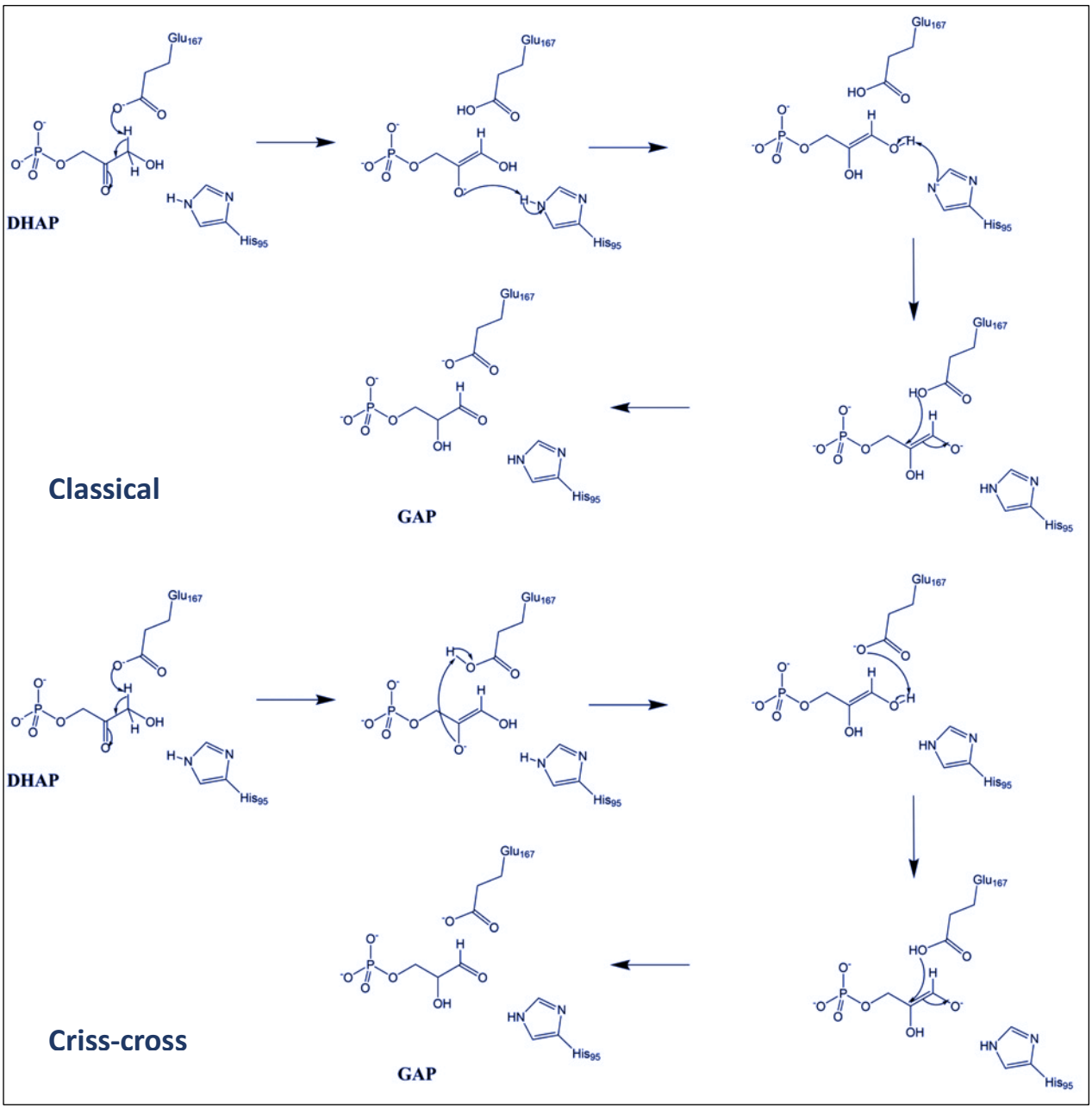

Figure 2. The formation of cis-enediolate intermediate during interconversion of DHAP to GAP catalyzed by TIM. The two proposed reaction mechanisms for proton transfer are classical (top) and criss-cross mechanism (bottom) (Adapted from https://doi.org/10.1107/S2052252521004619)

I.4.2. Outer membrane protein F as potential candidate for NMX studies

Outer membrane proteins are located exclusively in the outer membrane of Gram-negative prokaryotes, mitochondria and chloroplasts. These porins act as a permeability barrier protecting bacterial cell from harmful solutes such as toxins and antibiotics but at the same time allow the diffusion of size-limited hydrophilic molecules (<600 Da). It has a size-selective filter with high affinity for cations. Forty years ago, first three-dimensional crystals of a membrane protein, outer membrane protein F (OmpF) that were amenable to highest resolution X-ray diffraction were obtained [56]. However, it took another decade to solve the structure of this porin [57]. Since then 47 structures of this porin were deposited with a keen interest in it due to its high stability, easily crystallizable and permeability to several antibiotics (PDB accessed on 03/06/2021).

OmpF is one of the most abundant outer membrane protein and exists as a homotrimer consisting 340-residue monomeric unit [57]. Each monomer is a barrel composed of 16 amphipathic β-strands that form an aqueous channel spanning the outer membrane. Eight loops (L1-L8) are extended on the extracellular side and eight turned towards the periplasmic space. All barrels are surrounded by a water-filled pore with a solvent accessible area of 30-40 $Å^2$. Loop L3 (Arg100- Gly134) defines this area of limited access by connecting β-strands 5 and 6 that are bent towards inward of the barrel. Loop L3 forms a constriction zone at the barrel center where acidic residues (Asp 113 and Glu117) in the loop and the basic residues (Lys16, arg42, Arg82 and Arg132) on the opposite side of the size-limiting filter constricts the porin channel. These polar residues form a hydrogen bonding network inside the hydrophobic barrel [57, 58]. It has been inferred previously that size of the pore can be manipulated by making changes in the most flexible region (Pro116-Glu117–Phe118–Glu119–Gly120) of loop L3 [59]. The cluster of acidic and basic residues inside β-barrel gives rise to electric field that is assumed to affect solute transfer and ion permeation properties of channel. In addition to loop L3, loop L2 act as a latch between neighboring β-barrel subunits forming polar and ionic interactions [60]. Glu71 in Loop L2 is hydrogen bonded with guanidium groups of Arg100 and Arg132 of loop L3 across the interface of adjacent subunit. Another residue Glu74 in Loop L2 stabilizes this loop by forming intraloop hydrogen bonds. Thus, all these hydrogen bonds increase the stability of trimeric OmpF and indeed make it difficult to dissociate in presence of concomitant denaturants [60].

A striking feature of porins is that they can serve as receptor for numerous structurally unrelated substrates. This is the reason many structures of OmpF are deposited in complex with colicins and various β-lactam antibiotics [58]. Alteration of channel selectivity and permeability to ions has been investigated previously by Roux and coworkers to understand bacterial susceptibility of OmpF to antibiotics [61]. To further understand, various mutations of key residues in restriction zone of OmpF have also been conducted previously. It was concluded that alterations of charged residues in Loop L3 has a substantial impact on antibiotic susceptibility of bacteria and this can help in fine tuning antibiotic uptake rate or designing new molecules [62]. However, a better understanding of bacterial resistance triggered by modification of membrane permeability is still necessary for the development of new antibiotic therapy strategies.
PEFGGD fragment at the tip of Loop L3 is the conserved sequence in all enterobacterial porins and is known to interact with the wall of β-barrel by forming hydrogen bond between the backbone nitrogen atom of Glu117, Glu296 and Asp312. The proximity of acidic residues Glu296 and Asp312 with the PEFGGD fragment indicates that atleast one of them is protonated [63]. Protonation of Asp312 is speculated to weaken the hydrogen bond between carboxylate

of aspartate and backbone amide of Glu117 resulting in pore closure. Thus, clearly demonstrating the importance of protonated state of Asp312 in maintaining structural and permeability properties of porin. In addition, simultaneous protonation of both acidic residues Asp312 and Glu296 would lead to electrostatic repulsion triggering the movement of Asp312 and PEFGGD fragment into the permeation pathway of the aqueous channel. Similar studies have been investigated previously in OmpC by replacing Asp315 (Asp312 in OmpF) with alanine (protonated state analogue) resulting in lack of hydrogen bond with Glu 117 and simultaneous pore closure [64]. Further investigation of protonation/deprotonation state of these acidic residues is possible by neutron structure of OmpF. Thus, making OmpF a suitable candidate for NMX studies.

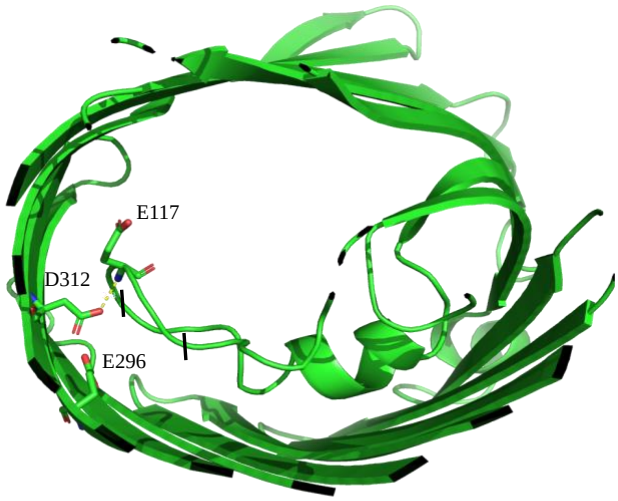

Figure 1. Partial view of Ompf X-ray structure. Acidic residues Glu296 and Asp312 are involved in interaction with conserved PEFGGD fragment of constriction zone. Carboxyl group of Asp312 is hydrogen bonded to backbone amide of Glu117, thus mainting the eyelet structure of β-barrel. Black solid lines indicate ends of PEFGGD sequence in loop L3.

I.5. Need of crystallization

I.6. Factors affecting protein crystallization

Crystallography is a method for studying the arrangement of atoms in the crystal inner structure, which obviously requires forming crystals. The structural information allows to understand the basic principles of biological processes. In case of proteins, this knowledge is applied in development of drugs. X-ray, neutron and electron diffraction are the major techniques employed by crystallographers to construct an atomic arrangement model in order to distinguish and characterize any solid material. Such findings can help in understanding the chemical composition, defects if any and polymorphic form. With time, crystallography has become more efficient and less arduous with improved sample preparation methods and technology development in data collection at synchrotrons. Research emphasis has inclined from determination of simpler structures to very complex ones and even to imperfectly formed crystals.

Crystallization is a three-stage process that begins with nucleation of protein molecules, continues to crystal growth stage and lastly, cessation of growth once protein molecules are depleted in the solution. The different stages of crystallization are presented in Figure 3. A

critical nucleus is formed by the three-dimensional association of protein molecules to form a stable crystal lattice. Growth stage is the continuous diffusion of protein molecules in organized manner to the surfaces of critical nuclei to form an ordered assembly onto the growing crystal. Destabilization of the crystal lattice with increasing deposition of impurities with the depletion of protein molecules in the solution leads to end of crystal growth [65]. Creation of a supersaturated state is required to crystallize a macromolecule. Supersaturation is a non-equilibrium condition wherein some part of the macromolecule reaches the solubility limit under specific conditions. To re-establish the equilibrium and attain the saturation limit, a solid phase (precipitate or crystal) from solution is formed. This solid phase can be achieved by changing various factors like temperature, pH, salt concentration or even addition of a ligand [66].

There are numerous challenges with producing protein crystals and monitoring their growth. A two-dimensional tool known as phase diagram is used to monitor the state of protein molecules as function of relevant variables. These variables could be protein concentration, temperature or characteristics of precipitant such as concentration, pH or ionic strength of salts in buffer [67]. Crystal growth requires a phase transition between two phases: soluble and crystalline. Change in the solubility of the protein with precipitant conditions can studied with phase diagrams as shown in schematic diagram in Figure 3. A phase diagram is divided into three regions: undersaturated zone, metastable or labile zone and precipitation zone. Crystals dissolve in the undersaturated region and start growing with the increase in supersaturation above the protein solubility. However, if the supersaturation is too high the protein enters precipitation zone. Controlling supersaturation is an ambiguous process and varies with protein to protein. Once the phase diagram is understood, it can help in predicting the right conditions for protein crystallization. A rational way to grow large crystals is by controlling the width of metastable zone which can be determined by phase diagram. Due to lack of sample availability, phase diagrams of handful of soluble proteins [68-71] and membrane proteins [72, 73] has been reported.

When it comes to membrane proteins, additional solubilization agent such as detergents are also to be considered along with conventional crystallization for soluble proteins. This adds an additional dimension to be evaluated for screening conditions. The crystals formed with detergents often lead to low-resolution structures or twinning. To overcome such challenges, a drastic improvement has been observed over the years in crystallization techniques. Crystallographers can set up plates without human intervention using efficient and automated robotic systems with very low amount of sample. However, general complexities in membrane protein crystallization will not be discussed in details here. Instead, major inclination will be on crystallization techniques employed in growing large soluble and membrane protein crystals.

I.7. Crystallization techniques for Neutron crystallography

Various techniques have been established to convert a protein solution into a supersaturated state. The commonly used methods are vapor diffusion, batch, dialysis and free interface diffusion [65, 74, 75]. A schematic diagram of various crystallization methods phase diagram indicating metastable zone is shown in Figure 4. To grow large crystals, some physical apparatus is required to optimize the solubility of protein

I.7.1. Vapor diffusion method

This technique is based on the principle of evaporation, diffusion and condensation of volatile substances (usually water) between a droplet of protein-buffer solution and precipitant, and a reservoir composed of similar buffer and precipitant at a higher concentration. To maintain the equilibrium, the container is sealed. Once water vapor from the protein solution is equilibrated with the reservoir solution, it causes supersaturation of protein. This eventually leads to nucleation and initial crystal growth. The droplet can be set up in three ways: hanging, sitting or sandwich drop. In hanging drop method, drop mixed with reservoir solution is placed on the underside of the siliconized glass cover slides that is inverted over the well solution (Figure 5a). In the sitting drop method, a droplet of the protein mixed with reservoir solution at a lower concentration is placed inside the well on a platform or bridge above the well (Figure 5b). In case of sandwich drop, protein mixed with reservoir solution is placed between two siliconized glass cover slips (Figure 5c).

Vapor diffusion is an optimal technique for screening numerous crystallization conditions and growing large protein crystals. Initial screening can be done manually or using robots against a wide range of commercially available screens. A general thumb of rule, large proteins (>30kDa) crystallize at lower protein concentration (2-5 mg/ml) unlike small proteins that reach supersaturation only at higher protein concentration (10-50 mg/ml). This is the most commonly used technique for crystallizing soluble and membrane proteins.

I.7.2. Free interface diffusion (FID) or counter-diffusion method

In this technique, precipitant solution is carefully layered over concentrated protein solution inside a capillary with ends sealed by wax. Due to narrow diameter of capillary, natural mixing by convection is minimized, thus allowing protein and precipitant solution to slowly inter-diffuse. Once the system is equilibrated to reach supersaturation level with liquid-liquid free inter-mixing, nuclei formation takes place. As the time proceeds, the two solutions dilute each other along the axis of capillary promoting growth of few large crystals by dissolving smaller ones. This is a technique of choice for neutron crystallographers, as large sample volume is required to obtain few high-quality crystals. It's easy to differentiate small and large crystals in the capillary as microcrystals usually appear at the protein-precipitant interface and large crystals towards the distal end of the capillary [76].

A different approach to this method is use of gelling agents such as high melting agar to perform the experiment. This can be done in various ways, either by placing a gel plug between protein and precipitant or other possibility is gelling of one of the solutions. To improvise, capillary with protein solution sealed with one-end is placed in a small crystallization vessel containing gelled medium overlayered with precipitant solution [77]. Use of agarose as gelling medium greatly reduces the natural convection and improves the internal order of protein crystal. Capillary counter-diffusion experiment has been previously attempted for membrane protein crystallization where protein solution (SERCA) was mixed with low-melting agarose to obtain few crystals in large diameter capillaries [78]. However, there are some drawbacks such as delicate handling of fragile capillaries and large sample requirement. One can optimize many variables such as gel volume, precipitant agent and protein concentration to decrease supersaturation for growing few large crystals using capillary counter-diffusion technique.

I.7.3. Batch crystallization

No equilibration is required for crystallization in batch method. Instead, direct supersaturation can be achieved by mixing the protein and precipitant to form a homogeneous mixture leaving it undisturbed. These initial conditions generally remain stable for 2-3 weeks. To avoid evaporation, the droplet is covered by oil. This method is not the best for growing large crystals as controlling equilibration is not easy. However, it can be improved by combining batch and vapor diffusion. In this method, a homogeneous suspension of protein and precipitant to their final concentration is prepared and stored with a precipitant at same concentration. This maintains the evaporation and also resolves the issue of slow evaporation of water molecules from the crystallization drop due to presence of oil.

I.7.4. Dialysis

In this technique, a semi-permeable membrane is used to allow passive diffusion of precipitant into a crystallisation chamber that leads to supersaturation of macromolecules where it crystallizes. Dialysis membrane of appropriate molecular weight cut-off is chosen according to size of protein in case of soluble proteins. However, protein-detergent micelle is to be considered for diffusion of detergent molecules through the membrane in case of membrane proteins. In the experimental setup, protein solution is added in a small button and carefully covered with dialysis membrane closed with an elastic band avoiding any bubbles. This button is then immersed in the precipitant solution. This method is advantageous for screening the best conditions for large crystals. One can recycle the same protein solution by just switching the reservoir solution from one condition to another. On the other hand, this method is not effective with higher PEG concentration as they draw all water from the dialysis button resulting in precipitation of protein solution. Another approach to slow down the equilibration for better crystal growth is to use double dialysis where in a dialysis button placed inside a reservoir is sealed with dialysis membrane and placed in second reservoir solution at slightly higher precipitant concentration [79]. Recently, micro dialysis buttons have also been used for crystallization of membrane proteins to obtain well diffracting crystals.

I.7.5. Seeding

One of the most commonly used approach to grow large crystals for NPX is seeding. It can be either single or repeated macroseeding, microseeding or just crystal feeding into large vapor diffusion crystal drops [80, 81]. Seeding techniques provide with preformed crystal surface onto which more molecules may be added in an orderly manner to give large crystals at lower degree of supersaturation [82]. In microseeding, microcrystals from are added to a supersaturated crystal drop wherein supersaturation should be lower than its nucleation point. To produce a seed stock, few crystals are crushed and washed with reservoir solution. Repeated vortexing with an interval of 30 sec is done to crush them even finely. This solution obtained is then diluted typically in the range of 10^{-3} to 10^{-5} as initial tube is excessively rich in nuclei. Streak seeding can also be done, however, it's not suitable for growing large crystals as number of seeds transferred cannot be controlled. For macroseeding, a single crystal is introduced into a new drop preequilibrated for crystal growth preferably in metastable zone of phase diagram. The crystal to seeded can be picked either by using a glass/quartz capillary or a fishing loop of crystal size. The crystal is then rinsed repeatedly (at least twice) in a stabilizing solution to clean the precipitant and any misoriented macromolecules or microcrystals deposited on top layer. The washed crystal is then transferred to the new crystallization drop. Seeding has been a powerful tool for controlling crystal growth, however, microseeding is preferable over macroseeding helping in obtaining large crystals for NPX [83, 84].

I.7.6. Temperature control

Temperature is an important factor to regulate the supersaturation level of protein solution. By varying temperature, growth of crystals can be moderated within the metastable zone of phase diagram [85]. It maintains a balance between the enthalpy and entropy to maintain the equilibrium of the system. Temperature-solubility is a function of protein-solution system; thus, choice of protein buffer is crucial. Depending on whether crystallization is enthalpy-driven or entropy-driven, protein solubility is influenced by temperature variation [85]. For a few soluble proteins, temperature effect on solubility and consequently supersaturation has been explicitly shown in phase diagrams [85-87]. Previously, temperature dependency during phase separation of detergent solutions for membrane protein crystallization has also been reported [88, 89]. Therefore, temperature control is a prerequisite for reproducible protein crystallization experiments. An automated bench for temperature-controlled protein crystallization using dialysis method has been designed for crystallization of soluble proteins [90]. This temperature-controlled batch setup has been successfully used to grow neutron-sized crystals by continuously monitoring the nucleation and crystal growth [15, 91].

I.8. Membrane protein-based crystallization

In general, membrane proteins produce type I and type II crystals based on their packing [92, 93]. In type I, a three-dimensional lattice is formed by two-dimensional stacking of layers on top of each other. In one layer, membrane proteins pack side-by-side providing crystal contacts with hydrophobic surfaces. Crystals grown in lipid phase produce type I crystals. On the other hand, in type II crystal packing, hydrophobic regions are covered by detergent molecules. Hence, crystal contacts are formed only by water-exposed region of membrane protein. Usually, detergent based crystallization produces such crystals and they often diffract to lower resolution.

I.8.1. Detergent-based crystallization

Most popular and conventional method for crystallization of membrane proteins. Detergents are used to isolate membrane proteins from the cell and purified protein-detergent complex is crystallized using general techniques used for soluble proteins. However, this approach has drawbacks of unstable protein in detergent micelles that might hinder formation of high-quality crystals. Due to few available crystal contacts, protein molecules are not arranged in an ordered fashion and the crystals produced often diffract to lower resolution.

I.8.2. Lipid cubic and sponge phase

Lipid cubic phase is composed of a single bilayer organized into a well ordered 3-D lattice permeated by aqueous channels. Membrane protein is embedded into this cubic phase by mixing protein solution with the LCP component i.e. monoolein in an optimum ratio. This method has seen a lot of improvements resulting in crystallization of human G protein-couples receptors, high-resolution details of photosynthetic reaction center and human A2A Adenosine Receptor Bound to an Antagonist [94-96]. Proteins crystallized with LCP produce stabilized crystals due to extensive contacts between hydrophilic and hydrophobic regions of proteins. However, it’s not the preferred method for growing large crystals due to practical difficulties in crystallization set up and fishing crystals out of lipid medium. In few cases, when LCP liquefies before the crystal formation, it gives rise to lipidic sponge phase (LSP). LSP has larger

aqueous pores and easy to handle due to its liquid state. Thus, suitable for vapor-diffusion experiments to grow large crystals.

I.8.3. Bilayered micelles crystallization

Bilayered micelles are formed by a suitable mixture of a lipid and a detergent. Long chain lipids such as 1,2-dimyristoyl-sn-glycerol-3-phosphocholine (DMPC) or 1,2-dihexanoyl-sn-glycerol-3-phosphocholine (DHPC) forms the bilayer micelle and detergents such as 3-[(3-cholamidopropyl) dimethylammonio]-1-propanesulfonate (CHAPSO) covers the edges of hydrophobic layer in the bicelles. Phase diagram of bicelle crystallization has several phase transitions and dependent on various parameters such as lipid-detergent ratio, temperature, protein and bicelle concentration. In this method, crystallization can take place in both the liquid and the gel phase. Varying the above-mentioned parameters packing of protein molecules can be optimized paving the way for growing large crystals. Moreover, bicelles mimics the in vivo lipid bilayer composition, thus proteins retain their native structure and remain stable for longer duration [97].

Chapter II. Sample preparation for NMX studies

II.1. Introduction

Producing isotopic labeled proteins for techniques like NMR and SANS has been a practice for several decades. The main purpose here is to take advantage of contrast variation unlike requirement of increased signal in NMX to avoid the negative ^{1}H scattering. Thus, Moore introduced the production of perdeuterated protein using M9 media and deuterated acetic acid as a cheap carbon source using *E. coli* as expression system [98]. Since then various protocols were proposed to produce perdeuterated protein, however, they were not easy to follow and not giving enough protein yield. Minimal media optimization with additives, partially deuterated protein using hydrogenated carbon source and deuterated algal hydrolysate as a carbon source were major breakthrough in production of perdeuterated proteins a decade ago [99-101]. This improved with time and various works on different choice of deuterated carbon source were reported such as perdeuteration of cytochrome P450cam using d-glycerol and production of perdeuterated human aldose reductase utilizing d-succinate [102, 103]. Currently, d-glycerol is the preferred choice of carbon source due to its low cost as compared to d-glucose.

E. coli due to its fast growth rate, easily manipulative genetics, inexpensive growth media and high biomass/substrate yield is an ideal expression system for recombinant protein production. Due to its well-known genetic and physiological characteristics, it's easier to understand the effect of new growth conditions on *E. coli* as compared to other organisms. However, plasmid choice with kanamycin-resistance is recommended to avoid leaky expression. Perdeuteration using plasmids with ampicillin resistance leads to lower final optical density of cells or sometimes even failure of expression [104]. Thus, expression control by transformation of optimum plasmid in *E. coli* strain is very important for persistent bacterial cultivation in deuterated conditions.

The classical method to produce deuterated protein involves adaptation of a bacteria to D_2O based medium by subsequent sub-culturing in media with increasing deuteration content [30]. This method is not only time consuming but also impractical in terms of additional cost of material required for adaptation. So, in this chapter a methodology to optimize perdeuterated protein expression without adaptation process has been demonstrated. Perdeuteration of recombinant TIM variants and OmpF has been demonstrated very similar to conventional hydrogenated bacterial heterologous protein production, once it was established to be reproduced with consistent yield.

II.2. Materials and methods

II.2.1. Production and characterization of OmpF

II.2.1.1. Plasmids and strains

The expression plasmid, pET-24(+)_ompF, was made by Genescript. It contains the *E. coli ompF* gene modified with a coding sequence of a hexa-histidine tag followed by a TEV endopeptidase cleavage recognition sequence placed between the OmpF signal sequence and natitve OmpF. The gene for *ompF* was deleted from the production strain, *E. coli* DA1(DE3), using the λ-Red recombinase-mediated gene deletion method [105]. A PCR product harbouring 50 bp end sequences homologous to ompF and a chloramphenicol resistance marker was amplified with plasmid pKD3 as template and primers ompF_up and ompF_down (ompF_up:ATTGACGGCAGTGGCAGGTGTCATAAAAAAAACCATGAGGGTAATAA ATAGTGTAGGCTGGAGCTGCTTC.
ompF_down:AAACAGGACCAAAGTCCTGTTTTTTCGGCATTTAACAAAGAGGTGTG CTAATGGGAATTAGCCATGGTCC). The *ompF* PCR product was transformed into *E. coli* DA1(DE3) that harbored the λ-Red recombinase expression plasmid pKD46, and subsequently transformants were selected on media plates containing chloramphenicol. Deletion of *ompF* was verified by amplifying the appropriate chromosomal region by PCR.
The OmpF construct (pET(24(+)_ompF) was transformed into electrocompetent DA1(DE3) cells lacking the *ompF* gene (*ompF::cat*) by electroporation and spread on Lysogeny broth agar plates (LA) plates containing 50 µg/µl Kanamycin.

II.2.1.2. Cultivation and preparation of algal extracts for deuterated medium

A culture of *Botryococcus braunii* was grown at 23°C under 12:12 light-dark cycle of LED lights using Multitron Pro (INFORS HT) incubators with constant shaking at 60 rpm in modified Bolds 3N medium (Schwartz, 1975). The composition of media was: 8.82 mM $NaNO_3$, 0.17 mM $CaCl_2$, 0.3 mM $MgSO_4$, 0.43 mM K_2HPO_4, 1.29 mM KH_2PO_4, 0.43 mM NaCl, 2 mM $Na_2EDTA•2H_2O$, 0.36 mM $FeCl_3•6H_2O$, 0.21 mM $MnCl_2•4H_2O$, 0.037 mM ZnCl2, 0.0084 mM $CoCl_2•6H_2O$ and 0.017 mM $Na_2MO_4•2H_2O$. The pH of the medium was adjusted to 7.8 and supplemented with thiamine to final concentration 1 µM, vitamin B12 and biotin to final concentration 0.1 µM. The culture was grown for 14 to 28 days in 3L glass bottles with maximum volume of 1L per flask. Once the culture turned dark green, 95% was harvested by centrifugation at ~6000 g for 10 min in a JLA 8.1 rotor (Beckman) and rest was used for inoculating the subsequent batch. Harvested cells were used for preparing algal extracts as described by (Weston Kightlinger, 2013). The pelletized cells were washed with distilled water and centrifuged at 4000 x g for 5 min. The washing step was repeated twice. 40 mL of D_2O was added to 10 g (wet weight) of algal cells. After resuspending, algal cells were placed in a 50°C water bath for 24 h to autolyze. The autolyzed cells were centrifuged at 4000 x g for 10 min and the pink colored supernatant was collected and used as carbon source in deuterated M9 medium.

II.2.1.3. OmpF Expression test in rich and minimal media

A comparative study for the optimized production of OmpF was done considering various parameters. Initially, parameters such as temperature, media, induction point for cell expression (OD_{600}) and isopropyl β-D-1-thiogalactopyranoside (IPTG) concentration were tested empirically.
LA-Kan plate was streaked with appropriate strain and incubated at 37°C overnight. 25 ml growth medium (LB) supplemented with kanamycin (50 µg/ml) was inoculated with few colonies and incubated overnight at 37°C with shaking at 200 rpm. This culture was then added to fresh 25 ml medium to an OD_{600} of 0.1 in an Erlenmeyer flask.

Six different bacterial cultures in LB media were grown with agitation at 200 rpm at 37°C until the cultures reached an OD_{600} of 0.6, 1.0 and 1.2. Once bacterial cells grew up to the desired OD_{600}, *ompF* expression was induced by adding 0.1 mM or 1 mM IPTG. To optimise the growth conditions in LB media at 18°C, bacterial cells were grown up to OD_{600} 0.6 and induced with varying IPTG concentrations (0.05 mM, 0.1 mM or 0.5 mM).

For all growth conditions a 1 ml sample was collected at the time of induction and stored at −20°C. For cultures grown at 37°C a 1 ml sample was collected 4 hours after induction and 18 hours after induction for cultures grown at 18°C. All collected samples were centrifuged at 20000 x g for 2 min at 4°C. The supernatants were removed and pellets were resuspended in 0.25 ml cold buffer (50 mM Tris, 100 mM NaCl, 10 mM EDTA (pH 8.0)). The next step was sonication of all the samples on ice (Vibra Cell disruptor, output control ~20, 3 second pulses). After sonication, 40 µl whole cell fraction was removed and stored on ice. The remaining part of the sample was stored at -20°C. SDS-PAGE of whole fractions was performed to select the best optimised conditions by observing band intensity. 20 µl 5 x SDS-PAGE sample buffer was added to the samples and incubated at 95°C for 10 min. All the tubes were then cooled on ice and spinned briefly. 10 µl sample per lane was loaded on an SDS-PAGE gel. Tris-glycine SDS (TGS) was used as a running buffer and Coomassie staining (SimplyBlue Safe stain) was used to visualise the bands. Destaining of gel was done in milli-Q water.

For optimization in minimal media M9 (composition in Table 1), bacterial cultures were grown at 30°C and 37°C [30]. At an OD_{600} between 0.5 and 0.6, *ompF* expression was induced with 0.1 mM, 0.05 mM or 0.5 mM IPTG. Optical density was recorded at different time points to calculate growth rate. Logarithmic (ln) OD_{600} versus time (hours) was plotted and the slope of the linear best fit line was used to calculate specific growth rate (μ). The doubling time (t_d) equals to $\ln 2/\mu$.

Growth curves (OD_{600} versus time) for all the samples were plotted. 1 ml sample before and after induction were collected and stored at -20°C. Samples were sonicated as described above and all the samples were then loaded on SDS-PAGE to observe the band intensity. Duplicates for each condition was performed.

Table 1. Components of M9 media. 100 ml of 10 X M9 media base was added to 1 l of medium. All the components were dissolved in D_2O for deuterated media.

M9 Base (10X)	**Amount (g/l)**
$Na_2HPO_4 \cdot 2\ H_2O$	7.6
KH_2PO_4	2.99
NaCl	0.5
Additives	
NH_4Cl	2
Glycerol	8
$MgSO_4$	0.12036
$CaCl_2$	0.01
thiamin	0.002
$FeCl_3$	0.0029

II.2.1.4. OmpF expression test in deuterated M9 media using glycerol as carbon source

Minimal media (M9) was used for production of deuterium-labelled protein. Protein expression was performed in three different ways with D_2O as the solvent and using either protiated glycerol, perdeuterated glycerol or perdeuterated algal extract as the carbon source. All media components were dissolved in D_2O (99.8 atom% D, Sigma-Aldrich) and sterilized with a 0.22 μm filter. Stock solutions of IPTG and kanamycin were also prepared in D_2O.
Overnight 25 ml hydrogenated M9 medium (H-M9) starter cultures were setup by inoculating few colonies from LA-Kan plate streaked with OmpF strain and incubated at 37°C, 200 rpm shaking. To reduce the carry-over of hydrogen to deuterated media, the overnight culture was diluted equivalent to OD_{600}=0.1 in a sterilized glass tube and centrifuged at 8000 x g for 8 minutes at room temperature. The pellet was then resuspended in 25 ml deuterated M9 medium (DM9) with glycerol as carbon source and incubated at 37°C with shaking at 200 rpm. The following day new bacterial cultures with two different carbon sources were set up using the harvested pellet from overnight culture. Partially deuterated medium was supplemented with 0.8% (w/v) protiated glycerol (referred to as DM9) and labelled glycerol-d8 (≥98 atom% D, Sigma-Aldrich) was added to the fully deuterated medium (referred to as DDM9). Duplicate bacterial cultures were then incubated at 37°C with shaking at 200 rpm. Expression of *ompF* was induced with 0.1 mM or 0.5 mM IPTG concentration once the OD_{600} of the cultures reached a value of 0.6-0.8. Samples were harvested at specific intervals to measure OD_{600} using a spectrophotometer and stored at -20°C for later SDS-PAGE analysis.

To maximise the deuterated protein yield, another expression trial using labelled glycerol-d8 was performed wherein initial fresh medium was inoculated with higher starting OD_{600} of 0.2, 0.3 and 0.1 was used as a reference culture. All the cultures were then induced with 0.1 mM IPTG and 1 ml sample was collected at specific intervals up to 86 hours of induction. The collected cultures were centrifuged at 20000 x g for 2 min at 4°C and the pellet was resuspended in 0.25 ml cold 50 mM Tris, 100 mM NaCl, 10 mM EDTA (pH 8.0) and stored at -20°C. The following day all the samples were sonicated on ice and SDS-PAGE was run on whole cell fraction as described in Section **II.2.3.**

II.2.1.5. Growth experiments in deuterated M9 media using algae extract as carbon source

An initial expression test was performed to optimize the final concentration of algal extract to be used in M9 medium. The starter culture was prepared in similar way as expressed above in Section **II.2.4.1.** The fresh bacterial cultures were set in an Erlenmeyer flask using algal extract filtrate and freeze-dried powder as carbon source. In initial experiments, we added 3g, 5g and 7g of freeze-dried algal extract powder and v/v 10%, v/v 15% and v/v 20% algae extract filtrate as carbon source in 10 ml of media. Duplicates of all the bacterial cultures were then incubated at 37°C with shaking at 200 rpm. Once bacterial cells reached an OD_{600} of 0.5-0.6, *ompF* expression was induced with 0.1 mM and 0.5 mM IPTG. The OD_{600} between 0.1 and 0.6 at

different time points was recorded using a spectrophotometer to calculate the growth rate. For large scale protein production from deuterated algal extract, the deuterated medium was prepared in the same way except 12% (v/v) algal extract was used as the carbon source which will be further referred as DAlgae. The harvested bacterial cultures were sonicated and samples were run on SDS-PAGE following the procedure as described in Section **II.2.3.**

II.2.1.6. Outer membrane extraction with and without Triton X-100

Outer membranes were extracted by using the lysozyme/EDTA method [106]. The pellet from 10 ml of bacterial suspension was resuspended in 200 µl 0.2 M Tris-HCl pH 8, 1 M sucrose, 1 mM Na-EDTA (pH 8.0). 40 µl of lysozyme with a final concentration of 5 mg/ml was added and incubated for 5 min at room temperature (RT). 800 µl of dH_20 was added after 5 mins and incubated for 20 min at same conditions. Samples were then observed under a microscope in order to observe spheroblast formation. 1.2 ml 50 mM Tris-HCl pH 8, 2% (w/v) Triton X-100, 10 mM $MgCl_2$ and 50 µl DNase I with a final concentration of 1 mg/ml was added to the solution and mixed by inverting the tube several times until the suspension was clear. This suspension was then centrifuged at 100 000× *g (50 000 rpm in Beckman Optima TL with TLA 100.4 rotor)* for 25 min at 4 °C. The obtained pellet containing outer membrane was washed again in 7.5 ml 50 mM Tris-HCl pH 8, 2% (w/v) Triton X-100 and centrifuged. After centrifugation, pellet rich in outer membranes was washed thrice in 500 µl dH_2O and stored at -20°C. Outer membrane extraction was also attempted without using Triton X-100 detergent in buffers.

II.2.1.7. Membrane solubilization test in different detergents

The frozen outer membranes extracted with and without Triton X-100 were thawed and further solubilized in two different detergents; β-octyl glucoside (OG) and n-Dodecyl β-D-maltoside (DDM). 50 µl of cell pellet was resuspended in 200 µl of buffer A (Table 2) supplemented with 6% (w/v) OG and 3% (w/v) DDM. Samples were incubated with shaking at room temperature for 1 hour and centrifuged at 100 000 × g for 25 min at 4°C. Most of the outer membranes remain in the supernatant after this step. SDS-PAGE was used to estimate the solubilized pellet and supernatant. 20 µl of each sample was mixed with 5 µl of 5 x SDS-PAGE and loaded on gel.

II.2.1.8. OmpF large scale expression and purification

OmpF expression was performed in 1 l of either hydrogenated or deuterated medium using previously optimized conditions. The harvested cell pellets from all the expressions above were lysed using lysozyme/EDTA lysis method followed by selective detergent treatment to extract outer membrane as mentioned in previous sections. Initially, the pellet obtained from 1 l of culture was resuspended in 4 ml 0.2 M Tris-HCl pH 8.0, 1 M sucrose, 1 mM Na-EDTA. The resuspended cell pellet was lysed with 400 µl of lysozyme (5 mg/ml) and incubated for 5 min at RT. After addition of 8 ml distilled water, another round of incubation was performed for 20 mins and then the cells were resuspended in 24 ml of 50 mM Tris-HCl pH 8.0, 10 mM $MgCl_2$ and 500 µl DNase I (1 mg/ml in dH_2O). The next step was centrifugation of suspension at 100000 × g for 25 min at 4°C. The membrane pellet obtained from centrifugation was first resuspended in 10 ml buffer A (Table 2) without detergent and later kept for constatnt stirring at room temperature for 2 h with an additional 10 ml of buffer A with 6% (w/v) β-octyl glucoside. After 2 h, the solubilized membranes were centrifuged at 100000 × g for 1 h at 4°C

and the supernatant was collected and filtered with 0.2 μm membrane filter to load onto a nickel-charged immobilized metal-affinity chromatography 1 ml HisTrap FF column (GE Healthcare) pre-equilibrated with buffer B (Table 2). The column was washed up to 10 column volume (CV) to obtain a stable UV signal at 280 nm and then eluted with a linear gradient of imidazole by elution buffer C (Table 2) over 20 column volumes.

Peak fractions from affinity chromatography were pooled and mixed with appropriate amount of TEV protease at enzyme: substrate mass ratio 1:20. This solution was dialysed overnight into a buffer B (with 1 mM DTT and 1 mM Na-EDTA) at 4°C using dialysis membrane (32 mm, Spectrapor, molecular weight cutoff: 12-14 kDa). The next day buffer B was replaced with a same buffer without DTT and dialysis was continued for at least 2 hrs before loading on HisTrap FF column (1ml, GE Healthcare). The flow-through containing purified and cleaved OmpF was concentrated to 10 mg/ml using Millipore Amicon ultrafiltration spin columns (molecular weight cutoff: 30 or 100 kDa) and loaded on HiLoad 26/600 Superdex 75 pg gel filtration column (120 ml, GE Healthcare) with a flow rate of 1 ml/min in buffer D (Table 2) supplemented with 0.8% (v/v) n-Octylpolyoxyethylene (Octyl-POE). Peak fractions containing non-aggregated (trimeric) OmpF were pooled and stored at 4°C. Protein purity for all the samples was analysed by SDS-PAGE and the concentration was measured by observing the absorbance at 280 nm with a Nanodrop UV/Vis microspectrophotometer. A schematic representation for the production of perdeuterated OmpF is shown in Figure 1.

Table 2. Buffer composition for protein purification

Buffer A	50 mM sodium phosphate, 300 mM NaCl, 10 mM imidazole, pH 8.0.
Buffer B	50 mM sodium phosphate, 300 mM NaCl, 10 mM imidazole, pH 8.0, 0.05% (w/v) n-Dodecyl β-D-maltoside
Buffer C	50 mM sodium phosphate, 300 mM NaCl, 500 mM imidazole, pH 8.0, 0.05% (w/v) n-Dodecyl β-D-maltoside
Buffer D	20 mM Tris pH 8.0, 100 mM NaCl, 0.8% (w/v) n-Octylpolyoxyethylene (Octyl-POE)

II.2.1.9. Mass spectrometry analysis

The level of D incorporation in OmpF purified from different conditions was measured by mass spectrometry analysis. The mass difference between H and D protein samples was calculated. The intact mass of all samples was analyzed by MALDI TOF/TOF mass spectrometer (Bruker Auto flex Speed TOF/TOF MALDI MS) in positive reflector mode. Sample preparation was done in protiated buffer with a protein concentration of 1 mg/ml. 1 µl of protein sample was mixed with 2 µl of 0.1% trifluoroacetic acid (TFA). 1 µl of TFA treated sample was mixed with 0.5 µl of matrix (5 mg/ml α-cyano-4-hydroxy cinnamic acid and 80% acetonitrile) and spotted on a MALDI stainless steel plate. The obtained mass spectra were calibrated using Intact BSA (Bruker Daltonics) software where four signals from the internal standard bovine serum albumin (BSA) were used for calibration $[M+H]^+$, m/z 66431 (average

mass); $[M+2H]^+$ average 33216 (average mass); $[M+3H]^+$, m/z 22144 (average mass) and $[M+4H]^+$, m/z 16607 (average mass).

II.2.1.10. Thermal stability by nano differential scanning fluorimetry (nano-DSF)

Protiated (H) and deuterated (D) protein samples were diluted to a concentration of ~0.2 mg/mL in hydrogenated and deuterated buffers, respectively. Each sample was loaded into capillaries (Prometheus NT.48 Series nanoDSF grade standard capillaries) in duplicate and placed into a Prometheus Nano Temper NT.48 (Nano Temper Technologies GmbH; Germany). The nanoDSF method detects change in intrinsic fluorescence largely of tryptophan and to a lesser degree of tyrosine residues when protein is slowly exposed to denaturing factors like temperature. OmpF contains 2 and 29 tryptophan and tyrosine residues, respectively. A temperature ramp of 1°C/min from 20 to 95°C was used. The melting temperatures (Tm) were calculated using the software PR ThermControl.

III. Results

III.1. OmpF Expression test in hydrogenated rich and minimal media

It was important to establish suitable conditions for OmpF expression to obtain as high protein yield as possible. The initial expression test was performed at 37°C using LB media. Moreover, optimization of other parameters influencing protein production in *E. coli* is necessary. Therefore, an evaluation of optimum induction point and best IPTG concentration was also performed at lower scale and estimated by protein band intensity using SDS-PAGE (Figure 1a). Overexpression of membrane protein in form of inclusion bodies was observed when cells were grown at 37°C and an IPTG concentration of 1 mM IPTG was used. This higher rate of protein synthesis likely saturates the Sec translocon machinery leading to impaired translocation across the inner membrane resulting in aggregation of OmpF in the cytoplasm [107].

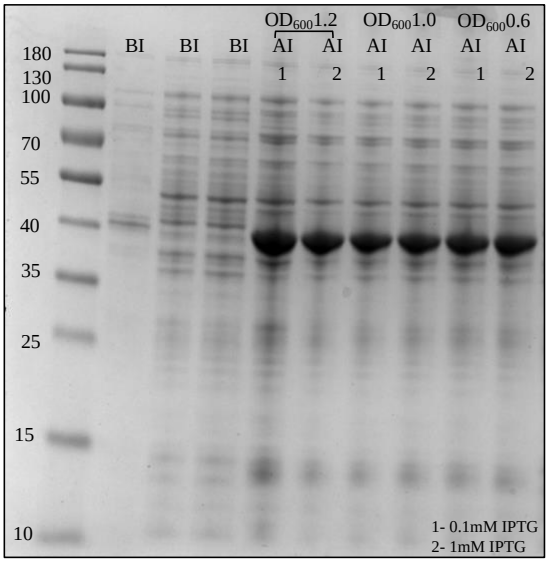

Figure 1. **Expression level of OmpF in cells grown in LB**. Each lane was loaded with a protein sample corresponding to 1 ml of culture and protein marker (in kDa) is labelled on the left. BI and AI denotes for before induction and after induction sample, respectively. a). SDS-PAGE of protein samples expressed at different cell densities and induced with varying IPTG concentration in LB media. b). SDS-PAGE profile of expressed OmpF obtained from cultures induced with 0.05 mM IPTG or 0.1 mM IPTG once the culture reached OD_{600} of 0.6.

It has been previously shown that bacterial growth slowed down at suboptimal temperatures producing more correctly folded proteins and reduce protein aggregation in form of inclusion bodies [108]. In the case of membrane proteins, slower cell growth is more advantageous for proper folding of proteins on the membrane. Thus, to avoid inclusion body formation, in LB media, bacterial cell cultures were grown at 18°C with induction at mid-log phase (OD_{600} = 0.6) of the growth curve. Since there was no significant difference observed in protein band intensities between cells induced with 0.1 mM and 0.05 mM IPTG, the lower IPTG concentration was chosen for large scale production of OmpF at 18°C (Figure 1b).

An initial expression test at 37°C was performed for M9 media where optimal induction point and IPTG concentration were established. Inducing bacterial cells at a later stage of the exponential phase could result in higher protein yield as recombinant membrane proteins can be toxic for bacterial growth. This increase in protein yield was observed with increasing cell density up to OD_{600} of 1.2 (Figure 2a) which could be further increased up to OD_{600} value of 2. Induction point did not have a significant effect on final protein yield as observed in Figure 2a. To avoid the over expression problem as observed with rich media, another expression test was performed in lower temperature. Even though no inclusion bodies were observed in minimal media, bacterial growth was slower at 30°C as expected. In general, doubling time of *E. coli* in M9 media is five times higher than LB [109]. This makes production of protein in minimal media time consuming. Protein expression levels of OmpF increased with increasing IPTG concentration from 0.1 mM to 1 mM as observed by visual comparison of band intensities in SDS-PAGE (Figure 2b). A similar trend was observed both at 30°C and 37°C. Thus, large scale production of OmpF in M9 media was performed at 37°C and cells were induced at 0.1 mM concentration of IPTG (Figure 2a).

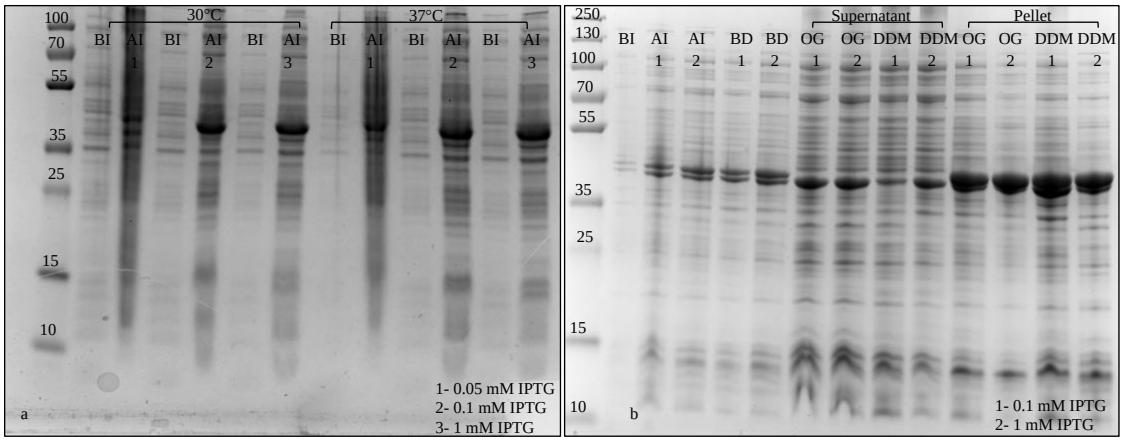

Figure 2. **Expression level of OmpF in M9 media**. Each lane was loaded with a protein sample corresponding to 1 ml of culture and protein mass marker (in kDa) is labelled on the left. BI and AI denotes for before induction and after induction sample. a). SDS-PAGE profile of protein samples when bacterial culture was grown at different temperature and *ompF* expression was induced with varying IPTG concentration. b). Expression levels of *ompF* when cells were grown at 37°C and 30°C in minimal media. Once the optical density of culture reached to 0.5-0.6, cells were induced with varying IPTG concentration

III.3. Optimization of OmpF production in deuterated M9 media using glycerol as carbon source

E. coli DA1(DE3) transformed with with plasmid pET-24(+)_ompF carrying the *ompF* gene was grown in deuterated minimal media with different carbon sources. The growth behavior of cultured cells was monitored and the optical density (OD_{600}) as a function of time was plotted as shown in Figure 3. Estimating the generation time during exponential growth is a real-time indicator of bacterial culture health and helps in predicting approximate induction time. From growth curves of all the samples, it was observed that cells grew fastest in media supplemented with deuterated algae extract with a doubling time of 1.4 h which was comparable to the doubling time (1.7 h) of regular HM9 media at 37°C. Growing bacteria in deuterated condition is time-consuming as due to the slower growth; doubling time of ~4.5 h in case of DM9 and DDM9. However, there was no significant doubling time difference in cell growth when using hydrogenated and deuterated glycerol as carbon source in D_2O. Addition of deuterated algae showed a positive impact on bacterial cell growth with 20% increase in cell density after 5 hours of growth in comparison with HM9. Often a small lag phase was observed when cells were grown in deuterated meida, however, growth proceeded normally after exit of the lag phase. Although, bacterial growth was still very slow and it took approximately 18 hrs for cells to reach optimum induction point. However, using adapted strain *E. coli* DA1(DE3) made the whole process time-efficient as the pre-adaptation of bacteria in D_2O medium was omitted [29].

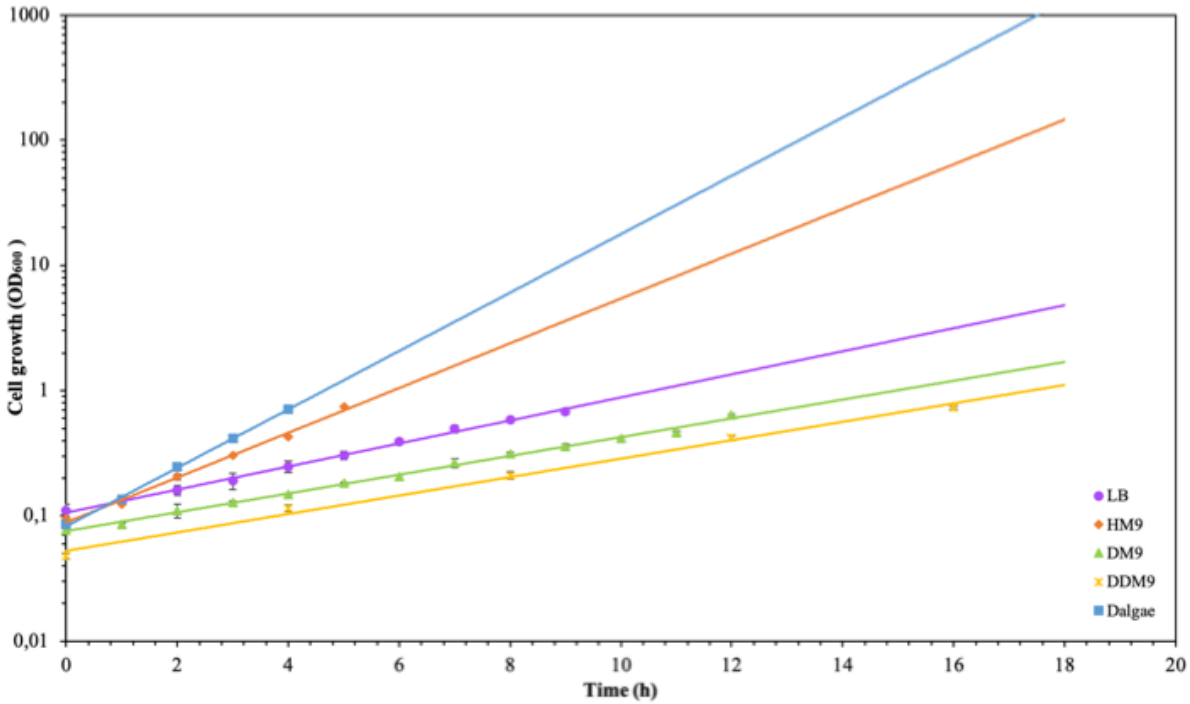

Figure 3. Growth curve of *E. coli* DA1(DE3) grown in minimal media. Deuterated minimal medium was supplemented with different carbon sources and OD_{600} up to a value of ~0.7 was measured for all samples. For each medium duplicates were analyzed. Mean of all data points was plotted and error bars represent the standard deviation. Error bars close to average data point are not visible. Each line represents an exponential fit of the corresponding growth data points.

Considering the cost and time for production of deuterated protiens an initial expression test to optimize the IPTG concentration, expression time and optimal induction point (OD_{600}) is essential. Bacterial cultures were induced with 0.5 mM IPTG and 1 mM IPTG and cells were grown for upto 47 hours to examine preferred time of harvest with highest protein yield (Figure 4b). There was no significant difference in protein expression 18 hours of post-induction with OD_{600} not increasing above value of 2.5. Similar protein expression level was observed with 0.5 mM and 0.1 mM IPTG, therefore, for large scale production, cells were induced with 0.5 mM IPTG and harvested after 18 hours of incubation.

Increased cell mass and higher protein expression level was observed when large culture was inoculated with higher number of bacterial cells (Figure 4a). Thus, it is advisable to start the bacterial culture in D_2O at higher OD_{600} (0.2-0.3) than regular initial OD_{600} of 0.05-0.1. This could also save few hours of experimental work considering the long incubation time in deuterated media.

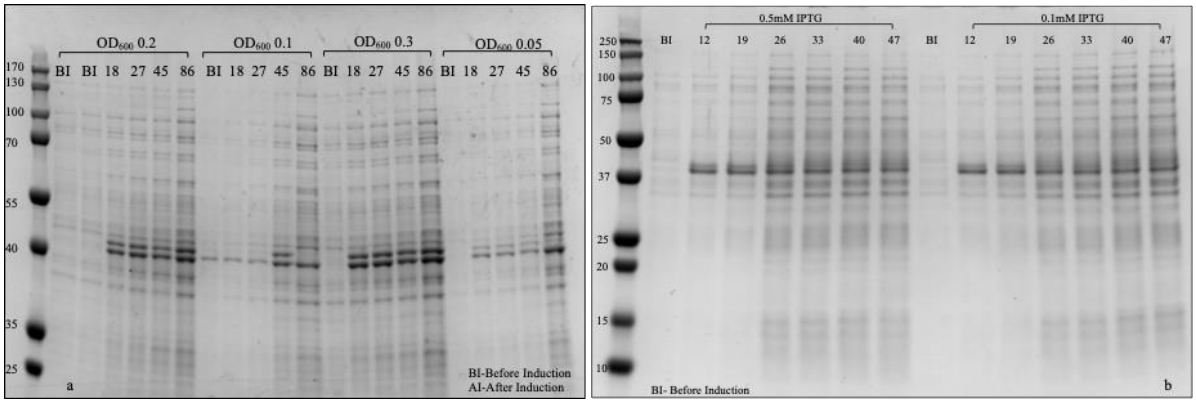

Figure 4. OmpF expression level test in DM9 and DDM9 media. Each lane was loaded with a protein sample corresponding to 1 ml of culture and molecular mass marker (in kDa) is labelled on the left. BI and AI denotes for before induction and after induction sample. a). Comparison of protein expression when bacterial culture was started with higher cell density. All the samples were induced at 0.5 mM IPTG. b). SDS-PAGE of protein soluble fractions when induced with 0.5 mM and 0.1mM concentration of IPTG added once cells reached an OD_{600} of 0.7. OmpF band is close to ~37 kDa.

III.4. Optimization of OmpF production in deuterated M9 media using deuterated algae as carbon source

Algae autolysate was prepared using simple autolysis method wherein cells own hydrolytic enzymes located in cellular matrix was used to breakdown cellular components of *B.braunii.* The supernatant of the autolysed algae extract is generally dried and the powder obtained is used as a supplement in media. Typically, yield of dried powder is ~1g per litre of algal culture. The effect of obtained algae extract on the bacterial growth was analysed by using algae powder as a supplement in media. 25 ml bacterial cultures in hydrogenated minimal media were supplemented with 3 g/l, 5 g/l and 7 g/l of lysate powder. Similar growth was observed in all the cultures and pre-post induction samples were run on SDS-PAGE (Figure 5 and 6b). Due to this and no significant difference observed in protein expression between 7 g/l and 5 g/l, further deuteration experiments were conducted using 5 g/l. The protein expression was induced at a later stage of exponential phase to obtain high-cell density. As the material was expensive negative control of growth curve was conducted on agar plate. 100 µl of bacterial culture media with and without algal extract as supplement was plated. The media was slightly turbid after adding algal extract, plating on media would also confirm that algal extract was not contaminated. No bacterial colonies were observed in negative control. All the experiments were conducted once due to the cost and limited availability of algae extract.

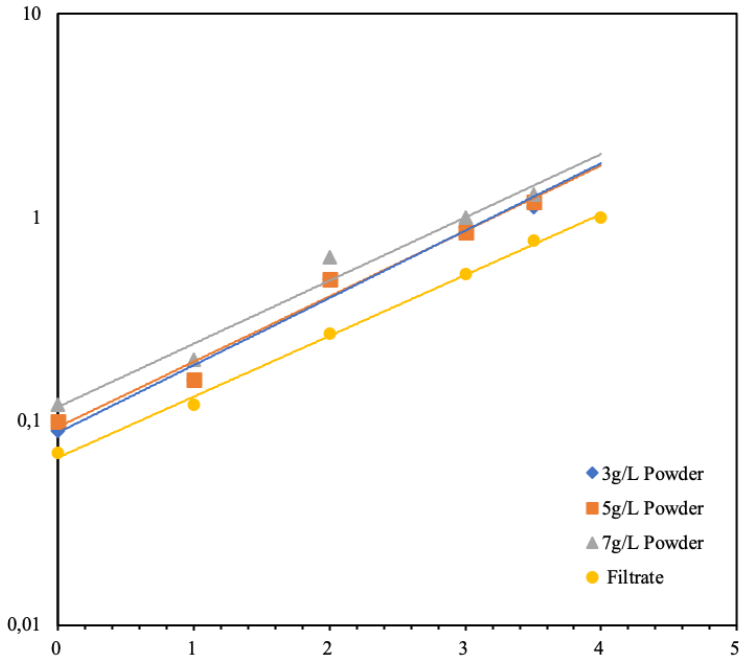

Figure 5. Optimization of algal extract as carbon source in medium. Growth curve of *E. coli* DA1(DE3) cells transformed with OmpF expression plasmid in deuterated media supplemented with algal lysate in form of powder and filtrate. Algae autolysate powder was supplemented in varying concentration of 3g/L, 5g/L and 7g/L. Each line represents an exponential fit of corresponding growth data points. This experiment was performed with no replicates.

The concentrated dry powder negatively affected *ompF* expression and aggregation of *E. coli* cells was observed after induction. Due to this and to avoid an extra step of freeze-drying required in preparation of dry lysate, a growth experiment was performed using supernatant obtained after autolysis (filtrate) as carbon source. This supernatant was filtered with 0.45 µm membrane-filter and supplemented as it is to the media. Surprisingly, growth rate was comparable to dry lysate, though slightly lower cell density was observed (Figure 5). To advocate this result, SDS-PAGE analysis was repeated using pre-post induction samples of dry lysate (powder) and filtrate (Figure 6a). After visual observation, band intensities of algal powder samples gave almost the double protein yield as compared to filterate. However, considering the amount of algal cells required to produce enough powder for this experiment was higher than used for filterate. Thus, filtrate was used as a supplement in media for large scale production instead of dry lysate.

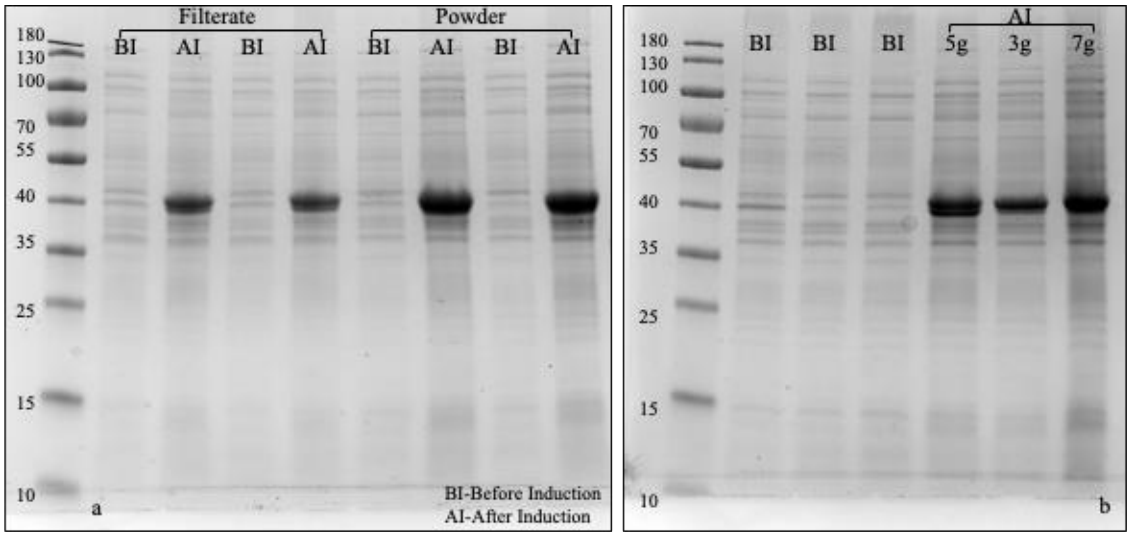

Figure 6. SDS-PAGE analysis of pre and post induction cell culture supplemented with algal extract. Each lane was loaded with a protein sample corresponding to 1 ml of culture and protein marker (in kDa) is labelled on the left. BI and AI denotes for before induction and after induction sample. OmpF band is close to ~37 kDa. a). Comparison of algal dry lysate and filtrate as carbon source in minimal media. b). Expression levels of OmpF in minimal media using different concentration of algae extract as carbon source.

III.4. Membrane separation and solubilization in different detergents

Traditionally physical methods have been used to disrupt the cells to extract membrane proteins. However, these have inherent advantages of protein denaturation due to localized heating produced by equipment. Therefore, to aid the disruption process, we used reagent-based method for lysing bacterial cells. It is a rapid and gentle method that gives high reproducible protein yield [106]. Lysozyme/ EDTA method is used to digest the lipopolysaccharide layer of bacterial cell wall that leads to spheroblast formation. Outer membrane (OM) is isolated from spheroblast where *ompF* resides. Outer membrane is usually difficult to extract and solubilize, thus, mild non-denaturing detergent like Triton X-100 detergent was used for membrane extractions. Moderate concentration of Triton X-100 (2% w/v) proved to be the best for destabilizing the membrane protein interaction with peptidoglycan layer and facilitating extraction of protein in its native form as they bind to hydrophobic parts of membrane proteins. Protein soluble fraction yields was estimated by SDS-PAGE as shown in Figure 7. Higher correspondence was observed at the estimated molecular size (37 kDa) of *ompF* protein band when solubilized with Triton.

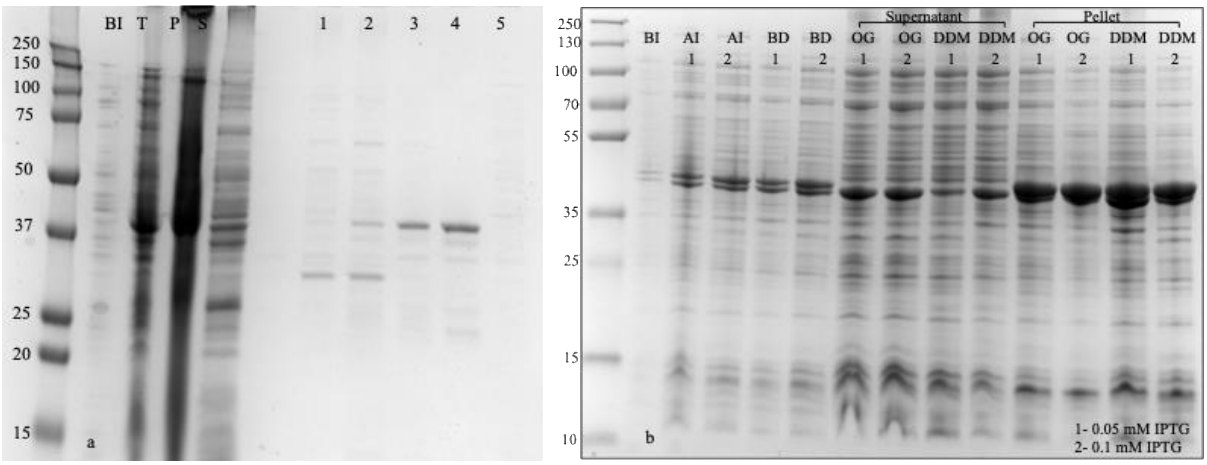

Figure 7. SDS-PAGE of membrane protein solubilized with Triton X-100, DDM and OG. a). Outer membrane was extracted by using the Triton X-100/EDTA method and insoluble cell debris were removed by ultracentrifugation. BI-before induction, T-Total protein, P-Triton-solubilized pellet and S-Solubilized protein fraction. Lane 1-5 are protein fractions from Ni-NTA chromatography. b). SDS-PAGE analysis of solubilized outer membrane using OG and DDM. 3% (w/v) DDM 6% OG (w/v) was added to 50 µl of cell pellet and incubated at room temperature for 1 hr. Supernatant and pellet were obtained after ultracentrifugation of solubilized membranes. BD signifies before detergent addition. Sample volume loaded was 20 µl, thus band intensities correspond to protein yield. OmpF protein band is expected at 37 kDa.

Triton can sometimes damage the protein by producing peroxides when exposed to air for long time. Even though extraction by Triton X-100 was beneficial for initial lysis of cells, subsequent crystallization applications with extracted proteins required solubilization in other detergents. We used SDS-PAGE analysis to study the solubilization efficiency of DDM and OG. Both the detergents solubilized OmpF, however, OG solubilized more protein as observed in supernatant bands in Figure 8. Using DDM and OG, protein was not fully soluble but OG solubilized better than DDM as demonstrated by intense protein bands in pellet fraction of DDM. This result resonates with previous protocols established for porin purification . Moreover, OG is very soluble in aqueous solutions and most importantly easily removable by dialysis if detergent is to be exchanged for protein assays/ crystallization applications. Therefore, OG was chosen as OmpF solubilizing detergent in further experiments.

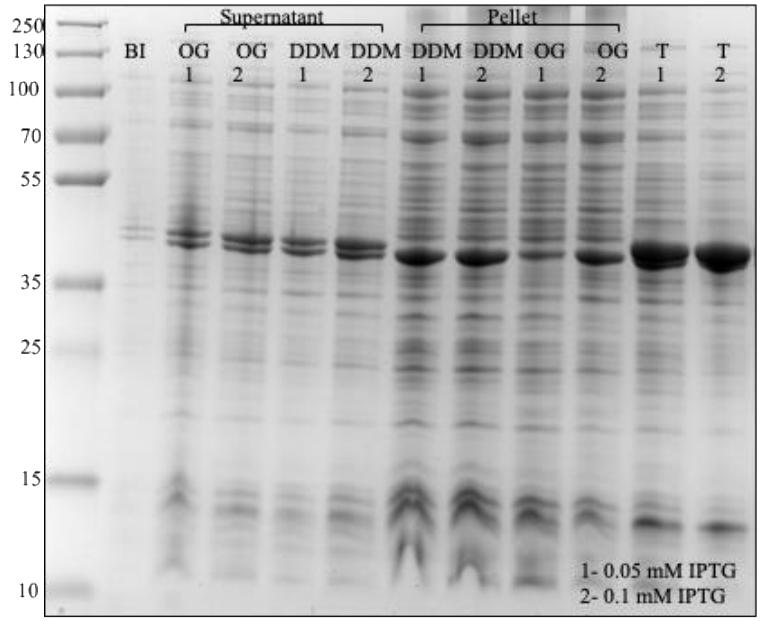

Figure 8. A comparison of solubilized fractions of OmpF using two different detergents (DDM and OG). Supernatant and pellet were obtained after ultracentrifugation of solubilized protein. BI signifies before induction and T denotes total protein. *ompF* protein band is expected at 37 kDa. Sample volume loaded was 10 µl, thus band intensities correspond to protein yield.

III.4. Protein Purification

To minimize the cost and improve the protein yield, optimization of protein production at lower scale is an essential requirement. With the optimized expression conditions as described above, large cultures of 1 l were grown to produce OmpF in hydrogenated and deuterated media. Pure protein was obtained using two-step protocol of immobilized metal affinity chromatography (IMAC) and size exclusion chromatography (SEC). While hydrogenous and deuterated protein expression conditions were different, purification was done in similar way in hydrogenous buffers for all the samples. Protein purity and size was analyzed by SDS-PAGE with no apparent difference in H and D versions of protein (Figure 9).

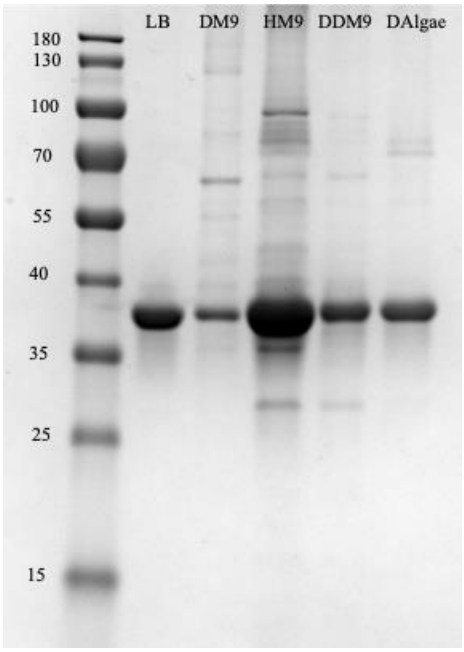

Figure 9: SDS-PAGE of purified OmpF from bacterial cells expressed in hydrogenated and deuterated media. OmpF protein band is expected at 37 kDa as observed in gel.

In few batches, we observed bands in addition to the prominent OmpF band in SDS-PAGE even after SEC. Therefore, an additional purification step of ion-exchange chromatography (IEC) was added to the purification process. This improved the sample purity and removed remaining impurities. Sample purity in all purification steps was assessed by SDS-PAGE (Figure 10). A distinct OmpF peak was observed in SEC chromatogram for all samples indicating monodispersity of protein solution (**Figure 11**). Protein eluted quite far from the void volume ensuring good separation from unwanted protein aggregates.

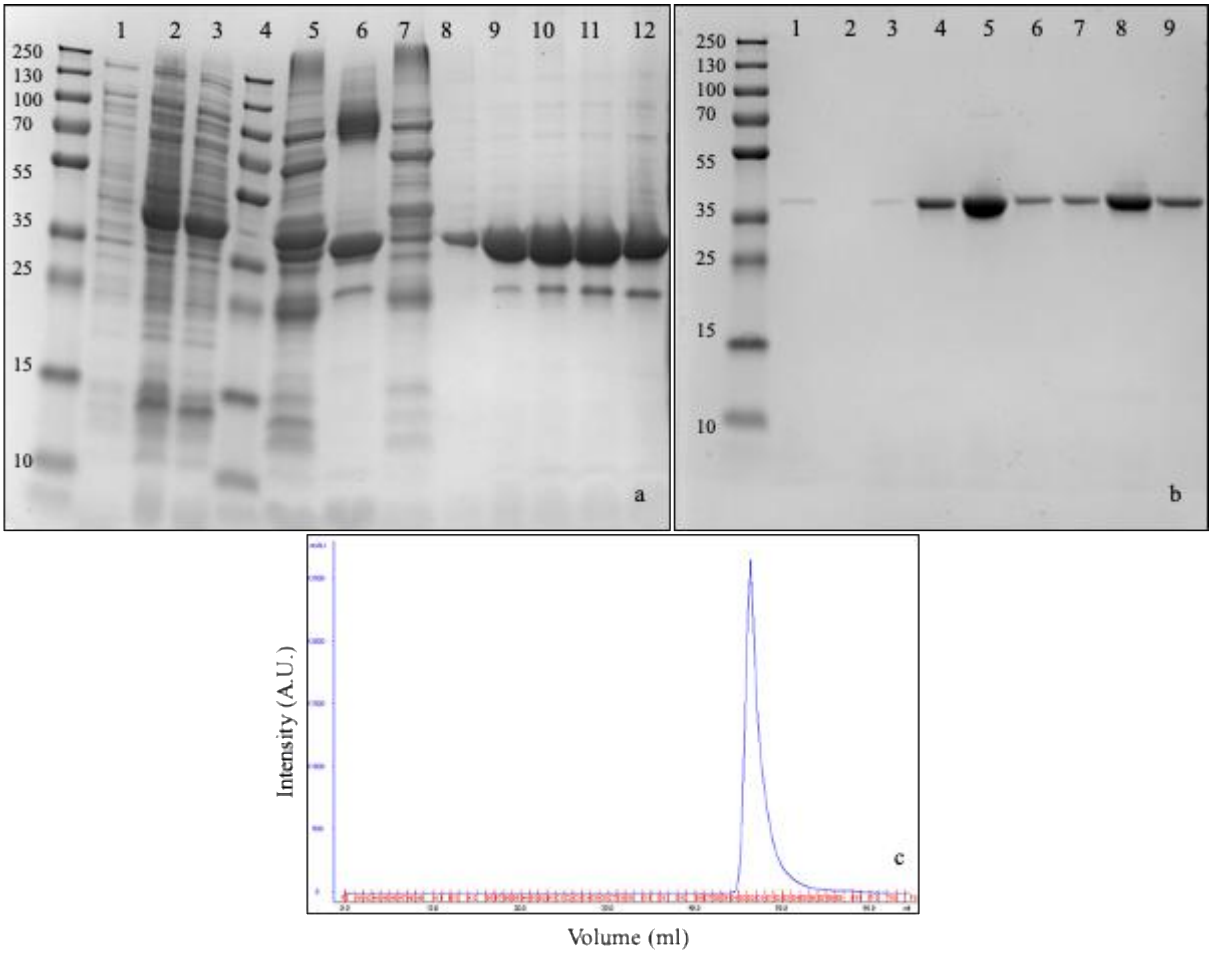

Figure 10. SDS-PAGE and SEC chromatogram after IEC. *ompF* was expressed in LB and protein band was expected at 37 kDa as observed in gel. a) Lane 1- Before Induction of expression, Lane 2:3- After induction Lane 4- Flow Through of IMAC, Lane 5- Elution of IMAC, Lane 6- Flow through of Reverse-IMAC, Lane 7- Elution of Reverse-IMAC, Lane 8:12- SEC elution fractions b). Elution fractions after IEC. c). SEC chromatogram of OmpF with high purity level after ion-exchange chromatography.

The yield of purified deuterated protein was lower than for the protiated protein. For the different carbon sources tested in minimal media, there was no appreciable difference observed in protein yield after 18 h of expression (Table 3). Even though protein yield of 1 mg in deuterated media was lower when compared to soluble protein, it was still remarkable for membrane protein expression in D_2O. The amount of purified protein was enough for further biophysical characterization and crystallization experiments. To obtain high-cell density culture in deuterated conditions, bacterial cells were first grown in LB media upto OD_{600} 0.6 and then cells were harvested by centrifugation to further inoculate into deuterated minimal media [110] incubated at lower temperature. Once the cells adapted, *ompF* expression was induced after 2 hours. This approach was effective for producing higher amount of deuterated soluble protein so far but reduced protein yield was observed in case of membrane protein.

Growth media used	Protein yield (mg/l)
LB	1.5
M9	1
DM9	1
DDM9	1
DAlgae	1

Table 3. OmpF yield comparison in different media. Protein yield is expressed in total amount in mg from 1 l of culture. Yield is based on peak fraction from size exclusion chromatography and UV 280 nm measurement using a Nanodrop spectrophotometer.

III.5. OmpF characterization

It is essential to analyse the quality and homogeneity of the over-expressed recombinant protein for crystallization experiments for consistent results. Unfortunately, quality control is often overlooked resulting in irreproducible observations and failure of experiments at later stage. Three important factors should be carefully evaluated for consistent results: protein sample homogeneity, precise assessment of concentration and protein solubilization in active state. This section describes how two techniques, mass spectrometry and nano-DSF, were used for biophysical characterization of the protein samples and also calculate the deuteration level in protein.

III.5.1. Mass Spectrometry analysis

Protein purity and level of D incorporation in purified OmpF from different media was assessed by mass spectrometry. All the measurements were done on intact protein and relevant masses for all samples measured by MALDI TOF are shown in Table 4. The calculated mass of the protiated version of OmpF is 37070.7 Da composed of 2452 protons (H) of which 612 are located at labile/exchangeable positions. Regulating fast H/D back exchange in mass spectrometry can be challenging, thus matrix was dissolved in hydrogenous buffers [111, 112]. This leads to ambiguous data interpretation and problems in deuteration level calculation due to uncertainty of partial H/D back exchange and loss of D. This was clearly evident with unexpectedly higher deuteration level of DM9 protein sample. Usually, 60%-80% D incorporation is expected in partially deuterated samples, unlike 90% deuteration recorded for protein samples in this study [16]. This can be improved by using deuterated matrix in future experiments.

A mass deviation of 54 Da and 56 Da was observed from the calculated OmpF mass of 37070 Da to the measured mass of 37124 and 37126 for LB and M9 samples, respectively. This was likely due to sodium adduction on protein ions from the sample buffer (Figure S2). As

expected, for perdeuterated samples DDM9 and Dalgae, deuteration level was greater than 90%.

For future labelling measurements, HX MS is higly recommended that can even give insights into location of deuteration in protein sample. This technique is helpful in providing conformational changes in protein due to deuterium labelling. However, there are some limitations to be implemented in membrane protein mass measurement due to presence of detergents.

Table 4. Theoretically and experimentally calculated mass of hydrogenated and deuterated OmpF in different media components.

Protein Sample	Calculated Molecular weight (Da)	Mass from MS (Da)	Deuteration level (%)
BSA	66463.0	66430.8	0
LB	37070.7	37124.2	0
HM9	37070.7	37136.3	
DM9	39539.6	38791.5	95
DDM9	39539.6	39054.5	>99*
DAlgae	39539.6	38860.7	99

* Higher deuteration level was observed in DDM9 due to incomplete or reversible back exchange of labile hydrogens.

III.5.2. Thermal stability by nano-DSF

After the assessment of purity and integrity, next step is to ensure the homogeneity of protein sample. Nano-DSF because of its rapidity and very low consumption of protein sample, is used to evaluate the monodispersity and thermal stability of protein solution. Very often protein aggregates can be formed while up-concentrating the protein for crystallization experiments. To ensure the reproducibility, analytical evaluation of concentrated protein is an important step especially in case of membrane proteins due to presence of detergents. The information obtained by thermal studies could also be implied in finding the optimum conditions for storage of protein.

The thermal unfolding temperature for all the protein samples was in the range of 80°C to 90°C with a sigmoidal curve of DSF profile as shown in Figure 10a. Steep thermal transitions were observed indicating cooperative unfolding of protein at high temperature. All the samples showed similar thermal stability; however, deuterated samples were more stable than hydrogenated (Table 5). There was no significant difference observed in protein unfolding temperature between different deuterated samples.

Nano-DSF employs the intrinsic fluorescence of tryptophan (Trp) and tyrosine (Tyr) residues as a probe for monitoring thermal unfolding temperature. On this basis, thermal unfolding will vary with location and arrangement of fluorophores in OmpF monomeric structure to form a trimer. In the trimeric form, one Trp is solvent exposed and other is buried in hydrophobic region facilitating monomeric interaction to form trimers (Figure 10b). Generally porins are

easily modified by heat and an oligomeric form is denatured to monomeric OmpF above 70°C [113]. Similar results of thermal transition at higher temperature and trimeric porin dissociation to monomeric form were observed in OmpF from *Yersinia ruckeri*. [114]. Therefore, denaturing factors like temperature predetermines the oligomeric sructure of OmpF and provides information about conformation changes in porin. Nevertheless, mechanism of these conformational changes in the porin that lead to protein unfolding should be taken into account when preparing samples for crystallisation experiments.

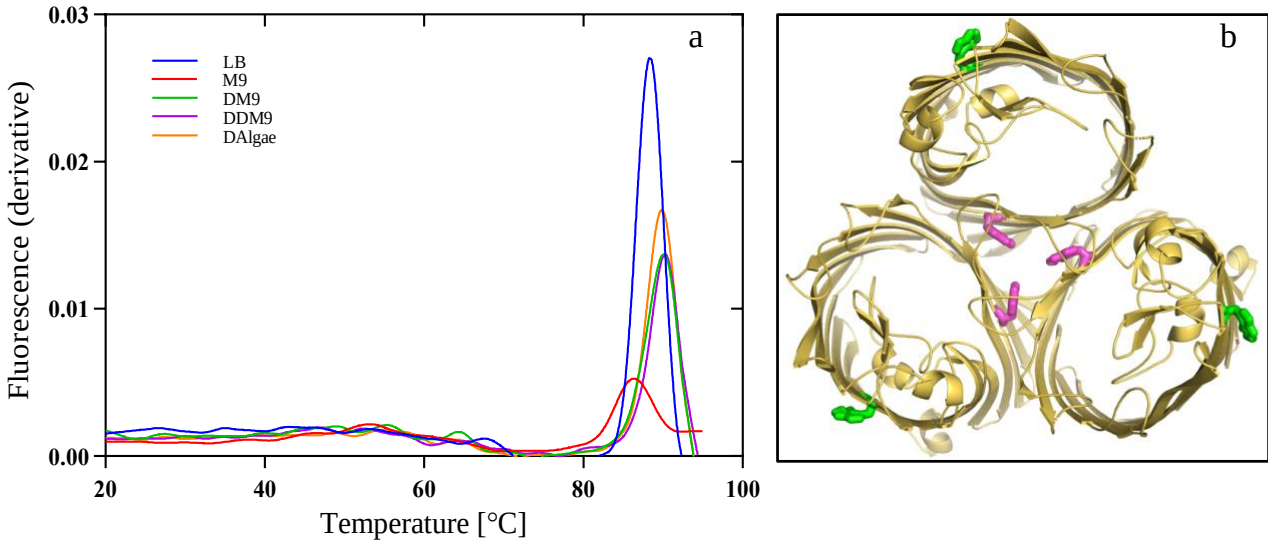

Figure 10. Protein unfolding temperature of OmpF as determined by nano-DSF (a) First derivative of thermal denaturation curve of H and D versions of protein measured as a function of temperature. All the samples were prepared in protiate buffers. (b) Cartoon representation for OmpF (PDB ID: 2ZFG) is shown here in trimeric form with solvent exposed tryptophan residues in green and buried residues in magenta. Structure presentations were produced using PyMOL (Schrödinger, Inc.).

Table 5. Values of protein unfolding temperatures (Tm in ºC) as determined by nano-DSF.

Protein Sample	**Protein Unfolding Temperature (°C)***
LB	88.3
M9	86.5
DM9	90.0
DDM9	90.2
DAlgae	89.9

***** Duplicate samples were analyzed with a calculated Tm variation of ±0.5 ºC.

III.5.3. Cost estimation

The minimal cost to produce 1 mg of hydrogenated OmpF porin in minimal media was 300 SEK as compared to 11447 SEK in deuterated media corresponding to ~38-fold increase in production of 1 mg of deuterated protein. This cost was decreased by ~1 fold when unlabeled glycerol was used a carbon source in comparison to labelled glycerol. However, still significantly higher than hydrogenated protein production. Perdeuteration cost sharply increased by ~95 fold when deuterated algae was used as a carbon source as compared to low-cost production of hydrogenated porin in minimal media. However, this cost of algae was the outcome of using filtered algae autolysate directly as a supplement in media as compared to exorbitant rates of dried auto lysate powder. Cost for producing 1 mg of deuterated of OmpF using algae powder was 377666 SEK. This evident the optimization of protocol previously described to minimize the cost of perdeuteration using rich growth medium.

Growth media used	**Protein yield (mg/L)**	**Cost of culture media per mg of protein yield per liter (SEK)***
LB	1.5	100
M9	1	300
DM9	1	5815
DDM9	1	11447
DAlgae	1	28325

***The **hydrogenated** media cost for 1 L LB is 150 SEK and 300 SEK for minimal media (cost includes material and labor) based on the current prices charged by LP3 (https://www.lp3.lu.se/). For **deuterated** media, cost of 1 L D_2O ~ 11330 SEK and d-glycerol (equivalent to 8 g/L) ~ 11264 SEK is added. Since recycled D_2O was used, thus cost calculation reduced to 50%.

III.3. Discussion

The protocol developed in this study serves as a convenient way to produce and improve the yield of perdeuterated membrane protein without the need of large fermenters by using commonly available laboratory equipment. The final optimized protocol for membrane protein expression in D_2O medium comprises of three major steps: pre-culturing in H_2O using H-glycerol, sub-culturing in D_2O with H-glycerol to reduce H-carry over and inoculation into large culture with labelled carbon source. To obtain high-cell density, protein expression was induced at a later exponential phase. The growth of *E. coli* is significantly reduced due to slower bacterial metabolism in deuterated media [22]. We observed a lag phase of 6-8 hours in bacterial growth at times. To resolve this problem, fresh media was prepared with all components in D_2O. Starter culture cell density also had a significant role in bacterial adaptation during lag phase. Thus, it is recommended that OD_{600} for starter culture should be between 4 and 6 for shorter lag phase. We found that these common practices that are sometimes neglected have a significant impact in producing consistent results.

Using algae extract as a carbon source supplement for deuterated minimal media has been reported previously for production of cytoplasmic proteins [110, 115-117]. However, this strategy had not been implied for production of labelled membrane proteins. Thus, effect on *ompF* expression in presence of algal autolysate was attempted in this work. Even though the yield and stability of the DAlgae sample was comparable with other carbon sources, production of algal secondary metabolites caused bacterial cell aggregation. This was more prominent by addition of concentrated algae powder as supplement, thus it was replaced by diluted algal autolysate filterate. Using the filterate would reduce the unwanted particles (maybe algal lipids) from the autolysate that improves the cell growth. Another reason was reduction in cost of process to produce to powder as compared to filterate.

Solubilization of the membrane to extract the protein of interest in an active form is the critical step in any in vitro analysis of membrane proteins. This aim to maximally disrupt the cell membrane while putting the protein in an in-vitro detergent environment without disturbing the stability makes it even more difficult. The most challenging part was to avoid the improper folding of protein and extraction of outer membranes to the maximum. A good detergent should be able to lyse bacterial cells, solubilize membrane proteins and be suitable for crystallization experiments. There is no ideal detergent for all applications, thus, trial and error with different detergents at different steps of purification are often necessary to find the optimal detergent for downstream applications. All detergent containing working solutions should be freshly prepared to avoid any hydrolysis and oxidation with course of time. Non-ionic detergents such as Triton X-100 are known to have oxidizing impurities that may interfere with protein crystallization and biophysical characterization [118]. Thus, it is mostly used for purification purpose. However, presence of Triton affected the crystallization propensity of OmpF as discussed in **Chapter III**. Thus, protein purification was performed without Triton using OG and DDM.

Protein solution homogeneity and purity was confirmed with mass spectrometry and thermal stability experiment using nano-DSF. Mass spectrometry showed >90% incorporation of deuterium in all samples while stability and purity were tested by thermal denaturation experiments and SEC. OmpF being a b-barrel and in deuterated state, makes the tryptophan residues very slowly exposed upon denaturation. Presence of intrinsic tryptophan at monomeric

interaction site greatly affected the unfolding temperature of OmpF. Moreover, deuteration effects the secondary structure motifs and hydrophobic surface exposure during the unfolding events [119]. This emphasize the onset of thermal unfolding at higher temperature primarily due to strong hydrophobic effect of D_2O. However, temperature induced unfolding can be very unclear and complicated. Oligomeric membrane proteins such as OmpF shows distinguishing physical effects that could be further explored by advanced techniques such as circular dichroism.

CHAPTER III. Growing large crystals for NMX studies

III. 1. Introduction

With the development of neutron protein crystallography, many structures have been deposited in PDB in the last decade. This recent growth is due to addition of new NMX beamlines giving access to more users, improved data processing software and pulsed neutron sources with higher flux. Despite this progress, sample preparation for NMX is still demanding with a requirement of large perdeuterated crystal volume of ~1 mm^3 for good diffraction at a higher resolution. Requirement of large crystal volume is due to the direct relationship between the incident flux of neutron source and unit cell volume as described below in Equation 1 [120]:

$$< I > \propto \frac{I_o \times |F|^2 \times V \times \lambda^2}{v_o^2} \qquad 1$$

Where $<I>$ is the diffracted intensity, I_o is the incident beam intensity, $|F|$ is the structure factor magnitude, V is the crystal volume, λ is the incident wavelength and v_o is the unit cell volume. As observed in above equation, volume of the sample is to be increased to compensate the weak diffracted intensity resulting from low flux incident beam of neutron source. For most successful experiments, crystal size reported is 1 mm^3 [12] and smallest crystals reported for NMX are in the range of 0.1-0.2 mm^3 [103] . Another limiting factor is the minimal unit cell dimension as the diffracted intensity is inversely proportional to its square (Equation 1). Current neutron diffractometers have a limitation of crystals with unit cell dimension of ~150 Å. With the ESS in pipeline and expected to be online in 2024, higher flux will enable data collection of small crystals as ~0.01 mm^3 in volume in a day instead of weeks with current neutron sources [121].

In order to collect diffraction data to a higher resolution and avoid hydrogen density cancellation effects, the protein should be perdeuterated or at least H/D exchanged, which is another major challenge as it requires extensive optimization of the process to be cost effective. Most of the structures deposited in PDB came from H/D exchanged protein crystallized by the vapor diffusion technique. As NMX is a technique complementary to X-ray and MX to study hydrogen related research questions, it requires a previously well studied protein. TIM and OmpF fulfill the criteria of being well characterized proteins with suitable unit cell dimensions and were hence chosen for this study. This chapter will further expand the methodologies used to grow large hydrogenated and perdeuterated crystals of a soluble and a membrane protein.

III.2. Material and methods

III.2.1. Crystallization of OmpF

Previously published crystallization conditions for OmpF were used to set up crystallization screens at room temperature [58]. Sitting drops in VDX vapour diffusion plates (Hampton Research) were prepared by mixing 1:1 ratio of protein (5 mg/mL in 20 mM Tris pH 8.0, 100 mM NaCl, 0.8% (w/v) octyl-POE) and precipitant solution (100 mM Tris pH 7.5, 18% (w/v) PEG_{2000} and 1 M $MgCl_2$) to a final volume of 2 µl in hydrogenated conditions. In deuterated conditions, precipitant solution was 100 mM Tris pH 7.5, 14%-16% (w/v) PEG_{2000} and 200 mM NaCl prepared in D_2O. Once optimized at small scale, large scale drops upto 100 µl were set in nine well sandwitch-box setup (Hampton Research). All plates were incubated at room

temperature and visually monitored under microscope for microcrystalline precipitates and single crystals.
In the batch crystallization setup, protein and reservoir solution were mixed together in a 1:1 ratio such that the solution was in a supersaturated state before addition into a Linbro plate well. A drop of 10 µl was prepared and centrifuged before dispensing into the well.
For the microdialysis crystallization setup, initial screening was performed with 5 µl dialysis buttons and semi-permeable dialysis membrane with a 12-14 kDa cut-off. The dialysis chamber was filled with protein solution mixed with and without reservoir solution (similar as above) at ratio of 2:1. This chamber was then placed in a Linbro plate well where 500 µl of reservoir solution was added. To guarantee a reasonable size meniscus on protein chamber and 10 µl of solution was prepared for 5 µl dialysis buttons. An extra care was taken to avoid bubbles while pipetting in the protein to the dialysis chamber. The dialysis membrane soaked in water was carefully released on the protein chamber from one corner. The applicator was immediately placed on the top of button and the membrane sealed with an O-ring. Excess membrane on the sides of the button was cut with scissors. The button was placed inside the well which was sealed with vacuum grease and a cover slip. Plates were incubated at RT and visualised on a daily basis.

In the capillary counter diffusion setup, the same protein concentration and reservoir solution were used as in the vapour diffusion except for a lower PEG 2000 concentration (12%). A stock solution of 1% low melting point agar was prepared in distilled water and repeatedly heated to dissolve it and form a clear solution. A custom syringe to dispense the solutions was prepared by attaching a 0.5 mm capillary at the front end of a syringe with the help of parafilm. The seal was made air tight to avoid any leakage. The 1 mm diameter capillary for the crystallization experiment was laid flat on a bench to mark with a ruler the positions to add protein and reservoir solution. This capillary was immobilized on modelling clay in an inclined position. Next the batch solution was prepared: 100 µl of protein was mixed with 70 µl of reservoir solution and incubated for ~8 hrs at RT. This undersaturated solution was then placed at 30 °C along with other materials required for the experiment. After 10-15 mins, 30 µl of molten agar was added to the tube and mixed. The batch-agarose mixture was quickly aspired into the capillary and left for a few minutes to set. Lastly, reservoir solution was added and the open end was sealed with silicone.

III.2.2. Crystallization of TIM mutants

Previously optimized conditions were employed in crystallizing TIM variants with slightly lower PEG 6000 concentration [83]. The protein in a hydrogenated buffer (10 mg/ml) was mixed in a ratio of 1:1 with reservoir solution (100 mM sodium acetate, pH 5.6, 16-24 % PEG 6000, 1 mM Na-EDTA and1 mM DTT) along with 10 mM 2 PG. Deuterated protein was prepared by exchanging H to D buffer using Amicon Ultra 0.5 ml filters (3000 Da). Several (atleast 4 cycles) centrifugation steps were performed consecutively at 10000 x g for 10 mins to reach the calculated deuterium level (~99%). Sitting drops were prepared using VDX vapor diffusion plates only after ~12 h of H-D exchange at 8°C. Initially, drops upto 2 µl drops were set to optimize the conditions in deuterated buffer. Once optimized large scale drops upto 200 µl were set in nine well sandwitch-box setup (Hampton Research) and incubated at 20°C.

III.2.3. Microseeding and Macroseeding of crystals

To grow large neutron-sized crystals of TIM variants and OmpF the microseeding technique was used [81]. One drop with few crystals obtained in small drops was chosen and crushed with crystal crusher. Once finely crushed, drop was pipetted to a microcentrifuge tube containing 30 µl of reservoir solution from the same drop and a seed bead (Hampton Research). Crushed crystal drop was washed with 20 µl of reservoir solution to extract all seeds. The tube with crused crystals was vortexed for 1 min with a short interval on ice and continued up to three cycles. Serial dilutions of seed stock were prepared with a constant dilution factor of 10 in 50 µl of volume and stored at -80°C. It is important to note here that crystals were always kept on ice and each time vortexed before making a dilution. While setting up the crystallization drops, seed stock was added in a ratio of protein:reservoir: seeds (3:2:1) of total drop volume with final reservoir volume of 500 µl. The protein solution was added to the drops first, followed by precipitant and seed stock. Optimized conditions where few large crystals were appeared were used to scale up to large drops.
For macroseeding, a reasonable sized crystal (100-200 µm) was washed in a solution with lower PEG concentration in 3-4 steps placed on cover slip. The washed crystal was then tranferred to either equilibrated or non-equilibrated batch solution or sitting vapour diffusion drop. Crystals were visually inspected under a microscope and evaluated as single/twinned crystals, non-aggregated, no or little precipitation in the crystal drops.

III. Results

III.1. Crystallization of OmpF

To obtain protein crystals, a standard two-step crystallization methodology is usually followed: firstly, the screening step where suitable crystallization agents are identified and secondly the optimization step, where conditions for crystallization are finely tuned to obtain better diffracting well-formed protein crystals [66]. In the case of OmpF, previously identified crystallization conditions were used to obtain better diffracting crystals. However, this also required fine tuning as the purification method employed was different from the previously published one affecting protein quality [58]. Various crystallization techniques such as vapor diffusion, microdialysis and capillary counter diffusion that favoured growth of large crystals are reported in this section. Additionally, seeding and feeding methods along with their strengths and limitations are also discussed.

III.1.1. Vapour diffusion crystallization method

Initial crystallization experiments were performed using the sitting drop vapour difffusion method. This method has been extensively used before to crystallize OmpF and conditions that produced well diffracting crystals (1.5 Å) were used to set up sitting drops in first experiments. However, the protein did not crystallize in initial experiments even after screening various precipitant conditions. The reason behind this was the use of Triton X-100 in extraction of outer membranes which is known for having negative impact on crystallization propensity of membrane proteins. Triton has a tendency to tightly bind to protein which is very difficult to completely remove even after SEC or dialysis. Crystallization experiments often require detergent concentrations to be lowered or just enough for protein stability. Thus, removing excessive amounts of Triton is imperative to avoid adverse effects on crystal packing. This

was clearly demonstrated with previous studies where only 0.3 % of total PDB structures used Triton X-100 for crystallization [122]. Moreover, presence of Triton in the protein sample increased the absorbance values A_{260} and A_{280} and reduce the A_{260}/A_{280} ratio. This would have direct effect on measuring the correct protein concentration, which is crucial for a successful crystallization experiment [123]. Thus, Triton was no longer used in future experiments to obtain better diffracting crystals. A comparison of initial crystallization trials with protein purified in presence and absence of Triton X-100 is shown in Figure 17.

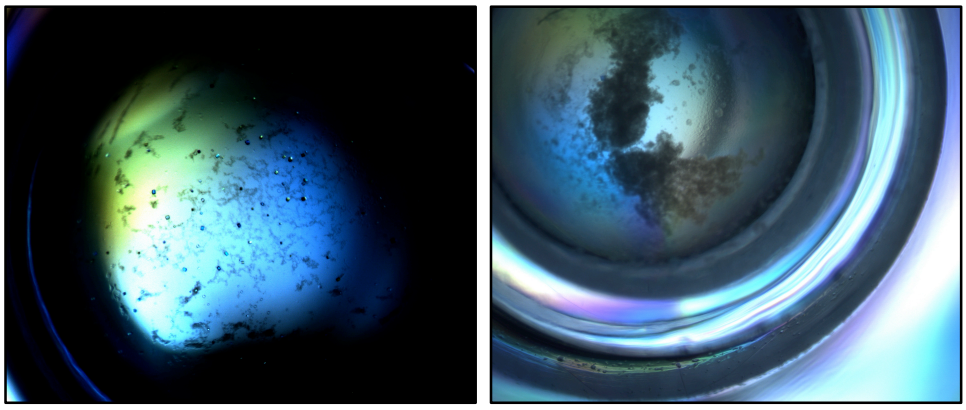

Without Triton X-100 With Triton X-100

Figure 17. Comparison of OmpF crystallization in presence and absence of Triton X-100. A 2 µl vapour diffusion sitting drop was set with a ratio of 1:1 of protein solution (OmpF 5mg/ml in 20 mM Tris pH 8.0, 100 mM NaCl, 0.8 % octyl-POE) and reservoir soultion (100 mM Tris pH 7.5, 1M $MgCl_2$, 20% PEG_{2000}). Crystal plates were visualized under microscope to monitor the appearance of crystalline, precipitate or crystals.

Lowering the PEG concentration was a key factor in obtaining large well-diffracting crystals of OmpF. It was also observed that metastable phase of OmpF has a narrow range of [PEG 2000]. This is clearly visible in Figure 18 where crystallization drops are set at varying concentration of PEG 2000, slight change had a significant impact on nucleation and appearance of crystals. Random aggregates and the number of crystals were increasing with higher concentration of PEG 2000 that aligns with previous studies [124]. The crystallization drops were clear at lower PEG concentration, which also implies that the PEG concentration induces nucleation at higher concentration. For growing large crystals, it is necessary to control the precipitant concentration which was successful after optimum PEG concentration screening. Salt screening was also performed, however, it did not have a significant impact in crystal growth, thus, only PEG was considered for setting up large drops.
In case of membrane proteins, the protein-detergent complex (PDC) interaction with PEG is an additional factor to be considered. At detergent concentrations below CMC, its mostly PEG molecules that form aggregates and they keep increasing with PEG concentration [125]. However at the CMC, PDCs form a crystal lattice by attractive micelle-micelle forces driven by PEG. It is well established that most membrane proteins crystallize near the detergent cloud point [126]. This represents the region where association of PDCs is promoted over non-specific aggregation by attractive interparticle forces between micelles and solvent. Thus, additives such as PEG in crystal growth significantly contribute to crystallization behaviour of PDCs and important to be optimized for growing large crystals to keep PDC stable .

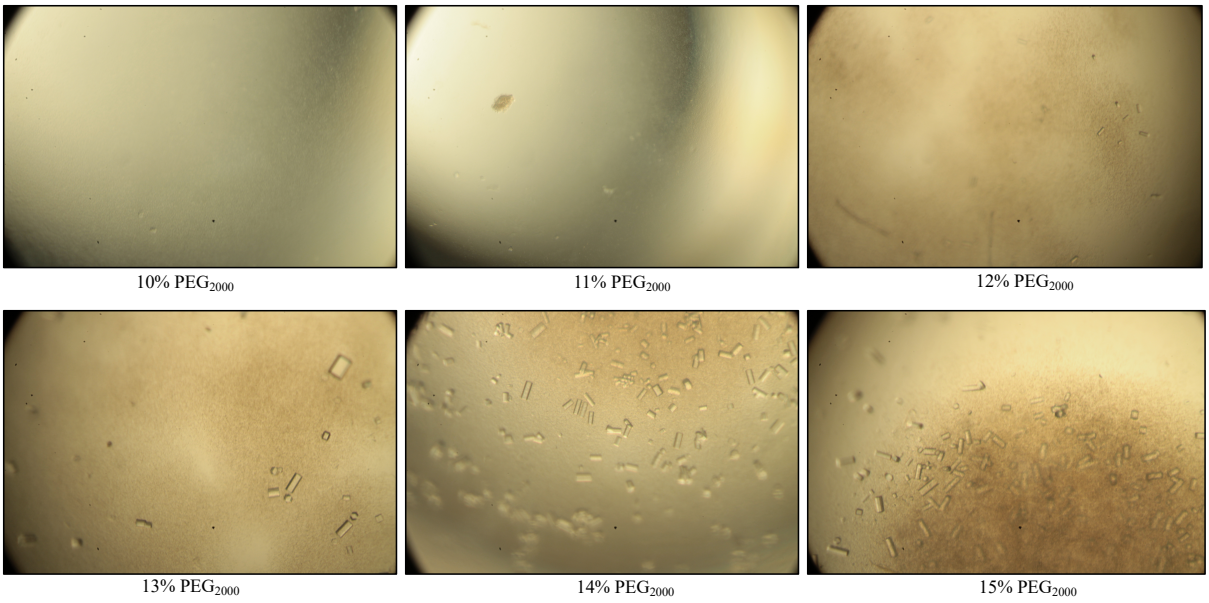

Figure 18. Optimization of precipitant in sitting drop vapour diffusion drops. A 2 µl vapour diffusion sitting drop was set with a ratio of 1:1 of protein solution and reservoir soultion with varying PEG_{2000} concentration. All other buffer components were kept constant. Crystal plates were visualized under microscope every day and nucleation was observed after 2 days.

After initial optimization of crystallization conditions in small scale, a nine-well sandwich-box was used to setup large drops in hydrogenated conditions. To obtain large neutron-sized crystals, drops were scaled up from 2 µl to 20 µl using the sitting drop method. A dark-colored precipitate and heavy nucleation was observed with increasing size of drops. This highlights the effect of changes in surface-area-volume-ratios on the crystallization drop dynamics. It was speculated that the problem might be impurities or precipitated protein before crystallization. To resolve the problem of precipitation, protein and precipitant in equal ratio were mixed and centrifuged before distributing as a sitting drop above higher precipitant concentration well. This strategy helped in reducing the precipitation and even controlling the nucleation as few crystals appeared. After extensive screening of PEGs and other precipitants, best conditions to obtain best-looking crystals were used to set up large 100 µl drops. The lower concentration of PEG 2000 (13%) and sample centrifuging before setting up large crystal drop tended to produce largest crystals upto 1.2 mm in the longest dimension (Figure 19).

First crystals appeared in 7 days which was expected as water-vapor equilibrium takes approximately 7 or more days to reach equilibration as this was consistent in all large drops' setup. The rate of equilibration in vapor-diffusion can have a substantial effect on the nucleation and dependent on distance from the crystallization droplet to the reservoir solution surface [127]. In case of 9 well plates, it is even slower as distance increases between the droplet and the reservoir solution surface. This also explains immediate nucleation and precipitation in Linbro plates when size of drop was increased. Often glass plates are not stable when placed on petri-plate inside sandwich box leading to more nucleation in drop. A potential solution to this problem was to seal the petri-plate on base of plastic box and then glass plate above it. This improvement in crystallization setup had a drastic impact on nucleation and lead to few crystals in the drop.

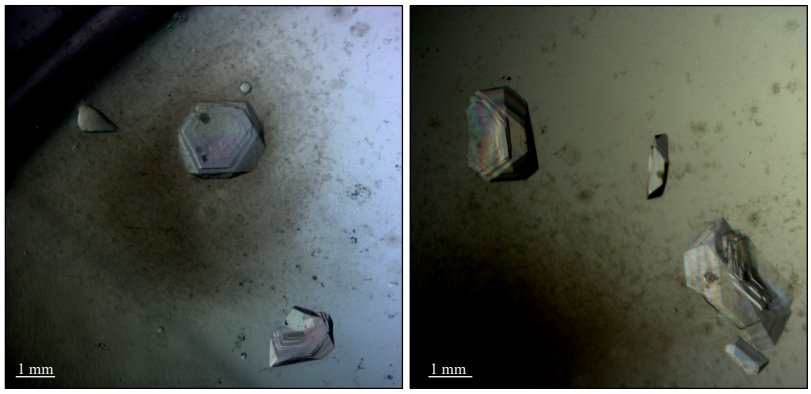

Figure 19. Large OmpF crystals in sitting drop vapour diffusion method. Identical 100 µl crystal drops were resuspended over 13 % PEG 2000 (10 ml) in 9 well plate placed inside a sandwich box. The first largest crystals appeared in 7 days and it took 20 days to reach a size of 1 mm in the longest dimension.

III.1.2. Vapour diffusion in deuterated conditions

Reproducing previous hydrogenated OmpF crystallization conditions was straightforward, but was more challenging for deuterated samples. Crystal morphology between protein samples purified from deuterated media using H and D carbon source was compared and shown in Figure 20. Mostly three types of precipitates were observed in crystal drops: crystals, phase separation droplets and random aggregates. Aggregates had no clear boundaries unlike round boundaries of phase separation droplets. Crystal morphology was different for hydrogenated and deuterated samples. Even after optimizing various parameters such as different precipitants and protein concentration, no crystals were formed from the DAlgae sample. The largest and best crystals were formed from protein purified in standard HM9 media with hydrogenated glycerol as the carbon source. It was observed that deuterated protein crystals were smaller and existed in a plate-like aggregated form (Figure 20). Compared to hydrogenated conditions, crystallisation in deuterated conditions (DM9 and DDM9) resulted in formation of numerous small crystals unlike few in HM9. Moreover, the protein was less soluble in the deuterated conditions and most of it was lost in precipitation. Another factor to be considered here is the use of hydrogenated detergents at otherwise fully deuterated conditions. It is speculated that micelle-micelle interaction between PDCs might be hindered due to low solubility of protein in D_2O resulting in defected crystals as observed in DM9 sample. Mass transport is also often responsible for distorting the steady state of crystal growth and might be the origin of defects in crystals [128]. Another reason could be an inhomogeneous distribution of supersaturation between the crystal corners and centre that eventually leads to morphological instabilities resulting in hoppered crystals as obtained with sample DM9 [128, 129]. Overall crystal morphology was similar between the hydrogenated and deuterated versions of the protein producing single crystals of similar shape. This also emphasize the need of fine tuning of crystallization conditions for deuterated protein which was not possible to investigate in this study due to limited sample and should be addressed in future experiments.

The crystallization behavior of the protein shifted slightly towards lower concentration of PEG 2000 – from 14% to 12-10 % in deuterated conditions. The crystal size was also comparatively smaller in D conditions when identical drops were set using H and D samples. Therefore, growing large crystals from perdeuterated protein would require a larger amount of protein that comes with great expense in cost and time. An alternative would be to grow large hydrogenated

crystals from perdeuterated protein and then perform H/D exchange in a capillary or vapor diffusion sitting drop to fully grown crystals. Since, the hydrogenated protein remained stable in deuterated precipitant conditions, this strategy should be applicable with perdeuterated protein, perhaps with a lower PEG concentration (see below Figure 22). Understanding the width of metastable zone better in deuterated conditions could be helpful in optimizing the conditions for growing large crystals.

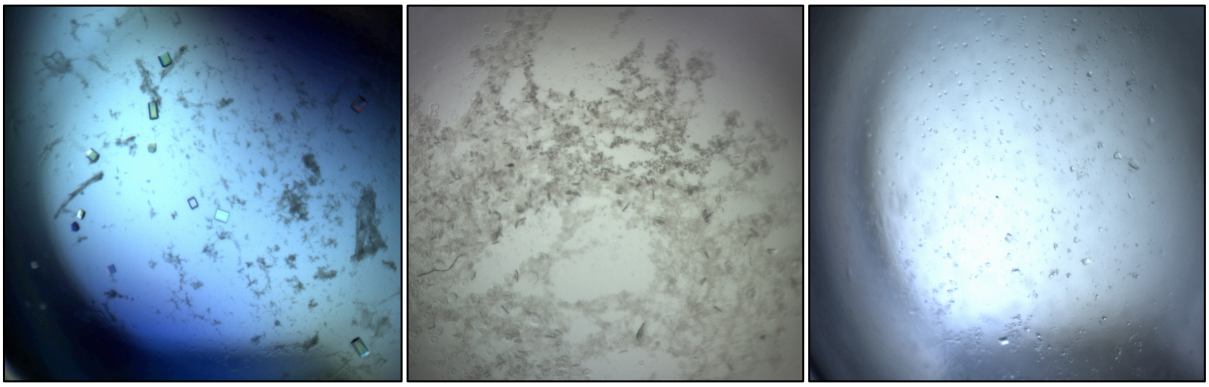

HM9 DM9 DDM9

Figure 20. Comparison of crystal morphology in H and D crystallization drops. 2 µl crystal drops were set up in similar precipitant conditions using H_2O and D_2O as the solvent. All the drops were imaged after 2 days of setup. Precipitation was observed in DM9 and HM9 after 2 and 5 days respectively.

III.1.3. Crystal Feeding

To increase the crystal size and quality, feeding of crystallization drops in a sitting drop was also attempted. In the first attempts, the precipitant conditions giving few and best crystals were used to set up 5 µl drops. Once the nucleation or a few crystals were observed, 5 µl of similar solution was added to the drop. The feeding procedure was repeated twice after a four day of interval. The addition of protein should contribute to existing crystals' growth with a smaller fraction of protein being lost to precipitation and nucleation. Even though the crystal size increased, more of the protein was precipitating with feeding (Figure 21). To resolve this issue, PEG concentration was decreased from 14% to 12% leading to five-fold increase in size of crystals (Figure 21). This again proves the point that PEG concentration had a significant effect allowing the existing crystals to grow further.
Thus, feeding had a resulted in crystal growth without the need of extra effort in screening conditions.

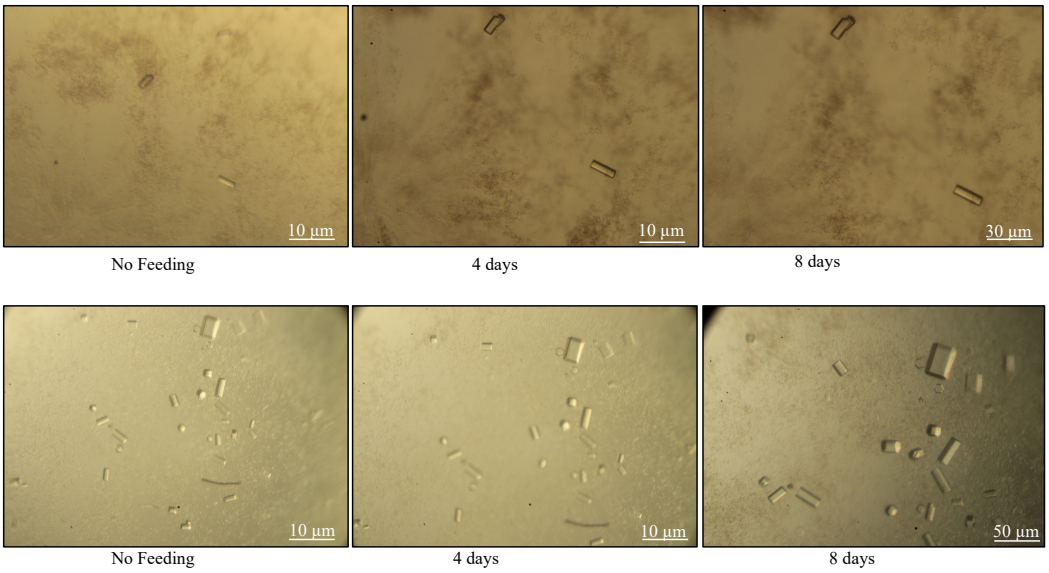

Figure 21. Effect of feeding on nucleation and crystal growth of OmpF. Identical 5 µl sitting drops (1:1) were set over 500 µl reservoir solution. PEG 2000 concentration was lowered from 14% in top panel to 12 % in bottom panel. The largest crystal appeared in 12% PEG after 2 cycles of feeding in 8 days.

Decoupling nucleation from crystal growth can be very effective in growing large crystals under deuterated conditions [130]. Thus, the feeding technique was used to grow large crystals under partially deuterated conditions. A 5 + 5 µl sitting drop with early stage crystals was fed with 5 µl of similar solution in D_2O and left for equilibration. After 2 days, a slight increase in crystal size was observed. Thus, the reservoir solution was also exchanged with a D_2O counterpart. A large fraction of the protein was lost to precipitation after second round of feeding. This might be due to the deuterated precipitant conditions that are known to reducing the solubility of protein [17, 131]. Most of this material was removed carefully without disturbing the crystals before adding a fresh batch of protein solution. Feeding was continued in D_2O solution and it was possible to grow crystals up to ~400 µm in the longest dimension (Figure 22). The drops were observed at specific intervals and crystal growth continued until 30 days. However, after 15 days precipitation increased and covered all the drop. Thus, feeding was not continued further as removing precipitant solution over the crystals might lead to a crack in the crystals as observed in previous trials. Each individual experiment varied and feeding in deuterated conditions requires more optimization. Moreover, irreversible loss of protein in precipitation eventually limits the size of crystals under deuterated conditions.

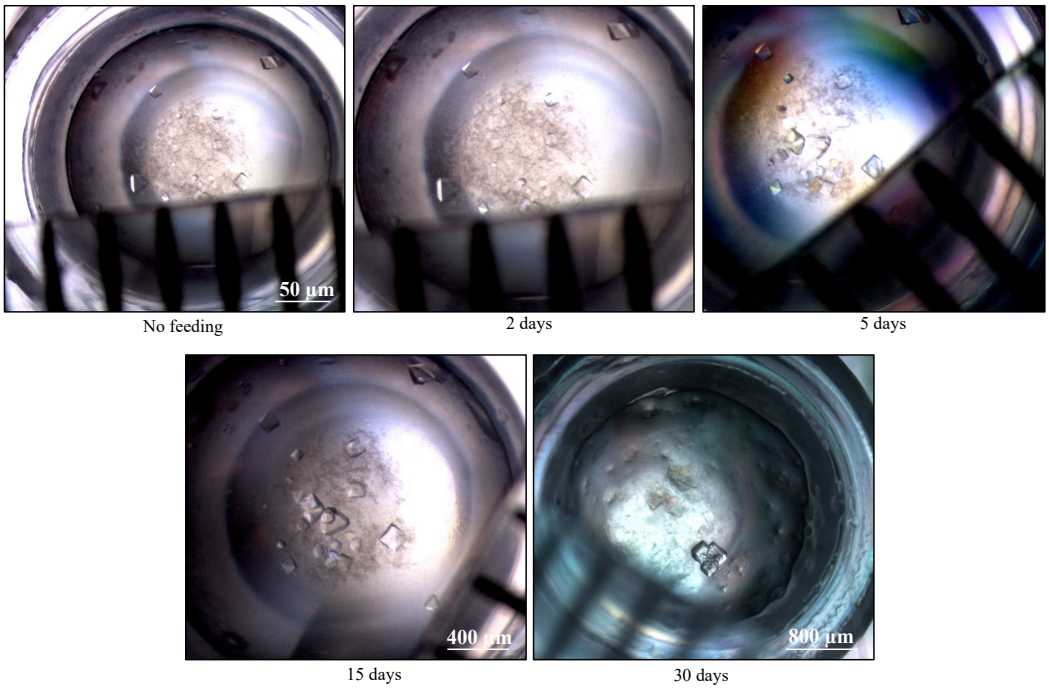

Figure 22. Effect of feeding on crystal growth under deuterated conditions. Identical 10 µl sitting drops were prepared by mixing protein solution (5 mg/ml) with an equal volume of reservoir solution composed of 100 mM Tris, pH 8.0, 1M $MgCl_2$ and 14% PEG 2000 over a 500 µl of reservoir solution in H_2O. The drops were left for equilibration for 2 days. After visualizing crystal growth, crystal feeding was performed by adding a suspension of protein and reservoir solution prepared in D_2O. Drops were visualized under microscope for any changes in size of crystals. The largest crystal grown by H/D exchange was ~400 µm in the longest dimension and 0.3 mm^3 in volume.

III.1.4. Microseeding in vapour diffusion

Crystal seed stock was prepared by following rMMS technique as described previously in **Section III.2.3.** Screening of the seed stock is a crucial step to control nucleation and promote crystal growth. By lowering the concentration of the seed stock, the level of nucleation could be controlled so that only the seed crystals would grow in the drop. Initially, a screening was performed by keeping all parameters constant except diluting the fresh seeed stock to 1000 times dilution. Initially, fresh seed stock was tested for protein solubility. If no precipitation was observed in the drops, the number and size of crystals were controlled by diluting the seed stock with the same reservoir solution to produce a fresh seed stock. Figure 23 shows an example of different concentrations of seed stocks when added to a crystal drop with constant precipitant concentration. The seed stock that produced least crystals in the drop was used to screen the optimum PEG concentration with low nucleation and few crystals. In the end, 1000X seed stock was used to prepare new 30 µl crystal drops with 18% PEG concentration. The new drop was empirically equilibrated up to a level of supersaturation that was enough for supporting crystal growth but not spontaneous nucleation. Only few seeded crystals were observed after 2 days which was good for protein availability for crystal growth. However, scaling up the drop volume did not favour the crystallization of OmpF and lead to heavy precipitation that increased over the course of time covering the seeded crystals. This resulted from the influence on kinetics of crystallization due to change in drop size from nanoscale to microscale [68].

The addition of oil was also tested and was not very effective leading to immediate heavy precipitation. Even though we obtained few well-formed crystals in small drops, it was not easy to scale up due to many constraints such as absence of detergent in the reservoir or preservation of all physical dimensions while seeding. Thus, microseeding was not further considered for testing in large crystal drops.
Few points to be considered here while seeding are not mixing the crystallization drop and always keeping seed stock on ice. The frozen seed stock was thawed numerous times to prepare crystallization drops and it never affected the results as in previous studies [132].

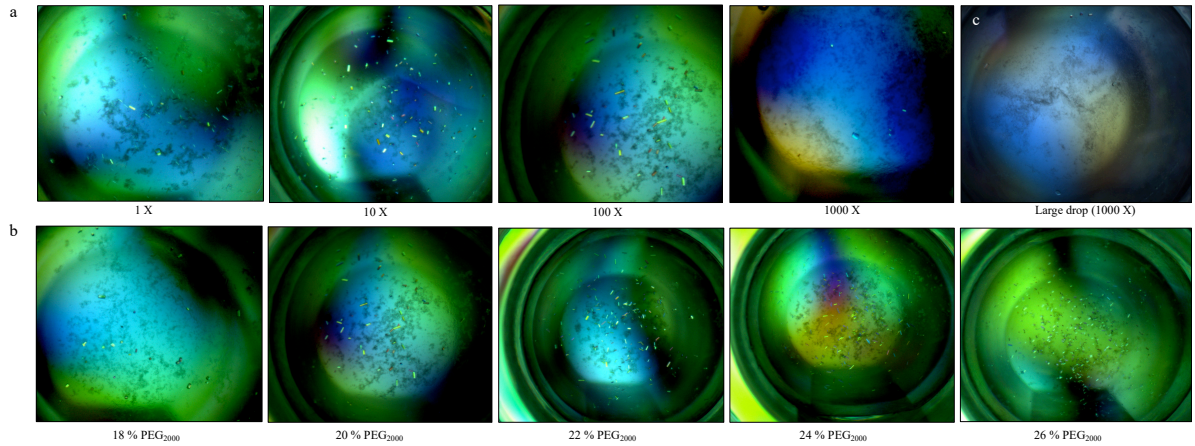

Figure 23. Effect of MMS on crystal hits and growth of OmpF. a. Initial screening of diluted seeds of OmpF seeded in crystallization screen close to the seed stock condition. **b**. Optimized seed stock (100 X) was used to screen the optimum precipitant conditions for protein to be in metastable phase emphirically. All the components in reservoir solution were kept constant except PEG_{2000}. **c**. 30 µl crystal drop with 1000X seed stock and 18% PEG_{2000} was prepared in duplicate to observe effect of seeding. Protein sample was purified from cells grown in LB media.

III.1.5. Macroseeeding

Another approach in crystallization techniques to aim for large crystals is macroseeding where a large crystal was seeded into a new or pre-equilibrated siting drop. Macroseeding was attempted with protein samples purified from LB and HM9 media and seeds were prepared as described in **Section III. 2. 3.** All the parameters were kept constant and early stage crystal was seeded into new drops. Surpisingly, a large difference in the crystallization drop was observed between M9 and LB purified samples. The macroseeded crystal with M9 sample crystal drop did not lead to any nucleation and slowly dissolved in few days. However, in the crystal drop with LB sample, the crystal dissolved immediately and led to heavy precipitation and nucleation the next day after macroseeding. This suggests that LB sample drop was supersaturated from the beginning even though initial precipitant conditions were at a lower PEG concentration. As mentioned previously, it is a prerequisite for macroseeding that the drop is in the metastable phase, which leads to lower nucleation and better crystal growth. Since the macroseeding results with the HM9 sample looked promising, a new crystal drop at lower PEG concentration (10%) than previous experiment was prepared. Crystal seeds dissolved from sides and were expected to act as a template for further addition of protein molecules to assemble and grow in size. However, they fully dissolved in ~24 hours leading to precipitation of the drop in the end. Even though the precipitant concentration was reduced, it was difficult to optimize the right time required for drop to equilibrate and connecting crystallization with

light scattering experiments could give more information on incubation time before seeding [133]. Another issue foreseen here is the evaporation of drop when it is opened to add seeds and affect move the supersaturation to labile zone from metastable zone. This is always a problem in vapour-diffusion and could be resolved by reproducing macroseeeding in batch setups. With these failures under hydrogenated conditions, macroseeding experiments were not continued further neither under hydrogenated nor deuterated condtions to grow large crystals for NMX.

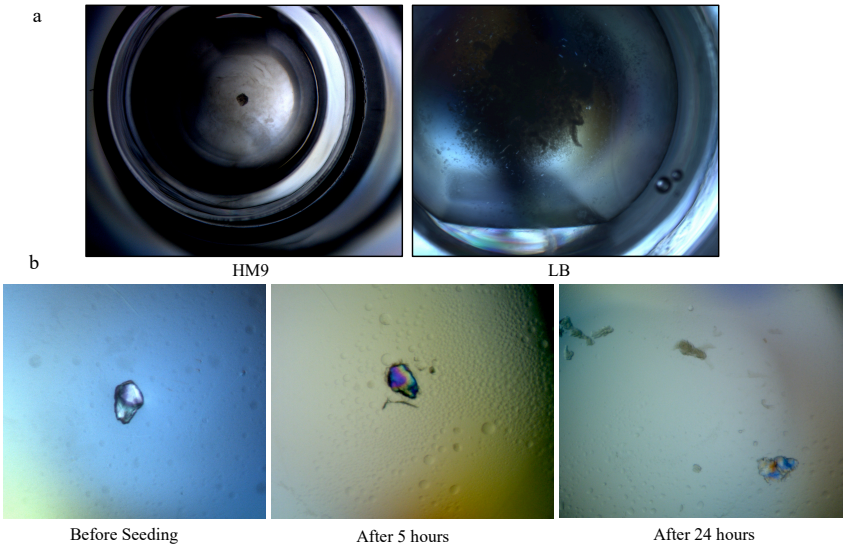

Figure 24. Effect of single crystal macroseeding. a. A 10 µl crystallization drop was prepared by mixing an equal volume of protein solution purified from LB and HM9 and precipitant solution at 12% PEG concentration. The crystal to be macroseeded was picked from similar precipitant conditions. **b**. A similar 5 + 5 µl crystal drop was prepared with lower PEG concentration of 10% in precipitant solution and mixed with HM9 protein sample. The crystal was stable for few hours and then dissolved leading to precipitation in the seeded drop.

III.1.6. Capillary counter diffusion

Vapour diffusion has a major limitation of excessive solute convection during the crystal growth process. Thus, other techniques such as capillary counter diffusion with its inherent advantage for growing large crystals was applied in crystallization of OmpF [78]. Convection is reduced by slow diffusion of protein and precipitant solution in a restricted geometry of capillary that also helps in controlling the supersaturation and nucleation. An added advantage of mounting the capillary directly on a goniometer without damage to crystal makes it more promising for NMX. Moreover, deuterium exchange can be easily implemented by simply refilling the capillary with new reservoir solution from sides without any physical manipulation of the crystal.

Counter diffusion experiments can be set up in various ways and we opted for free liquid interface wherein protein and precipitant solution are in direct contact with one another in a narrow diameter of capillary. Previous studies have shown that mixing the protein with gel reduces the convection and maintains the concentration gradient along the length of capillary [76, 78]. Thus, without wasting much protein sample in other optimisation, we gelled the protein in 0.1% low-melting point (LMP) agarose. Since OmpF is a quite thermostable protein as shown in **Section II**, experiments performed at 30 ºC did not have an adverse effect on

protein stability. No immediate precipitation of protein when mixed with gel in a PCR tube at 30 ºC was observed, which further proved this point.
For this technique, previously optimized precipitant conditions that produced few and single crystals in vapour diffusion were used for initial screening. After preparation of molten agar, we incubated all the materials required for the crystallization experiment at 30 ºC for 10-15 min. A batch solution of protein and varying precipitant concentration was prepared and left for incubation for ~8 h and centrifuged just before addition of agar. To this solution, molten agar was added and the solution was thoroughly mixed before dispensing it into the capillary. It was observed that incubating the batch solution for ~8 hrs before dispensing into a capillary gave less precipitation compared to the solution without incubation. Crystallization in capillary followed a similar trend as in vapour diffusion technique. Heavy precipitate was observed in capillaries with higher precipitant conditions and best well-formed crystals appeared in capillaries with lower concentration (14% PEG 2000) as shown in Figure 25. A crystallization gradient was generated with smaller protein crystals grown at the protein-precipitant interface and large crystals away from the interface along the length of the capillary (Figure 25). Even though we obtained several crystals, they were not suitable for NMX as size was significantly smaller than the minimum requirement. While this could be optimized further, the results were not very consistent, which might be due to batch to batch variation of the protein or other physical parameters like a new batch of protein reservoir solution. Capillary experiments are challenging and require careful handling due to fragility of glass and quartz capillaries. If broken during setup, a large amount of precious sample could be lost. Moreover, it requires large volumes of sample to perform the experiment, which was the major constraint as deuterated samples are limited in amount and not much sample could be wasted for optimization. As mentioned previously, solubility is affected in D_2O, so the batch solution initially prepared might require some more optimization along with precipitant screening. In future experiments, large crystals could be grown in hydrogenated conditions and exchanging solvents by vapour diffusion inside the capillary as a potential solution.

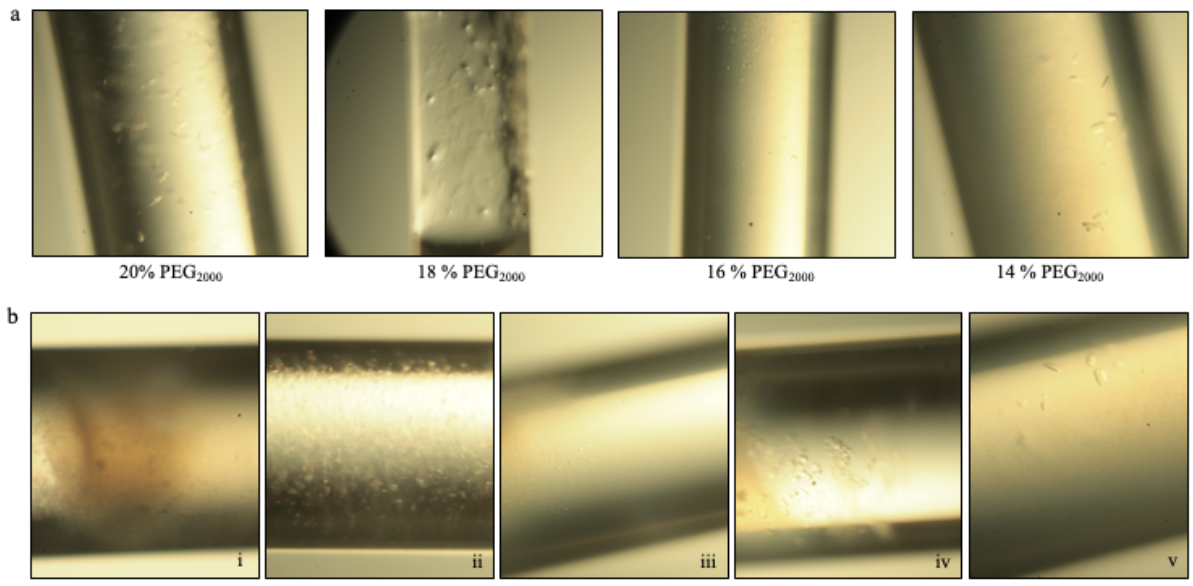

Figure 25. OmpF crystals grown using capillary counter diffusion in gelled protein solution. a. A 0.5 mm glass capillary was filled with batch solution of 100 µl of protein solution (5 mg/ml), 70 µl of reservoir solution and 30 µl of LMP-agar. Over this batch solution, 500 µl of reservoir solution with varying PEG 2000 in each capillary was dispensed while avoiding any air gap at the gelled protein-reservoir interface. All the capillary images shown are from

the side of sealed end. **b.** A capillary prepared in similar way as described above with 14% PEG_{2000} as precipitant. Various stages of crystallization experiment were visualised under microscope. Protein solution was clear for 4 days. Moving along the capillary towards the opposite of open bulb end, supersaturation was observed. i. Gelled protein-reservoir interface, ii. High rate of nucleation with concentration of protein and reservoir at their peak, iii-iv. Microcrystalline and several small crystals, v. Crystals reducing in number and growing in size towards the end of capillary.

III.1.7. Microdialysis crystallization

Even though vapour diffusion and capillary diffusion techniques are favourable for growing large crystals, controlling all parameters precisely is not possible, which is what the microdialysis technique offers. Microdialysis allows thorough estimation of all components within a crystallization system from mother liquor to protein solution [78, 121]. A salting-out phenomenon is followed where precipitant penetrates a semi-permeable membrane to equilibrate the protein solution leading to nucleation. As the system reaches solubility limit, crystal growth is halted, but it can be re-initiated by an increase in precipitant concentration as shown in Figure 26. A further increase in precipitant concentration led to the dissolution of the crystal with brown precipitation inside the dialysis button. Unlike other techniques, crystal growth occurs with increase in precipitant concentration in microdialysis, however up to an extent where protein was not precipitated. The crystal morphology was similar to other methods with much clearer drops resulting in higher stability of OmpF in dialysis method than other techniques. Due to slow diffusion, crystal growth was slower, which was expected and considered good for growing large crystals without an undesirable increase in crystal mosaicity. Results from this study gives a possibility to grow crystals without secondary nucleation and make the process reversible if the rate of PEG/detergent influx across the membrane is controlled.

For the microdialysis setup, protein solution was added to a dialysis chamber (10 µl) and sealed with a semipermeable membrane corrresponding to protein-detergent complex size. This dialysis button was then placed in a Linbro plate that holds reservoir solution. Drops as big as 350 µl can be set by using dialysis buttons and reservoir solution can be changed without much physical manipulation or disturbance of drop. This also means that optimization of best crystal growth conditions are possible with same amount of protein unless it has not precipitated which was not the case in our scenario as protein precipitated [121]. There are two possibilities for precipitation: osmotic shock due to increase in precipitant concentration or change in detergent concentration leading to disturbance of crystal lattice. In case of membrane proteins, optimization of detergent concentration in reservoir solution could be explored further as this might have a significant impact on crystal packing. However, addition of detergent would increase the cost of experiment making it more expensive than other crystallization methods.

Setting up a dialysis experiment requires particular care in placement of membranes on the dialysis buttons which might lead to air bubble if not careful. With the introduction of air bubbles, its difficult to visualize the drop and it also affects the diffusion across the membrane. Its always recommended to prepare extra protein sample than required loading amount to form a round meniscus over the protein chamber to avoid bubbles. Another constraint is harvesting, disturbing the membrane might damage the crystal especially membrane proteins due to high levels of solvent and increased fragility. Despite these limitations, microdialysis can be promising for growing large neutron-sized crystals for NMX studies and can be even implied in understanding protein phase diagram due to its proven advantage of precise control over

parameters and lower volume of sample required for optimization [90]. In future experiments, using hydrogenated crystallization conditions, there is a possibility of optimizing perdeuterated protein crystallization in small volume as scaling up is much easier than vapour diffusion and capillary counter diffusion methods.

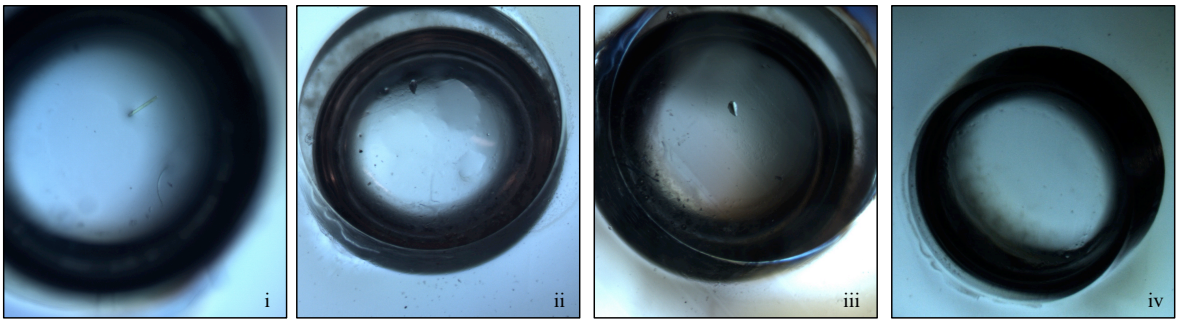

Figure 26. OmpF crystallization using microdialysis technique. 10 µl of protein batch solution (5 mg/ml, 4% PEG 2000) was added in the protein chamber which was placed in 500 µl of 8% PEG 2000 to prepare understaurated solution. i. A small needle appeard in 4 days, ii. Crystal (10 µm) appeared in 6 days after increasing precipitant concentration to 10 % PEG 2000, iii. Crystal increased in size (30 µm) with further increase in PEG 2000 (12%), iv. Dissolution of crystal when precipitant increased to 14 % PEG 2000 after 15 days.

To grow large crystals, seeded batch method under controlled temperature was also employed. OmpF was crystallised in vapour diffusion setup using previously mentioned conditions to give few crystals. One single crystal was picked and used as a macroseed in a new batch solution which was prepared by suspending equal volumes of protein and precipitant solution at a slightly lower PEG concentration (12% PEG 2000). Before macroseeding, batch drop was left for equilibration for ~1-2 hours and then trasnferred to a specially designed quartz cell . One single was was then treanferred from the vapour diffuion drop to this batch solution. The quartz cell was then sealed tightly and placed inside a brass transport. The temperature of this experiment is monitored by Peltier elements and quartz cell was visualised under an inverted microscope aimed at the bottom. To begin with, experiment was set at room temperature (20 °C) and crystal growth was observed in ~24 hours. The next day temperature was then reduced to 18 °C to observe further crystal growth and left for a week. Crystal grew upto a size of ~200 µm, however with further lowering of temperture to 15 °C, no crystal growth was observed. After a week protein started precipitating so experiment was not continued further. With this experiment, it can be concluded that lowering the temperature is not the optimal strategy for growing large crystals of OmpF as it seems to reduce the solubility of OmpF, thus leading to precipitation in the end.

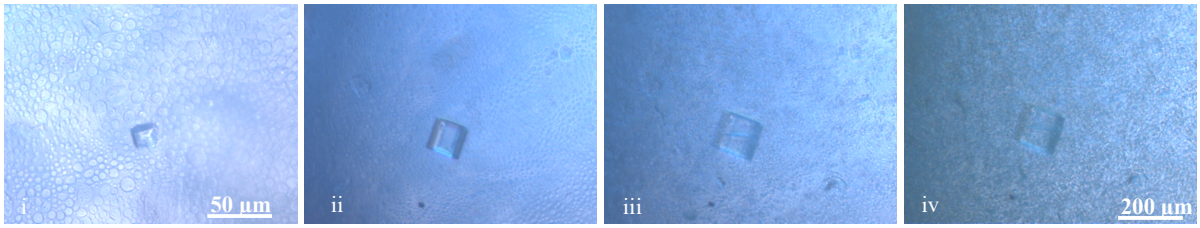

Figure 27. Growth of macroseeded OmpF crystals within temperature-controlled crystallization apparatus. A single crystal (~50 µm) was placed in a 100 µl of batch solution (5 mg/ml protein in 12 % PEG 2000): (i) observed immediately after set-up; (ii)

crystal growth observed after ~24 hrs at 20°C; (iii) crystal grew further at 18 °C; (iv) precipitation at 15°C.

III.2. Crystallization of TIM

Crystals of TIM variants E97Q and E167Q were successfully obtained by vapor diffusion set ups following previously optimized conditions [83]. During initial screening of mutants, crystals did not appear by spontaneous nucleation, so hetero-micro-seeding was used to induce nucleation. An old seed stock of TIM E65Q mutant was used as a micro seed stock to crystallize the TIM E97Q variant in similar conditions as for variant TIM E65Q. A similar process was followed to crystallize TIM E167Q mutant using a TIM E97Q seed stock. Crystals appeared within three days and were stable for months in precipitant conditions comprising of 100 mM sodium acetate, pH 5.6, 16-24 % PEG_{6000}, 1 mM Na-EDTA and1 mM DTT. Even though crystals appeared by spontaneous nucleation for E97Q variant, implementing hetero-micro-seeding was just a strategy for future structural studies of variant proteins that are difficult to crystallize.
Protein crystallization is known for difficulties in reproducibility, so each experiment was set up in duplicates for qualitative comparison.

To set up the crystallization drops in deuterated conditions, protiated protein buffer was exchanged to deuterated buffer and drops were set only after ~12 h of H/D exchange. For initial screening, 2 µl drops were set up in similar conditions as hydrogenated protein for both mutants. Random matrix microseeding (rMMS) was used to prepare stock seeds from H-TIM E97Q and H-TIM E167Q complex with 2PG and PGH as shown in Figure 13. An initial crystallization plate was set to test the seed stock prepared by serial dilution. One single crystal was obtained in 1:1000 times diluted seed stock and was later used to optimize condition in deuterated solutions.

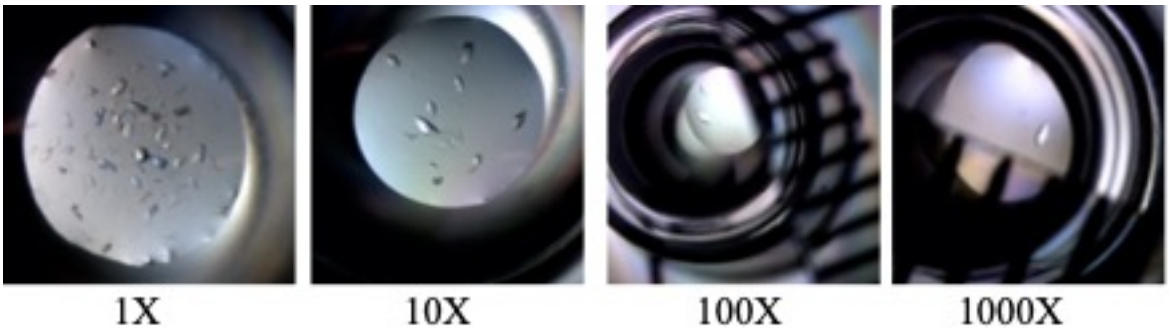

Figure 13. Microseeding screening of TIM E97Q complex with 2PGA in protiated buffer. A non-equilibrated sitting drop was prepared with 1:0.8:0.2 ratio of protein (10 mg/ml), reservoir solution and seed stock. Reservoir solution was 100 mM sodium acetate, pH 5.6, 14% PEG 6000, 1 mM Na-EDTA and1 mM DTT and seed stock was obtained from 16% PEG 6000. The seed stock was kept on ice and vortexed just before pipetting to the drop.

After the seed stock optimization, crystallization drops were prepared with both variants in hydrogenated and deuterated versions of the reservoir solution and protein buffer. In the case of D-TIM E97Q, drops remained undersaturated for 10 days under fully deuterated conditions in contrast to a protiated buffer where crystals appeared in three to four days. Therefore, streak seeding was performed using cat whisker. Spontaneous nucleation with a shower of crystals was observed within two days and these crystals continued growing up to the solubility limit of the drop. On the contrary, spontaneous nucleation was observed in D-TIM E167Q drops

similar to hydrogenated trials. Deuterated seed stock using rMMS was prepared and a seeding trial with optimized precipitant conditions was performed. Once the right dilution seed stock was optimized with a small number of crystals, drops were scaled up to ~150 µl in 9-well sandwich plates (Figure 13). The crystallization drops were clear for many days in fully deuterated conditions and mild precipitation was observed in partially deuterated in D-TIM E97Q crystallization trials (**Figure 14**). A similar pattern was observed in large scale drops giving rise to perdeuterated crystals with a maximum volume of ~0.5 mm^3. Large drops were also set up in protiated conditions and later H/D exchange was performed in a capillary mounted with neutron-sized crystal of volume ~1 mm^3 (**Figure 14).** In the case of D-TIM E167Q variant, few crystals appeared in deuterated small-scale drops to be later used as seed stock for larger drops. Large drops in deuterated conditions yielded perfect three-dimensional crystals with a maximum dimension of 1.5 mm along the long axis, ready to be mounted in capillaries for neutron diffraction. It is to be noted here that seed was added in the new drop equilibrated at the metastable zone to avoid spontaneous nucleation and promote growth of only a few crystals.

The reduced protein solubility under deuterated conditions was consistent with previous studies [110, 134]. The stronger hydrophobic effect in D_2O cause additional compactness of protein structure/association into large aggregates that could be a cause for protein precipitation in deuterated conditions. The precipitate under deuterated conditions leads to loss of protein, instead of contributing to crystal growth explaining smaller crystal volumes under deuterated conditions. However, the overall crystal morphology was similar in both TIM variants under hydrogenated and deuterated conditions and these results were consistent.

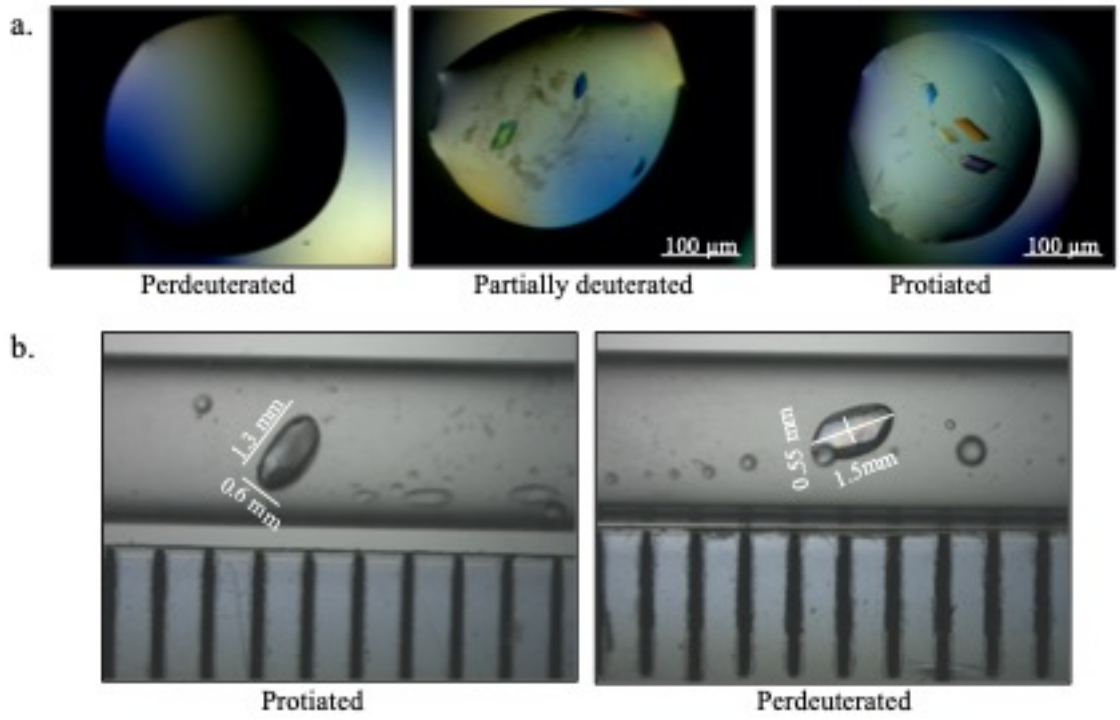

Figure 14. TIM E97Q crystals under deuterated and hydrogenated conditions. a. A seed stock was prepared and protein drops were set up in three different conditions: Protein and precipitant in D-buffer, protein in D-buffer and precipitant in H-buffer and protein and precipitant in H-buffer. The best conditions for large drops was protiated buffer. b. Crystals of TIM E97Q complex with 2PG mounted in a Vitrocom capillary for neutron diffraction.

Apart from microseeding, macroseeding was performed in a batch solution to aim for one large crystal in a drop. A well-defined crystal in size range of ~500 µm was washed in a 200 µl drop comprised of macro seed precipitant condition and then carefully moved to another 200 µl with subsequent two washing steps (lower PEG 200 concentration of 10%). After washing, the crystal was transferred to a new batch drop and crystal growth was monitored for few days. It is important to mention here that seeded crystal survived the washing steps without any damage. However, after transfer into new drop, small crack was visualized under microscope and half of the crystal dissolved within 4 h. With no occurrence of spontaneous nucleation, the seeded crystal showed slow growth and increased to double the size after five days. However, a small satellite was observed along with the crystal growth that grew over the course of time, thus experiment was not continued further. Results from macro seeded batch drops are shown in Figure 15. Satellite formation could be due to presence of precipitate or dissolved protein around seeded crystal that might lead to more crystal nuclei in the solution.

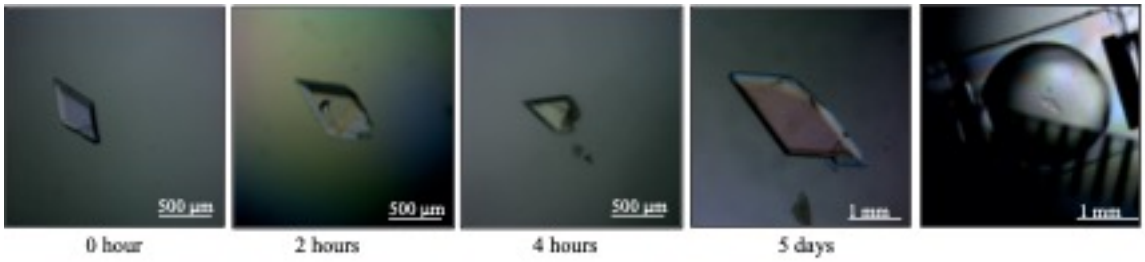

Figure 15. Growth of D-TIM E97Q crystal macro seeded into a batch experiment. A batch solution of 10 mg/ml D-TIM E97Q complex with 2PG and 10 % *w/v* PEG 2000 was prepared in microbridges and sealed before fishing seed crystal. The seed crystal was taken from a sitting-drop vapor diffusion experiment consisting 16% PEG 2000 and serially washed into 14-10% PEG 2000 placed on coverslips.

Another macroseeding experiment was performed where a crystal was seeded into a new large sitting drop with lower [PEG 2000]. No cracks or spontaneous nucleation were observed after seeding and crystal remained unchanged for several days. However, small nuclei appeared around the crystal after five days that turn into large crystals over extended period of time (Figure 16).

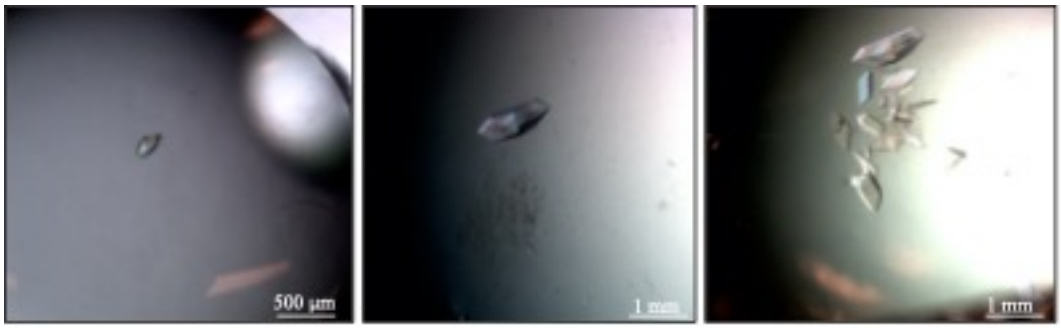

Figure 16. Growth of D-TIM E97Q crystal macro seeded into a sitting drop vapor diffusion experiment. A sitting drop with 1:1 ratio of 10 mg/ml D-TIM E97Q complex with 2PG and reservoir solution (12 % w/v PEG 2000) was prepared and sealed before fishing seed crystal. The seed crystal was taken from another sitting-drop vapor diffusion experiment consisting 16% PEG 2000.

A small screening test to find the suitable seeding conditions was performed before macroseeding crystal into the non-equilibrated drop. As previously tested optimized conditions for spontaneous nucleation were known (16%-18% w/v PEG 2000), a few drops were set to find the undersaturation level of protein by varying PEG 2000 concentration. No spontaneous nucleation occurred below 10% PEG 2000. This method was used to roughly estimate the conditions where protein will be in metastable zone. In the end, macroseeding was performed at two different PEG2000 concentrations. The solution remained in the metastable phase for an extended period of time with no nucleation (Figure 15). However, changing the precipitant condition slightly led to nucleation in macroseeded drops (Figure 16). This suggests that the metastable zone is very small for TIM E97Q. Compared to conventional seeding techniques, this method is distinct in its own way as making the phase diagram of a protein requires lot of protein and optimization. This strategy could be useful for proteins with a limitation of low expression yield, ligand cost and even membrane proteins. The solubility of a protein is greatly affected in D_2O, roughly estimating the conditions for seeding paves the way for growing large stable deuterated crystals for neutron diffraction.

III.3. Discussion

The results of this study show promising strategies to grow large membrane and cytoplasmic protein crystals for NMX studies. It was possible to grow crystals up to ~1 mm^3 and ~0.5 mm^3 in volume of TIM variants and OmpF respectively with standard crystallization techniques and thoroughly optimizing the precipitant conditions. *In surfo* techniques such as vapour diffusion and microdialysis have so far been the most successful techniques for crystallizing and preferably growing large crystals of proteins [78, 90]. This study proves that growing large crystals of membrane protein without any imperfections is a possibility using these techniques and can be further explored for other potential membrane protein targets for NMX studies.

While transplanting OmpF crystal in a new drop was not very successful, it indeed led to crystal growth in case of TIM. The presence of detergent in MPs is speculated to have major impact on macroseeding along with other physical dimensions such as effect of convection in vapor diffusion. Although appearance of crystal defects and mild precipitation was observed in both the scenarios, these results highlight that relocation of a crystal in a new drop is not very favorable for growing large crystals without any undesirable stress fractures. Based on the findings in this study, the most promising approach to maximize the size and quality of crystals would be slow feeding of the naturally nucleated drops containing few crystals. As expected, growing large TIM crystals using microseeding was effective and consistent, suggesting this as a potential method that could be explored further in growing large crystals of OmpF in batch mode for OmpF. However, preparing a seed stock of membrane proteins would require extra attention to obtain better diffracting crystals. The dialysis technique has been previously used to improve the resolution of trimeric photosystem I crystals diffracting X-rays showing the possibilities of exploring seeding techniques with OmpF and other MPs [135]. So far seeding has been underestimated in crystallization of membrane proteins and should be considered for future experiments to improve crystal growth. Addition/optimization of detergents in reservoir solution in the dialysis method is another alternative, though it will increase the cost given large volume setups for NMX studies. This was also the reason why no crystallization experiments of TIM using the microdialysis method undertaken, as it would require large quantities of the inhibitor adding to the cost of experiment.
Each individual crystallization experiment varies due to numerous factors. The major limitation is non-availability of same protein batch and precipitant solution throughout the experiment

which is usually unavoidable. The current study where TIM crystallization results were consistent as compared to OmpF already proves this point. Keeping all solutions same especially in case of membrane proteins is often not feasible due to limited purified sample from each purification batch. It is even worse in case of perdeuterated protein samples due to limited amount of protein and reduction in solubility leading to more sample loss due to precipitation as compared to protiated counterpart. This problem is inevitable and a thorough investigation of protein stability in solubilizing detergent and crystallization conditions at nanoscale will be at least time-efficient and cost-effective. Crystallization conditions of TIM and OmpF in D_2O were optimized at small scale and it was consistent for TIM once the setup was scaled up unlike OmpF again highlighting the challenges with MPs. Even though crystal morphology was similar in appearance for deuterated TIM and OmpF, a fine screening was still required for perdeuterated OmpF samples for consistent results.
Very few membrane proteins are crystallized by seeding previously [135-138] and this should be investigated in future being an effective solution for successful crystallization. Microseeding in deuterated solutions and perhaps even macroseeding in batch set ups in the undersaturated zone of the phase diagram could have favorable crystallization dynamics. However, seed stock preparation needs extra care with detergent being resuspended in reservoir solution while microseeding that makes MP more stable in new crystal drop [139]. Determination of the solubility curve of hydrogenated and perdeuterated protein as a function of temperature would definitely help in manipulating the supersaturation rates to cease nucleation and promote crystal growth [71]. Temperature as a physical changing parameter was not exploited much in this study and should be considered for future studies as it comes with a benefit of dissolving smaller crystals to allow large crystal growth [140].

From this study, it is clear that NMX studies of membrane proteins still presents specific challenges compared to soluble proteins. However, some of these challenges will be addressed with the operation of European Spallation Source in future and further expand the horizon of neutron diffraction studies to membrane proteins. With its powerful flux, requirement of crystal size would be down-sized to ~0.01 mm^3 and large unit cell dimension crystal data collection would be feasible. Traditional crystallization methods along with manipulation of multiple parameters such as precipitant concentration, temperature and pH should be exploited further in keeping the protein stable throughout the kinetic-trajectory of phase diagram. The methods used in this study would open doors for NMX studies of membrane proteins as demonstrated with large neutron-sized crystals of OmpF.

Chapter IV. Towards X-ray and neutron crystallography of model proteins

IV.1. Introduction

OmpF has been well studied porin over the years due to its high stability and yield as compared to other membrane proteins. Moreover, due to current unit cell limitation of detector edges of ~150 Å for neutron sources such as ILL, this model system is suitable for neutron crystallography studies with its unit cell dimension of a = 116.923, b= 116.923 and c= 51.346 (PDB ID: 2ZFG). To avoid the density cancellation effects (previously Outlined in Chapter 1) generated by hydrogens in the protein, perdeuterated crystals or atleast H/D exchanged crystals are a prerequisite for NMX studies. Due to lower solubility of protein in deuterated conditions as discussed in previous chapters, it was best to choose a model system that is crystallized easily and perhaps in various crystal forms. Ultimately, producing large crystals that would diffract at room temperature and remain stable for days during data collection was also expected to be achieved by using OmpF as a model system. Most of the above parameters such as high protein yield, stability and large crystal volume has been shown in previous chapters. In this chapter, data collection and structural studies of OmpF crystals will be discussed. In this study, structural comparison of protiated (H/H) and deuterated (DDM9) forms of OmpF will be presented.

IV.2. Data collection and refinement

Room temperature X-ray data collection for the protiated OmpF and perdeuterated TIM variant E97Q complex with 2PG was collected on the BioMax beamline at MAXIV laboratory, Lund. The large crystal of OmpF and TIM with a dimension of ~500 µm was mounted on a cryoloop and covered with a 2 mm diameter quartz capillary. A drop of reservoir solution was added in the capillary to avoid the dehydration and maintain the vapour pressure around the crystal. The capillary was then sealed to the base of the loop with help of plasticine. In case of TIM variant E167Q (complex with 2PG); protiated and perdeuterated OmpF, crystals were flash frozen in liquid nitrogen. X-ray diffraction was collected with a resolution range of ~1.0 to ~1.5 Å for both TIM variants.

Neutron quasi-Laue diffraction data for TIM variant E97Q complex with 2PG was collected at room temperature on LADI-III beamline at Institut-Laue-Langevin (ILL), Grenoble. Large single crystals of size ~0.5 mm^3 were mounted inside a 3 mm capillary using a custom-made large loop prepared from nylon fishing line. Deuterated reservoir solution was added inside capillary to allow H/D exchange of labile H atoms for a month before data collection. 24 images of crystal were collected for 8 days with an exposure time of ~8 h. All neutron data was processed using the LAUE suite program LAUGEN [141]. Wavelength normalization was done by using the program LSCALE and intensities were merged using SCALA [142]. The X-ray model of TIM E97Q complex with 2PG was used as a starting model for performing joint neutron- X-ray refinement in *phenix.refine* [143]. Once the R-values converged in X-ray data, water molecules were added in the model and refined. The next phase was the adding D atoms to the model, which was performed using *ReadySet* program in *PHENIX* program suite. Several rounds of refinements of individual coordinates, atomic occupancies of H/D atoms and individual B-factors was performed in *phenix.refine.* Model was inspected by using Coot [144] and further modelling was done by using a series of mF_o-DF_c and 2Fo-Fc electron and nuclear scattering length density maps. Manual adjustment of D_2O molecules was done and random orientations were fixed using omit mF_o-DF_c and $2mF_o$-DF_c maps.

IV.3. Results and discussion

IV.3.1. Effect of perdeuteration on OmpF structure

All the crystals used for X-ray data collection were obtained in protiated and deuterated conditions using sitting drop vapor diffusion method. For room temperature (RT) data collection, crystals mounted in a capillary were placed on the goniometer in BioMAX beamline at MAXIV. However, none of the crystals diffracted X-rays which could be due to many reasons such as instability of crystals at RT, crystal dehydration or radiation damage as it would increase at RT. Instability of large crystals at room temperature has been observed previously and was resolved by maintaining ambient data collection temperature using a cooling device [145]. After testing few crystals, it was concluded that neutron data collection for OmpF crystals should be performed at cryogenic temperature. For X-ray data collection with cryocooled crystals, both protiated and deuterated crystals diffracted with good statistics at a similar resolution range of 1.9-2.0 Å and belonged to the same space group P321 as shown in Table 4.

Table 4. Data collection, processing and refinement statistics for protiated and deuterated OmpF

	Protiated	Deuterated
Diffraction Source	FIP, BM30, ESRF	Biomax, MAXIV
Wavelength (Å)	0.979	0.976
Temperature (K)	293	293
Detector	Eiger	Eiger
Rotation range per image (°)	0.5	0.1
Exposure time per image (s)	0.011	0.011
Scaling Statistics		
Space group	P321	P321
a, b, c (Å)	116.03 116.03 49.57	116.03 116.03 49.57
α, β, γ (°)	90.00 90.00 120.00	90.00 90.00 120.00
Resolution range Å)	44.46-2.01 (2.08-2.01)	44.46-1.91 (1.98-1.91)
Total no. of reflections	153960 (23813)	
No. of unique reflections	25638 (4038)	
Multiplicity	0.166 (0.169)	
Completeness (%)	99.52 (97.23)	99.08 (91.38)
<I/*σ(I)*>	22.46 (3.05)	
Wilson B-factor	31.93	34.06
R-merge (%)		
R-meas (%)	6.3 (59.9)	
CC1/2 (%)	99.9 (81.7)	
Refinement Statistics		
Reflections used in refinement	25631 (2457)	29363 (2683)
Reflections used for R-free	1261 (123)	1472 (154)
R-work	0.2409 (0.2603)	0.2214 (0.2938)
R-free	0.2810 (0.3059)	0.2482 (0.3208)

Number of non- hydrogen atoms	2641	2633
Macromolecules	2641	2561
Protein residues	339	333
RMS (bonds)	0.032	0.007
RMS (angles)	1.12	0.82
Ramachandran favored (%)	95.52	96.07
Ramachandran allowed (%)	4.48	3.63
Ramachandran outliers (%)	0.00	0.30
Rotamer outliers (%)	2.97	3.12
Clash score	4.50	2.63
Average B-factor	37.06	38.32
Macromolecules	37.06	38.30

For deuteration studies, it is absolutely necessary to determine the effects of D_2O on protein conformation and structure. For the application of perdeuterated protein in NMX studies, it is best suitable to behave similarly like protiated protein. In case of perdeuterated OmpF, no difference in β- barrel side chain or constriction zone was observed. A defined aqueous channel with all the conserved acidic and basic residues residing on constriction zone inside OmpF barrel region was observed (Figure 1). Mg^{2+}, water molecules and acidic residues were perfectly hydrogen bonded in the L3 loop of β- barrel region. Thus, it can be concluded that perdeuteration had no significant effect on the overall structure of protein. However, these findings are in contrast to the thermal stability and crystallization behavior of perdeuterated protein as discussed in previous chapter. The structural comparison of the deuterated and protiated protein suggested that there is insignificant effect or change owing to deuteration, thus further studies can be carried out to grow large perdeuterated crystals for neutron crystallography.

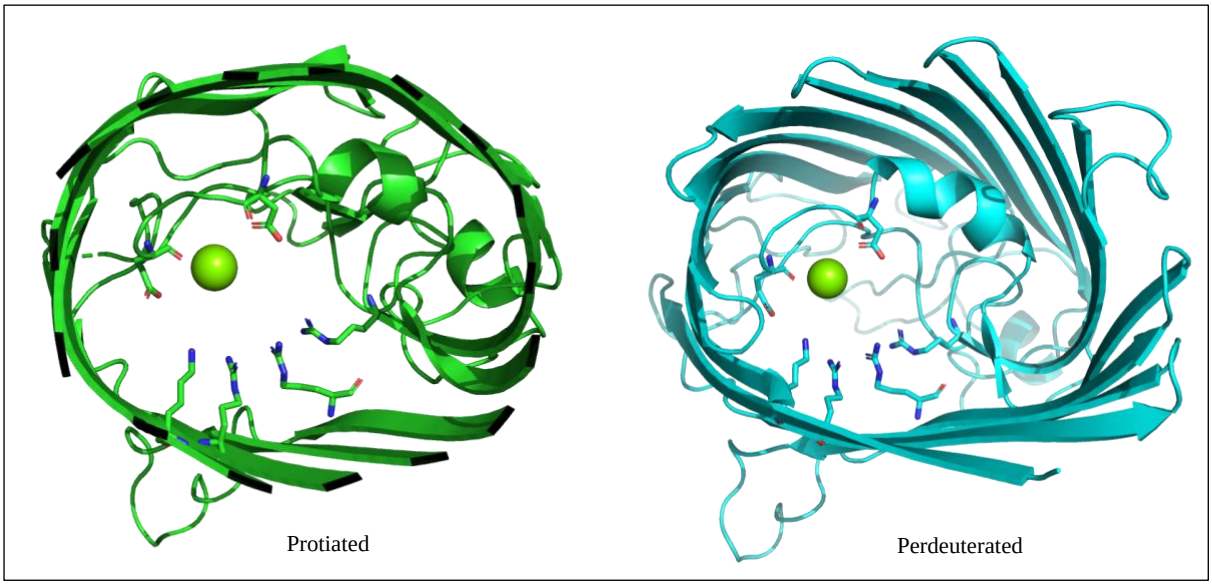

Figure 1: Structural comparison of protiated (green) and perdeuterated (cyan) OmpF. β-barrel region of OmpF where acidic and basic residues of the loop L3 in constriction zone are highlighted. All the conserved residues look similar in protiated and perdeuterated protein structures.

4.3.1. Neutron and X-ray structure analysis of perdeuterated TIM E97Q variant

The best crystals of perdeuterated TIM E97Q variant diffracted X-rays and neutrons at a resolution of 1.13 Å and 1.7 Å respectively. The two datasets were collected from different crystals at ambient temperature. Processing statistics are shown in Table 1 and 2. The active site in both neutron and X-ray structures was in the 'loop-closed' conformation and with the inhibitor 2PG bound. In this 'closed' state, conserved residues of active site such as Asn11 and H95 residues remain unchanged. However, small movement of E167 and a large conformational change in K13 residues was observed as reported previously by Samantha et al [54]. The geometry of the active site is primarily governed by loop-6 that switch between open and closed conformation providing information about hydrogen bond interactions between phosphate moiety PGA and main chain residues. Figure 3 compares the catalytic active site of wild-type TIM and the variant E97Q in the closed-liganded conformation with 2PG. In the wild type, ligand binding leaves the active site residues K13, H95, E167 and K13 unchanged. A large conformation movement in K13 was observed such that K13 is no more hydrogen bonded to E/Q97 as in the wild type (Figure 3). The N-O distance has increased to 4.7 Å in E97Q variant from 2.8 Å in wild type (liganded conformation).

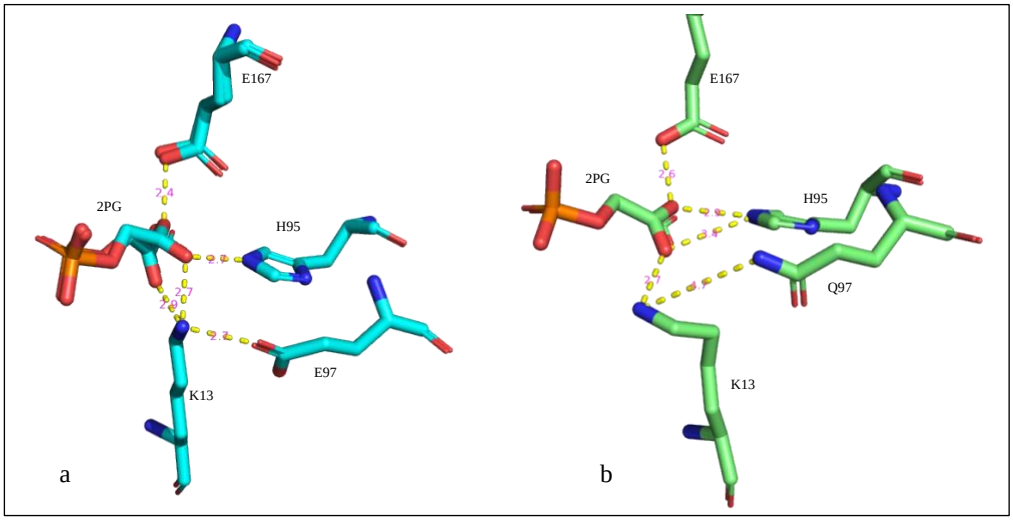

Figure 3. Comparative distance between active site residues of TIM. **a.** Wild-type *Lm*TIM (PDB ID:2VXN). **b**. *Lm*TIM variant E97Q. K13 moved away from E97Q with an increasing distance from 2.7 to 4.8 between the two residues.

Even though carboxamide of glutamine and carboxylic of glutamate side chains are isosteric, they still differ in their hydrogen-bonding formation abilities. In the wild-type enzyme, carboxylic acid moiety is involved in more hydrogen bonding interactions with its surrounding atoms as compared to variant enzyme. However, these changes made favorable condition for a water molecule to enter the vicinity of active site (Figure 4b). Moreover, Q97 moved closer to H95 giving a stearic hindrance with a shorter hydrogen bond between main chain amide of glutamine and side chain amide of histidine compared to wild-type as shown in Figure 4 a and b. The amide group on side chain of E97Q and introduction of extra hydrogen bonds might sterically crowd the catalytic K13 residue due to close proximity of ε-NH_3^+ of K12 to amide group of Q97. This could be the reason of ammonium group displacement and mispositioning of K13 consequently leading to 4000-fold decrease in catalytic activity of E97Q variant as suggested by Richard and Samantha et al [54, 55]. Because of all this movement in molecules,

E167 residue shifted closer to inhibitor 2PG such that inhibitor is no longer in two alternate conformations as in the atomic resolution structure of *Lm*TIM [49]. Movement of E167 closer to the carboxylate of 2PG caused steric hindrance that might be another add-on possibility for reduced catalytic activity.

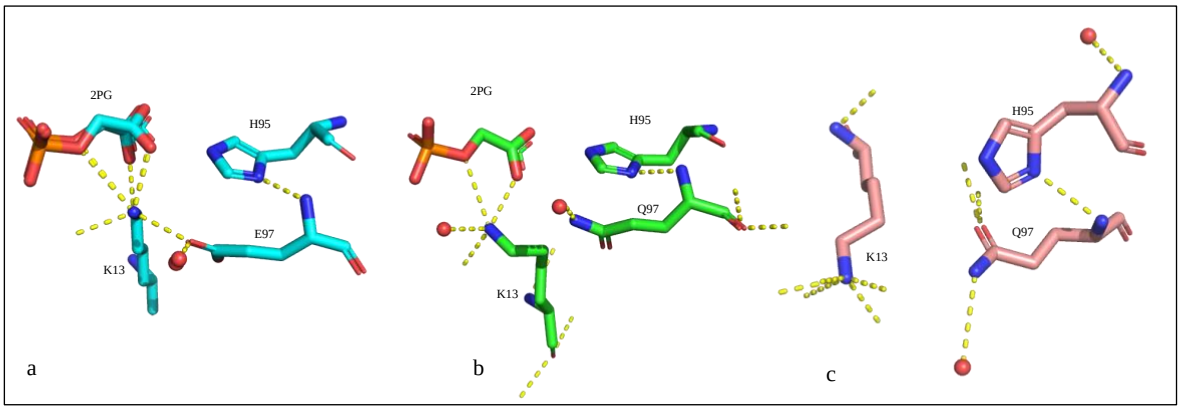

Figure 4. Hydrogen bonding interactions between active site residues and water molecules a. Wild-type *Lm*TIM (PDB ID:2VXN) **b.** *Lm*TIM variant E97Q in liganded conformation **c.** Unliganded *Pf*TIM variant E97Q (PDB ID: 3PSW).

It has been previously reported that E167 is protonated upon binding of PGA to TIM (https://doi.org/10.1107/S2052252521004619). However, protonation of Lys13 is also clearly observed in neutron structure of TIM variant E97Q when complex with 2PG forming a 2 Å hydrogen bond between amide group of K13 and O1 atom of inhibitor 2PG. Figure 5a shows the nuclear density between the two atoms when $2mF_o$-DF_c nuclear scattering length density map was contoured at 1.0σ level. This suggests K13 being a donor facilitating proton transfer from its amide group to O1 carboxylate of 2PG. Other active site residues such as H95 and E167 also showed nuclear density but at a lower $2mF_o$-DF_c contoured level of 0.5 unlike K13. No nuclear densities were observed on H atoms of 2PG, as expected revealing no exchange of H to D in 2PG and thus modelled as H in joint/X-ray refinement. The phosphate moiety of 2PG was well anchored with backbone amides of G173 and G235 which is in accordance with previous deposited PDB entry 7az3. However, one of the phosphate oxygens was stabilized by a water molecule instead of G234 unlike previous structures. This was clearly evident with scattering length density map between 2PG-phosphoanion and water when contoured at 1.0σ level as shown in Figure 5b. The phosphate binding energy with main chain significantly lowers the transition state free energy barrier [146]. In the liganded-closed conformation, the YGGS conserved sequence (residue 210-213) in loop-7 forms a binding site for phosphate anions such that G211-G212 peptide rotates by 90º and G211-Ser213 rotates by 180º allowing N(G234) and N(G173) to act as hydrogen bond donors for binding phosphates of 2PG. Residues G173 and G235 were slightly shifted by 0.45 Å from their position as compared to previously deposited sub-atomic resolution structure of TIM complex with PGA [48].

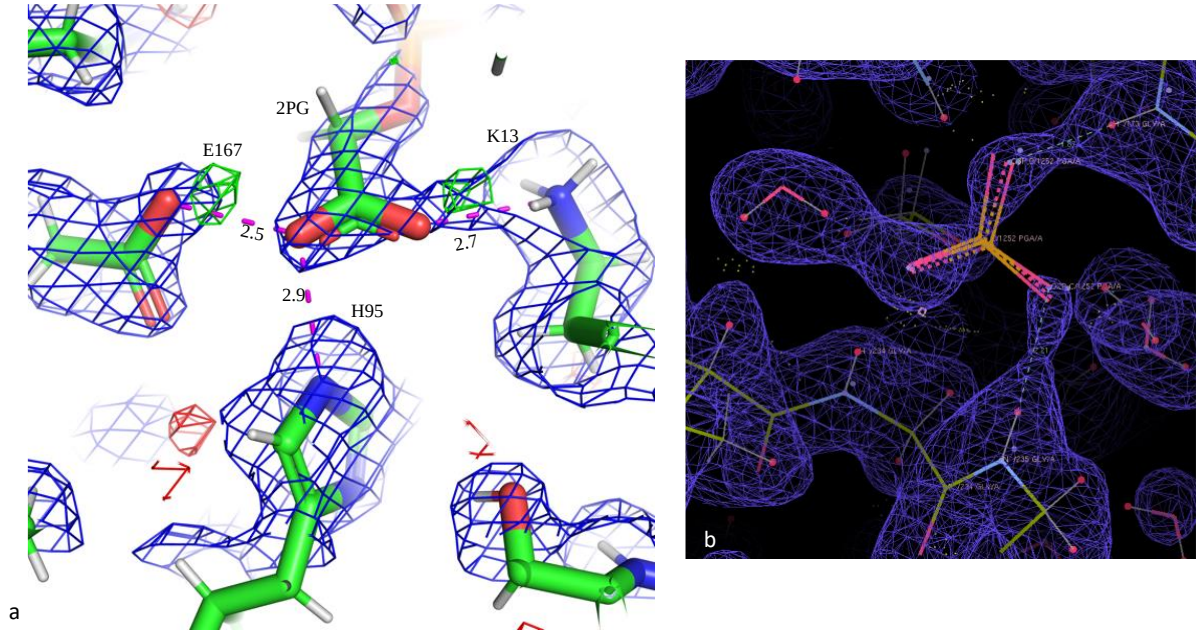

Figure 5. 2mF_o-DF_c nuclear scattering length density map of active site (contoured at 1.0σ level) a. Nuclear density between O1 of 2PG and K13 b. Stabilization of phosphate oxygens of 2PG by main chain amides and water network.

Apart from conventional refinement, advanced computational quantum refinement for the active site was also performed in order to validate the conclusions. Initially, only X-ray quantum refinement of 2PG-TIM complex was performed due to technical issues with ComQumU. Three possible proton transfer pathways were tested: a) protonation state of E167, K13 and deprotonation state of 2PG, b) E167 and 2PG protonated and K13 in deprotonated state, c) E167 deprotonated with D atom moved to O1 of 2PG and K13 in protonated state d) E167 in deprotonated, K13 in protonated and 2PG in deprotonated state. The calculations were in accordance with joint X-ray/neutron refinement for first three cases confirming that E167 and K13 are protonated. These findings support the previously established theory of E167 being the general base [48, 54, 55]. Recently, the first neutron structure of TIM complex with 2PG and PGH was published confirming the protonation state of E167 and K13 which is in accordance with this study (https://doi.org/10.1107/S2052252521004619). However, presence of low-barrier hydrogen bonds in intermediate states is still ambiguous and needs further investigation possible by computational analysis. Interestingly, a water molecule was observed inside active site which was opposing the dehydrated enzymatic mechanism of TIM catalytic end. Role of this water molecule should also be further investigated with QM calculations.

4.3.1.1. Possible role of E97 in catalysis

The extensive work of numerous researchers on several structures of TIM and its variants proposed the abstraction of a proton by the carboxylate of E167 in *Lm*TIM from the hydroxymethylene group of the substrate DHAP leading to the formation of an enediolate intermediate. The conserved active site residues such as H95 and K13 are proposed to have a direct role in electrostatic stabilization of intermediate states to facilitate isomerization reaction. A constant debate on the role of H95 has puzzled researchers that led Karplus and coworkers to perform QM/MM calculations that concluded the formation of an imidazolate anion when H95 donates a proton to the substrate [147]. However, the contribution of H95 and

K13 to stabilization of enediolate and polarization of DHAP carbonyl group is still not understood very well that might be explained by QM/MM calculations on joint X-ray/neutron refinement of TIM variant E97Q. Knowles et al pointed out a hydrogen bond with neutral group of imidazole and backbone amide group of E97 that would orient H95 in close proximity with DHAP leading to the proposal of its involvement in proton abstraction step [148]. However, Kelpsas et al. in recent studies confirmed that E167 is the general base and isomerization reaction begins with abstracting of proton from its carboxylate group. Neutron structures of transition state mimics PGH and 2PG were used to evaluate three proton transfer mechanisms, all of which were shown to be energetically feasible (https://doi.org/10.1107/S2052252521004619). The hydrogen bonding network formed by enediolate, neutral imidazole ring of H95, ammonium group of K13 and carboxylic acid of E97 seems to allow easy relaying of protons.

The observed of nuclear scattering length density between K13 and 2PG suggests a definite role of the K13-E97 pair in the stabilization of the reaction intermediates. There are two possible significant roles of K13: the neutralization of the negative charge of the phosphate group or stabilization of substrate carbonyl groups as previously suggested by Patricia and coworkers [149]. They showed by various mutations in active site that K13 positive charge has a significant role in balancing the overall electrostatic environment in the active site and not just neutralizing one negative charge on substrate. Its dramatic displacement in TIM variant E97Q structure brings it even closer to 2PG to form a well-defined hydrogen bond also suggesting the critical role in stabilization of substrate facilitated by the conserved E97. Even though dimerization is a requirement for the catalytic activity of TIM and E97 is in close proximity to dimer interface, the E97Q mutation left the dimeric interface uninterrupted again suggesting its indirect involvement in catalytic machinery of the enzyme [54]. Whether the reduction in catalytic activity in E97Q variant is due to mispositioning of K13 or by disturbance of a proton chain is still not clear and needs further investigation. QM/MM calculations on neutron structure of this variant would answer more questions on role of K13 and E97 in transition state stabilization during catalysis of TIM. Even though the joint X-ray/neutron refinement is in accordance with previous findings, understanding the role of specific amino acids is indeed challenging. Designing site-directed mutagenesis to evaluate catalytic mechanisms might introduce unwanted displacements or interactions of amino acids involved in active site as observed in this study. Extensive studies to evaluate second shell active residues such as E97 may facilitate the understanding of catalytically active residues and their importance in reaction mechanism without having an adverse impact on stability.

4.3.2. X-ray structure analysis of perdeuterated TIM E167Q variant

The best crystals of perdeuterated TIM E167Q variant diffracted X-rays at an ultra-high resolution of 1.08 Å. The dataset was collected at cryo-temperature for these crystals and processing statistics are shown in Table 3. After evaluating active site, it was observed that all the conserved residues in active site moved away from 2PG by a distance of 0.37 Å except H95 and E97 that moved closer. Due to the ultra-resolution, all the atom positions were visible with high accuracy including H atom at CE2 position in imidazole ring of H95 as shown in Figure 6. Ligand still binds to active site; however, no catalysis can be carried out due to loss of proton abstraction capability of glutamine and no deprotonation of substrate/inhibitor. Q167 is no more above the cis-enediolate plane but almost in the same plane as 2PG and H95. It was not totally in swung out position but a hydrogen bond with 2PG at a distance of 2.7 Å is still feasible. Due to the movement of glutamine away from 2PG, side chain came close enough to

S96 leading to formation of 2.8 Å H-bond between main chain amides and side chain O1 of Q167. This also increased the hydrogen bond length between enzyme-inhibitor from 1.8 Å in wild type to 2.75 Å in variant. Since amide of G167 and N^{δ} atom of H95 imidazole ring came closer, a stearic hindrance was observed between the two moieties.

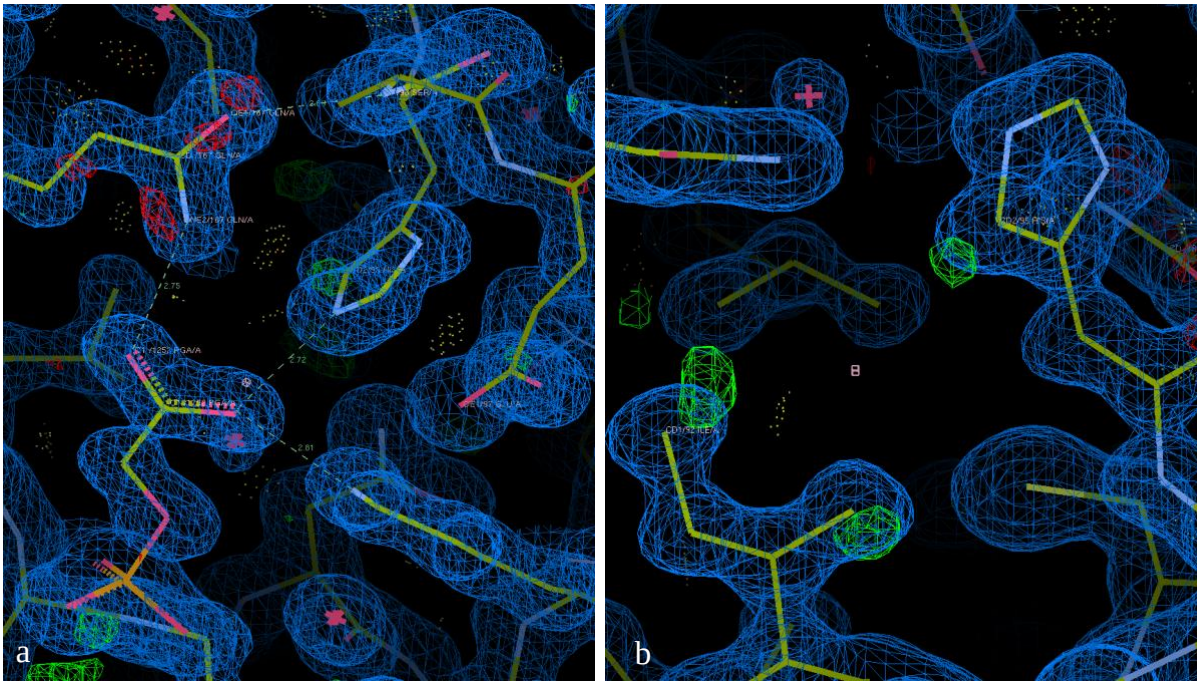

Figure 6. Orientation of catalytic active site in complex with 2PG in TIM variant E167Q
a) $2F_0$-Fc electron-density map (contoured at 1.0σ level) of active site conserved residues Q167, H95, K13 and E97. b) The Fo-Fc electron density map (green) indicates the H atom on the N^{δ} atom of H95 and C^{δ} of I172 residues.

The movement of hydrophobic side chains of amino acid residues I172 and L232 accompanies the closure of loop 6. A series of movement begins from the side chain of I172 towards the carboxylate group of E167 forcing it to swing towards 2PG and L232 resulting in ligand- closed conformation of enzyme [50]. These hydrophobic residues resulted in sequester of carboxylate side chain of E167 from bulk solvent clamping it tightly between the hydrophobic surrounding residues I172 and L232. This swinging in catalytic base and desolvation of active site is very important for effective enzymatic activity as it confines the movement of E167 side chain forcing it to protonate. However, due to replacement of E167 to Q167, this hydrophobic pocket formation was affected where I172 moved slightly away from E167 making space for a water molecule to enter the active site (Figure 7). Movement of water molecule perturbed its hydrogen bonding with surrounding bulk waters outside hydrophobic active site. Basicity of glutamate side chain increase from pKa value of ~4 to ~10 enhancing the driving force for protonation. Mutating glutamate with neutral glutamine results in no basic environment which is important for deprotonation of enzyme-bound ligand/substrate.

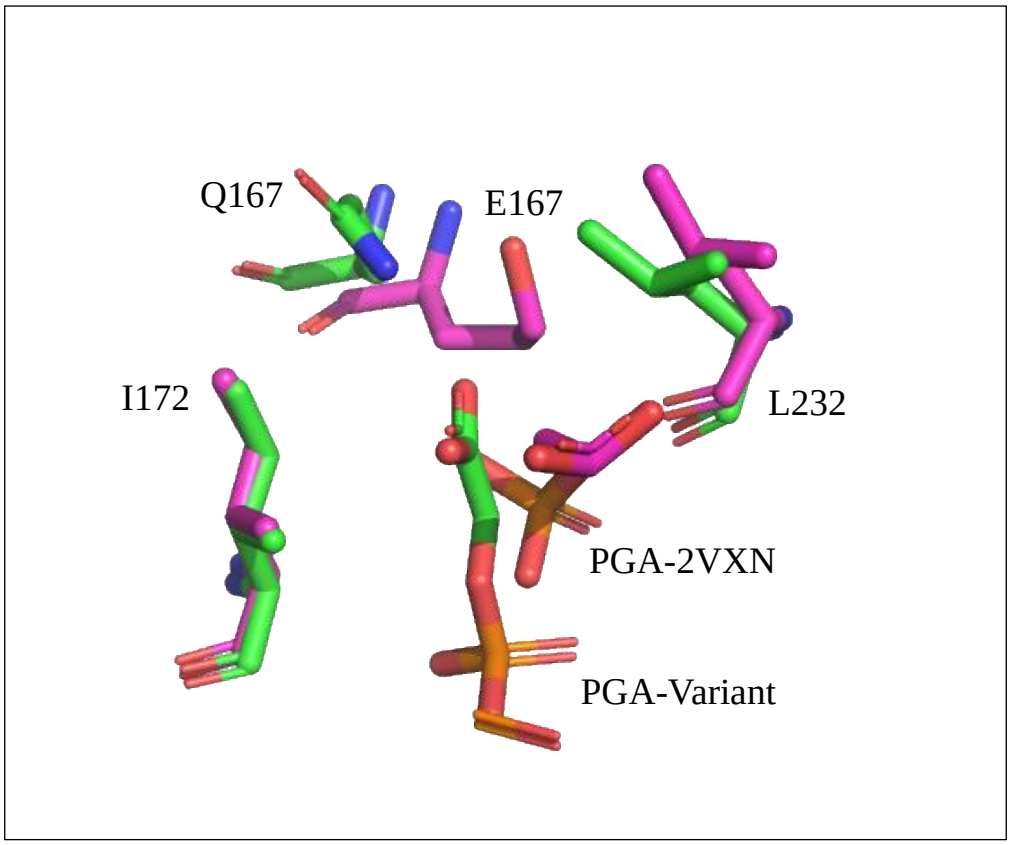

Figure 7. Models of superimposed active site of TIM variant E167Q (green) and PDB entry 2VXN (magenta). Loop 6 (residues 167-177) closure results in movement of I172 side chain towards catalytic base glutamate that further moves side chain of L232. This movement results in sequestration of catalytic base.

Table 3. TIM E167Q-2PG processing and refinement statistics

Values in parentheses are for the outermost shell.

Data Collection	
Diffraction Source	Biomax, MAXIV
Wavelength (Å)	0.976
Temperature (K)	293
Detector	Eiger
Rotation range per image (°)	0.1
Total rotation range (°)	180
Exposure time per image (s)	0.011
Scaling Statistics	
Space group	C2
a, b, c (Å)	99.3, 52.5, 58.7
α, β, γ (°)	90.0, 118.2, 90.0
Resolution range Å)	45.55 - 1.08 (1.15 – 1.08)
Total no. of reflections	623635
No. of unique reflections	189153
Multiplicity	3.29
Completeness (%)	85.7 (41.2)

<I/*σ(I)*>	10.09 (1.49)
Wilson B-factor	15.82
R-merge (%)	
R-meas (%)	6.6 (55.6)
R-pim (%)	
CC1/2 (%)	99.6 (84.8)
Refinement Statistics	
Reflections used in refinement	94001 (6815)
Reflections used for R-free	4711 (337)
R-work	0.1430 (0.2268)
R-free	0.1681 (0.2329)
Number of non- hydrogen atoms	2423
Macromolecules	1982
Ligands	25
Solvent	416
Protein residues	249
RMS (bonds)	0.004
RMS (angles)	0.75
Ramachandran favored (%)	97.98
Ramachandran allowed (%)	2.02
Ramachandran outliers (%)	0.00
Rotamer outliers (%)	0.47
Clash score	2.73
Average B-factor	26.11
Macromolecules	21.65
Ligands	42.14
Solvent	46.43

TIM is a well-suited model system for continuing the structural enzymatic studies of αβ-barrel proteins. Even though, vast experimental and computational studies give an elaborative insight into TIM reaction mechanism, there are still several unanswered questions. With the aim of using glutamine as an analogue of protonated catalytic base G167 we performed site-directed mutagenesis to further understand the electrostatic behavior and hydrogen bond geometry of active site residues. In principle glutamine will keep substrate bound to enzyme helping us to further understand the role of K13 and H95 in polarization of substrate. With the movement of Q167 away from ligand and H95 moving closer to form hydrogen bond, emphasized the previous findings that H95 has a significant role in polarization of carbonyl group of substrate or 2PG in this case [150]. Apart from proton abstraction, E167 also helps in ground state stabilization (GSD) of intermediate states of reaction mechanism. Despite the importance of GSD, it still needs further investigation and might play a role in understanding hydrogen-bond geometry and its effect on enzyme-substrate complex [151]. The enzymatic mechanism of TIM is a multi-step process with various transition states, by replacing charged glutamate with non-polar neutral glutamine, we have a possibility to lock the substrate in a specific intermediate state which can be further evaluated using QM/MM calculations. It is speculated that lack of carboxylate group might lead to stronger binding of substrate. However, X-ray structure alone of TIME167Q variant will not provide all this information and we need a neutron structure to evaluate further the catalytic contribution. It will be interesting to see if the nuclear density of K13 and H95 would still persist in neutron structure of this TIM variant.

Table 1. Data collection and processing statistics of TIM-2PG

Values in parentheses are for the outermost shell.

Diffraction Source	**Biomax, MAXIV**	**LADI-III, ILL**
Wavelength (Å)	0.976	
Temperature (K)	293	293
Detector	Eiger	Neutron image plate
Rotation range per image (°)	0.1	
Total rotation range (°)	180	
Exposure time per image (s)	0.011	
Space group	C2	C2
a, b, c (Å)	99.30, 52.67, 58.85	98.17, 52.20, 58.10
α, β, γ (°)	90.00, 118.00, 90.00	90.00, 118.11, 90.00
Resolution range (Å)	45.72 - 1.13 (1.19-1.13)	43.29-1.7 (1.86-1.70)
Total no. of reflections	561742	74411
No. of unique reflections	171724	21797
Completeness (%)	85.9 (40.4)	76.7 (60.5)
Multiplicity	3.27	3.4
<I/*σ(I)*>	10.68 (0.70)	6.4 (1.2)
R_{meas} (%)	5.4 (142.2)	0.19 (0.48)
CC1/2 (%)	99.8 (29.8)	

Table 2. Joint neutron-X-ray refinement statistics and structure determination of TIM-2PG

Values in parentheses are for the outermost shell.

	X-ray	Neutron
Resolution range (Å)	43.29 - 1.175 (1.217-1.175)	43.29 - 1.7 (1.761-1.7)
Unique reflections	83726 (6577)	21644 (1518)
Completeness (%)	97.02 (76.34)	75.33 (53.40)
Wilson B-factor	17.05	24.04
Reflections used in refinement	83724 (6577)	21613 (1515)
Reflections used for R_{free}	4143 (303)	1151 (82)
R_{work}	0.1467 (0.3343)	0.2322 (0.3723)
R-free	0.1651 (0.3279)	0.2917 (0.3472)
Number of non-hydrogen atoms	2579	2579
Macromolecules	2015	2015
Ligands	18	18
Solvent	546	546

Protein residues	249	249
RMS (bonds)	0.016	0.011
RMS (angles)	1.23	1.28
Ramachandran favored (%)	98.38	98.38
Ramachandran allowed (%)	1.62	1.62
Ramachandran outliers (%)	0.00	0.00
Rotamer outliers (%)	1.37	1.37
Clash score	5.35	6.56
Average B-factor	34.13	34.13
Macromolecules	28.08	28.08
Ligands	22.13	22.13
Solvent	56.84	56.84

Supplementary Information

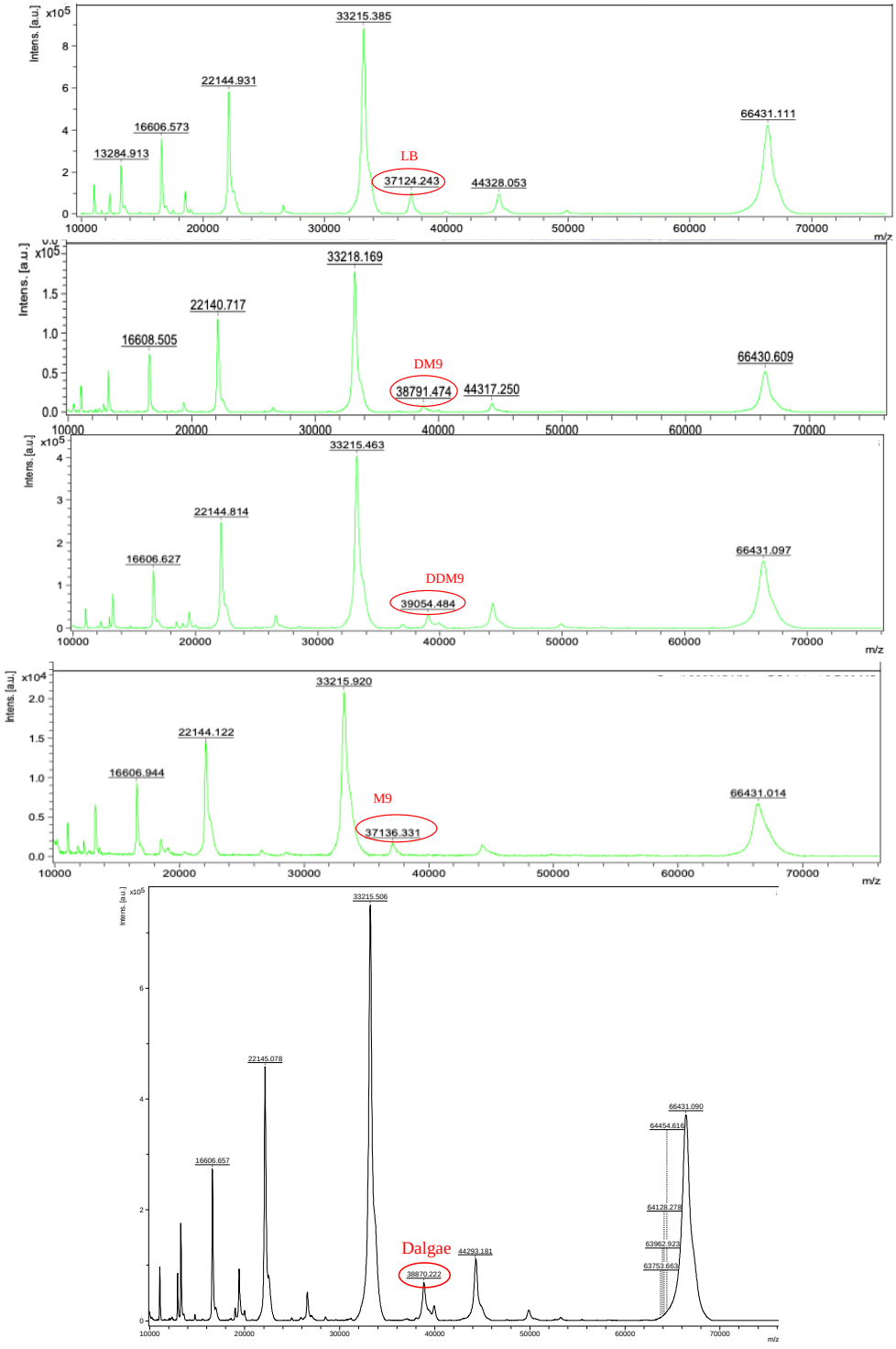

Figure S1. MALDI-TOF Mass spectra for all the protein samples wherein Bovine serum albumin (BSA) was used as an internal standard. BSA peak was observed at 66431, 22144 and 33215 Da approxiamtely in all samples. The protein samples peaks are enclosed in a red circle.

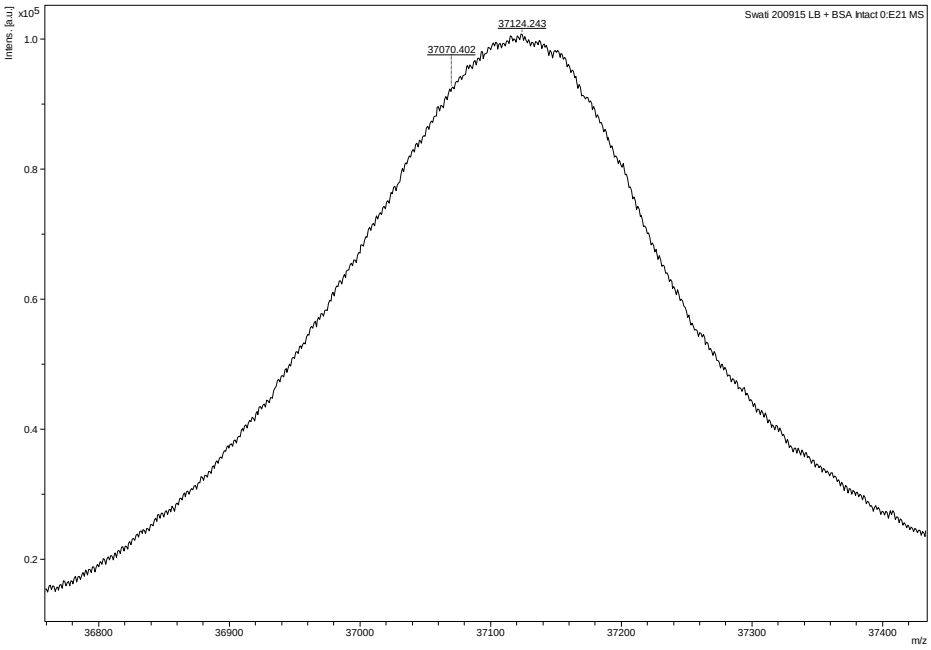

Figure S2. MALDI-TOF Mass spectra of protein sample purified in LB media. The maximum peak was observed at 37124 Da instead of theoritacal mass 37070 Da. A Na^+ on the peptide instead of H^+ was observed, thus mass increased by 23 Da which makes 54 Da with two oxidations.

Agah, S. and S. Faham (2012). Crystallization of Membrane Proteins in Bicelles. Membrane Protein Structure and Dynamics, Humana Press**:** 3-16.
Asherie, N. (2004). "Protein crystallization and phase diagrams." Methods **34**(3): 266-272.
Asherie, N., C. Ginsberg, S. Blass, A. Greenbaum and S. Knafo (2008). "Solubility of thaumatin." Crystal Growth and Design **8**(6): 1815-1817.
Ashkar, R., H. Bilheux, H. Bordallo, R. Briber, D. J. Callaway, X. Cheng, X.-Q. Chu, J. E. Curtis, M. Dadmun and P. Fenimore (2018). "Neutron scattering in the biological sciences: progress and prospects." Acta Crystallographica Section D: Structural Biology **74**(12): 1129-1168.
Ataka, M. and M. Asai (1988). "Systematic studies on the crystallization of lysozyme: Determination and use of phase diagrams." Journal of Crystal Growth **90**(1-3): 86-93.
Ataka, M., K. Shinzawa-Itoh and S. Yoshikawa (1992). "Phase diagrams of a crystalline membrane protein, bovine heart cytochromec oxidase, in the salting-in region." Journal of crystal growth **122**(1-4): 60-65.
Baker, M. R., G. Fan and I. I. Serysheva (2015). "Single-particle cryo-EM of the ryanodine receptor channel in an aqueous environment." European journal of translational myology **25**(1): 35.
Bergfors, T. (1999). Protein Crystallization: Techniques, Strategies, and Tips, International University Line.
Bergfors, T. (2003). "Seeds to crystals." Journal of structural biology **142**(1): 66-76.
Blakeley, M. P., S. S. Hasnain and S. V. Antonyuk (2015). "Sub-atomic resolution X-ray crystallography and neutron crystallography: promise, challenges and potential." IUCrJ **2**(4): 464-474.
Blakeley, M. P., P. Langan, N. Niimura and A. Podjarny (2008). Neutron crystallography: opportunities, challenges, and limitations. Current Opinion in Structural Biology.
Budayova-Spano, M., S. Z. Fisher, M.-T. Dauvergne, M. Agbandje-McKenna, D. N. Silverman, D. A. Myles and R. McKenna (2006). "Production and X-ray crystallographic analysis of fully deuterated human carbonic anhydrase II." Acta Crystallographica Section F: Structural Biology and Crystallization Communications **62**(1): 6-9.
Burada, A. P., R. Vinnakota and J. Kumar (2020). "Cryo-EM structures of the ionotropic glutamate receptor GluD1 reveal a non-swapped architecture." Nature structural & molecular biology **27**(1): 84-91.
Caffrey, M. (2009). "Crystallizing membrane proteins for structure determination: use of lipidic mesophases." Annual review of biophysics **38**: 29-51.
Chayen, N., J. Akins, S. Campbell-Smith and D. Blow (1988). "Solubility of glucose isomerase in ammonium sulphate solutions." Journal of Crystal Growth **90**(1-3): 112-116.
Chayen, N. E. (1997). "A novel technique to control the rate of vapour diffusion, giving larger protein crystals." Journal of Applied Crystallography **30**(2): 198-202.
Cherezov, V., D. M. Rosenbaum, M. A. Hanson, S. G. Rasmussen, F. S. Thian, T. S. Kobilka, H.-J. Choi, P. Kuhn, W. I. Weis and B. K. Kobilka (2007). "High-resolution crystal structure of an engineered human β2-adrenergic G protein–coupled receptor." science **318**(5854): 1258-1265.
Das, N., J. Dai, I. Hung, M. Rajagopalan, H.-X. Zhou and T. A. Cross (2015). "Structure of CrgA, a cell division structural and regulatory protein from Mycobacterium tuberculosis, in lipid bilayers." Proceedings of the National Academy of Sciences **112**(2): E119-E126.
Drenth, J. (2007). Principles of protein X-ray crystallography, Springer Science & Business Media.
Dubochet, J. and A. McDowall (1981). "Vitrification of pure water for electron microscopy." Journal of Microscopy **124**(3): 3-4.

Fadel, F., Y. Zhao, A. Cousido-Siah, F. X. Ruiz, A. Mitschler and A. Podjarny (2016). "X-ray crystal structure of the full length human chitotriosidase (CHIT1) reveals features of its chitin binding domain." PloS one **11**(4): e0154190.
Garavito, R. M. and D. Picot (1991). "Crystallization of membrane proteins: a minireview." Journal of crystal growth **110**(1-2): 89-95.
Garcia-Ruiz, J., A. Moreno, C. Viedma and M. Coll (1993). "Crystal quality of lysozyme single crystals grown by the gel acupuncture method." Materials research bulletin **28**(6): 541-546.
Gaucher, J.-F., M. Riès-Kautt, F. Reiss-Husson and A. Ducruix (1997). "Solubility diagram of the Rhodobacter sphaeroides
reaction center as a function of PEG concentration." FEBS Letters **401**(2-3): 113-116.
Glaeser, R. M. (1985). "Electron crystallography of biological macromolecules." Annual Review of Physical Chemistry **36**(1): 243-275.
Gonen, T., Y. Cheng, P. Sliz, Y. Hiroaki, Y. Fujiyoshi, S. C. Harrison and T. Walz (2005). "Lipid–protein interactions in double-layered two-dimensional AQP0 crystals." Nature **438**(7068): 633-638.
Henderson, R. (1995). "The potential and limitations of neutrons, electrons and X-rays for atomic resolution microscopy of unstained biological molecules." Q Rev Biophys **28**(2): 171-193.
Henderson, R., J. M. Baldwin, T. A. Ceska, F. Zemlin, E. Beckmann and K. H. Downing (1990). "Model for the structure of bacteriorhodopsin based on high-resolution electron cryo-microscopy." Journal of molecular biology **213**(4): 899-929.
Henderson, R. and P. N. T. Unwin (1975). "Three-dimensional model of purple membrane obtained by electron microscopy." Nature **257**(5521): 28-32.
Hjorth-Jensen, S. J., E. Oksanen, P. Nissen and T. L.-M. Sørensen (2020). "Prospects for membrane protein crystals in NMX." Methods in enzymology **634**: 47-68.
Huxford, T. (2013). "X-Ray Crystallography."
Ikeya, T., D. Ban, D. Lee, Y. Ito, K. Kato and C. Griesinger (2018). "Solution NMR views of dynamical ordering of biomacromolecules." Biochimica et Biophysica Acta (BBA) - General Subjects **1862**(2): 287-306.
Ikeya, T., P. Güntert and Y. Ito (2019). "Protein Structure Determination in Living Cells." International Journal of Molecular Sciences **20**(10): 2442.
Jaakola, V.-P., M. T. Griffith, M. A. Hanson, V. Cherezov, E. Y. Chien, J. R. Lane, A. P. Ijzerman and R. C. Stevens (2008). "The 2.6 angstrom crystal structure of a human A2A adenosine receptor bound to an antagonist." Science **322**(5905): 1211-1217.
Jacrot, B. (1976). "The study of biological structures by neutron scattering from solution." Reports on progress in physics **39**(10): 911.
Jaremko, M., L. Jaremko, S. Villinger, C. D. Schmidt, C. Griesinger, S. Becker and M. Zweckstetter (2016). "High-Resolution NMR Determination of the Dynamic Structure of Membrane Proteins." Angew Chem Int Ed Engl **55**(35): 10518-10521.
Junius, N., E. Vahdatahar, E. Oksanen, J.-L. Ferrer and M. Budayova-Spano (2020). "Optimization of crystallization of biological macromolecules using dialysis combined with temperature control." Journal of Applied Crystallography **53**(3).
Kanelis, V., J. D. Forman-Kay and L. E. Kay (2001). "Multidimensional NMR Methods for Protein Structure Determination." IUBMB Life (International Union of Biochemistry and Molecular Biology: Life) **52**(6): 291-302.
Katona, G., U. Andreasson, E. M. Landau, L.-E. Andreasson and R. Neutze (2003). "Lipidic cubic phase crystal structure of the photosynthetic reaction centre from Rhodobacter sphaeroides at 2.35 Å resolution." Journal of molecular biology **331**(3): 681-692.
Kelpšas, V., B. Lafumat, M. P. Blakeley, N. Coquelle, E. Oksanen and C. Von Wachenfeldt (2019). "Perdeuteration, large crystal growth and neutron data collection of Leishmania

mexicana triose-phosphate isomerase E65Q variant." Acta Crystallographica Section F: Structural Biology Communications **75**(4): 260-269.
Kendrew, J. C., G. Bodo, H. M. Dintzis, R. Parrish, H. Wyckoff and D. C. Phillips (1958). "A three-dimensional model of the myoglobin molecule obtained by x-ray analysis." Nature **181**(4610): 662-666.
Khoshouei, M., R. Danev, J. M. Plitzko and W. Baumeister (2017). "Revisiting the structure of hemoglobin and myoglobin with cryo-electron microscopy." Journal of molecular biology **429**(17): 2611-2618.
Koruza, K., B. Lafumat, M. Nyblom, B. P. Mahon, W. Knecht, R. McKenna and S. Z. Fisher (2019). "Structural comparison of protiated, H/D-exchanged and deuterated human carbonic anhydrase IX." Acta Crystallogr D Struct Biol **75**(Pt 10): 895-903.
Langan, P. S., V. G. Vandavasi, B. Sullivan, J. Harp, K. Weiss and L. Coates (2019). "Crystallization of a potassium ion channel and X-ray and neutron data collection." Acta Crystallographica Section F Structural Biology Communications **75**(6): 435-438.
Liao, M., E. Cao, D. Julius and Y. Cheng (2013). "Structure of the TRPV1 ion channel determined by electron cryo-microscopy." Nature **504**(7478): 107-112.
Lorber, B., L. J. DeLucas and J. B. Bishop (1991). "Changes in the physico-chemical properties of the detergent octyl glucoside during membrane protein crystallization using a salt as the precipitant." Journal of crystal growth **110**(1-2): 103-113.
Lu, P., X.-c. Bai, D. Ma, T. Xie, C. Yan, L. Sun, G. Yang, Y. Zhao, R. Zhou and S. H. Scheres (2014). "Three-dimensional structure of human γ-secretase." Nature **512**(7513): 166-170.
Mcpherson, A. (2004). "Introduction to protein crystallization." Methods **34**(3): 254-265.
McPherson, A. and J. A. Gavira (2014). "Introduction to protein crystallization." Acta Crystallographica Section F: Structural Biology Communications **70**(1): 2-20.
Mikol, V. and R. Giegé (1989). "Phase diagram of a crystalline protein: Determination of the solubility of concanavalin A by a microquantitation assay." Journal of crystal growth **97**(2): 324-332.
Mitchell, D. P. and P. N. Powers (1936). "Bragg reflection of slow neutrons." Physical Review **50**(5): 486.
Mitsuoka, K., T. Hirai, K. Murata, A. Miyazawa, A. Kidera, Y. Kimura and Y. Fujiyoshi (1999). "The structure of bacteriorhodopsin at 3.0 Å resolution based on electron crystallography: implication of the charge distribution." Journal of molecular biology **286**(3): 861-882.
Murata, K., K. Mitsuoka, T. Hirai, T. Walz, P. Agre, J. B. Heymann, A. Engel and Y. Fujiyoshi (2000). "Structural determinants of water permeation through aquaporin-1." Nature **407**(6804): 599-605.
Oksanen, E., M. P. Blakeley, F. Bonnete, M. T. Dauvergne, F. Dauvergne and M. Budayova-Spano (2009). "Large crystal growth by thermal control allows combined X-ray and neutron crystallographic studies to elucidate the protonation states in Aspergillus flavus urate oxidase." J R Soc Interface **6 Suppl 5**: S599-610.
Oksanen, E., M. P. Blakeley, M. El-Hajji, U. Ryde and M. Budayova-Spano (2014). "The neutron structure of urate oxidase resolves a long-standing mechanistic conundrum and reveals unexpected changes in protonation." PLoS One **9**(1): e86651.
Oksanen, E., J. C.-H. Chen and S. Z. Fisher (2017). "Neutron Crystallography for the Study of Hydrogen Bonds in Macromolecules." Molecules **22**(4): 596.
Ostermeier, C. and H. Michel (1997). "Crystallization of membrane proteins." Current opinion in structural biology **7**(5): 697-701.
Otálora, F., J. A. Gavira, J. D. Ng and J. M. García-Ruiz (2009). "Counterdiffusion methods applied to protein crystallization." Progress in biophysics and molecular biology **101**(1-3): 26-37.

Park, S. H., B. B. Das, F. Casagrande, Y. Tian, H. J. Nothnagel, M. Chu, H. Kiefer, K. Maier, A. A. De Angelis and F. M. Marassi (2012). "Structure of the chemokine receptor CXCR1 in phospholipid bilayers." Nature **491**(7426): 779-783.
Preiswerk, P. and H. von Halban (1936). "Preuve experimental de la diffraction des neutrons." CR Acad. Sci. Paris **203**: 73-75.
Pusey, M. L. and K. Gernert (1988). "A method for rapid liquid-solid phase solubility measurements using the protein lysozyme." Journal of crystal growth **88**(3): 419-424.
Rupp, B. (2009). Biomolecular crystallography: principles, practice, and application to structural biology, Garland Science.
Sears, V. F. (1992). "Neutron scattering lengths and cross sections." Neutron News.
Shi, D., B. L. Nannenga, M. G. Iadanza and T. Gonen (2013). "Three-dimensional electron crystallography of protein microcrystals." Elife **2**: e01345.
Stura, E. A. and I. A. Wilson (1990). "Analytical and production seeding techniques." Methods **1**(1): 38-49.
Stura, E. A. and I. A. Wilson (1991). "Applications of the streak seeding technique in protein crystallization." Journal of crystal growth **110**(1-2): 270-282.
Suloway, C., J. Pulokas, D. Fellmann, A. Cheng, F. Guerra, J. Quispe, S. Stagg, C. S. Potter and B. Carragher (2005). "Automated molecular microscopy: the new Leginon system." Journal of structural biology **151**(1): 41-60.
Traaseth, N. J., L. Shi, R. Verardi, D. G. Mullen, G. Barany and G. Veglia (2009). "Structure and topology of monomeric phospholamban in lipid membranes determined by a hybrid solution and solid-state NMR approach." Proceedings of the National Academy of Sciences **106**(25): 10165-10170.
Weber, I. T., M. J. Waltman, M. Mustyakimov, M. P. Blakeley, D. A. Keen, A. K. Ghosh, P. Langan and A. Y. Kovalevsky (2013). "Joint X-ray/Neutron Crystallographic Study of HIV-1 Protease with Clinical Inhibitor Amprenavir: Insights for Drug Design." Journal of Medicinal Chemistry **56**(13): 5631-5635.
Yonekura, K., K. Kato, M. Ogasawara, M. Tomita and C. Toyoshima (2015). "Electron crystallography of ultrathin 3D protein crystals: atomic model with charges." Proc Natl Acad Sci U S A **112**(11): 3368-3373.
1. Moore, P.B., *[50] The preparation of deuterated ribosomal materials for neutron scattering*, in *Methods in enzymology*. 1979, Elsevier. p. 639-655.
2. Olah, G.A., et al., *Troponin I encompasses an extended troponin C in the Ca2+-bound complex: a small-angle X-ray and neutron scattering study.* Biochemistry, 1994. **33**(27): p. 8233-8239.
3. LeMaster, D.M. and F.M. Richards, *Preparative-scale isolation of isotopically labeled amino acids.* Analytical biochemistry, 1982. **122**(2): p. 238-247.
4. Sosa-Peinado, A., D. Mustafi, and M.W. Makinen, *Overexpression and biosynthetic deuterium enrichment of TEM-1 β-lactamase for structural characterization by magnetic resonance methods.* Protein expression and purification, 2000. **19**(2): p. 235-245.
5. Meilleur, F., et al., *Production and X-ray crystallographic analysis of fully deuterated cytochrome P450cam.* Acta Crystallographica Section D: Biological Crystallography, 2005. **61**(5): p. 539-544.
6. Hazemann, I., et al., *High-resolution neutron protein crystallography with radically small crystal volumes: application of perdeuteration to human aldose reductase.* Acta Crystallographica Section D: Biological Crystallography, 2005. **61**(10): p. 1413-1417.
7. Anthony P. Duff*, Karyn L. Wilde*, Agata Rekas*, Vanessa Lake*, Peter J. Holden†, *Robust High-Yield Methodologies for 2H and 2H/15N/13C Labeling*
of Proteins for Structural Investigations Using Neutron Scattering and NMR. Methods in Enzymology, 2015. **565**.

8. Paliy, O., et al., *Improved methods of cultivation and production of deuteriated proteins from E. coli strains grown on fully deuteriated minimal medium.* Journal of Applied Microbiology, 2003.
9. Datsenko, K.A. and B.L. Wanner, *One-step inactivation of chromosomal genes in Escherichia coli K-12 using PCR products.* Proceedings of the National Academy of Sciences, 2000. **97**(12): p. 6640-6645.
10. Schnaitman, C.A., *Effect of ethylenediaminetetraacetic acid, Triton X-100, and lysozyme on the morphology and chemical composition of isolated cell walls of Escherichia coli.* Journal of Bacteriology, 1971. **108**(1): p. 553-563.
11. Baneyx, F. and M. Mujacic, *Recombinant protein folding and misfolding in Escherichia coli.* Nature biotechnology, 2004. **22**(11): p. 1399-1408.
12. Vera, A., et al., *The conformational quality of insoluble recombinant proteins is enhanced at low growth temperatures.* Biotechnology and bioengineering, 2007. **96**(6): p. 1101-1106.
13. Paliy, O. and T.S. Gunasekera, *Growth of E. coli BL21 in minimal media with different gluconeogenic carbon sources and salt contents.* Applied microbiology and biotechnology, 2007. **73**(5): p. 1169-1172.
14. Kelpšas, V. and C.v. Wachenfeldt, *Strain improvement of Escherichia coli K-12 for recombinant production of deuterated proteins.* Scientific Reports, 2019.
15. Koruza, K., et al., *Deuteration of human carbonic anhydrase for neutron crystallography: Cell culture media, protein thermostability, and crystallization behavior.* Archives of Biochemistry and Biophysics, 2018.
16. Rand, K.D., M. Zehl, and T.J. Jørgensen, *Measuring the hydrogen/deuterium exchange of proteins at high spatial resolution by mass spectrometry: overcoming gas-phase hydrogen/deuterium scrambling.* Accounts of chemical research, 2014. **47**(10): p. 3018-3027.
17. Resetca, D. and D.J. Wilson, *Characterizing rapid, activity-linked conformational transitions in proteins via sub-second hydrogen deuterium exchange mass spectrometry.* FEBS Journal, 2013. **280**(22): p. 5616-5625.
18. Weber, I.T., et al., *Joint X-ray/Neutron Crystallographic Study of HIV-1 Protease with Clinical Inhibitor Amprenavir: Insights for Drug Design.* Journal of Medicinal Chemistry, 2013. **56**(13): p. 5631-5635.
19. Naveed, H., et al., *Engineered oligomerization state of OmpF protein through computational design decouples oligomer dissociation from unfolding.* Journal of molecular biology, 2012. **419**(1-2): p. 89-101.
20. Novikova, O.D., et al., *Peculiarities of thermal denaturation of OmpF porin from Yersinia ruckeri.* Molecular BioSystems, 2017. **13**(9): p. 1854-1862.
21. Borek, E. and D. Rittenberg, *Anomalous growth of microorganisms produced by changes in isotopes in their environment.* Proceedings of the National Academy of Sciences of the United States of America, 1960. **46**(6): p. 777.
22. Kightlinger, W., et al., *Production and characterization of algae extract from Chlamydomonas reinhardtii.* Electronic Journal of Biotechnology, 2014. **17**(1): p. 3-3.
23. Franke, B., et al., *Production of isotope-labeled proteins in insect cells for NMR.* Journal of biomolecular NMR, 2018. **71**(3): p. 173-184.
24. Löhr, F., et al., *A strategy to obtain backbone resonance assignments of deuterated proteins in the presence of incomplete amide 2 H/1 H back-exchange.* Journal of biomolecular NMR, 2003. **25**(4): p. 291-311.
25. Ashani, Y. and G.N. Catravas, *Highly reactive impurities in Triton X-100 and Brij 35: partial characterization and removal.* Analytical biochemistry, 1980. **109**(1): p. 55-62.

26. Turowski, M., et al., *Deuterium isotope effects on hydrophobic interactions: the importance of dispersion interactions in the hydrophobic phase.* Journal of the American Chemical Society, 2003. **125**(45): p. 13836-13849.
1. O'Dell, W.B., A.M. Bodenheimer, and F. Meilleur, *Neutron protein crystallography: A complementary tool for locating hydrogens in proteins.* Arch Biochem Biophys, 2016. **602**: p. 48-60.
2. Blakeley, M.P., S.S. Hasnain, and S.V. Antonyuk, *Sub-atomic resolution X-ray crystallography and neutron crystallography: promise, challenges and potential.* IUCrJ, 2015. **2**(4): p. 464-474.
3. Hazemann, I., et al., *High-resolution neutron protein crystallography with radically small crystal volumes: application of perdeuteration to human aldose reductase.* Acta Crystallographica Section D: Biological Crystallography, 2005. **61**(10): p. 1413-1417.
4. Budayova-Spano, M., K. Koruza, and Z. Fisher, *Large crystal growth for neutron protein crystallography.* Methods in enzymology, 2020. **634**: p. 21-46.
5. Yamashita, E., et al., *Crystal structures of the OmpF porin: Function in a colicin translocon.* EMBO Journal, 2008.
6. Kelpšas, V., et al., *Perdeuteration, large crystal growth and neutron data collection of Leishmania mexicana triose-phosphate isomerase E65Q variant.* Acta Crystallographica Section F: Structural Biology Communications, 2019. **75**(4): p. 260-269.
7. Bergfors, T., *Seeds to crystals.* Journal of structural biology, 2003. **142**(1): p. 66-76.
8. McPherson, A. and J.A. Gavira, *Introduction to protein crystallization.* Acta Crystallographica Section F: Structural Biology Communications, 2014. **70**(1): p. 2-20.
9. Stetsenko, A. and A. Guskov, *An overview of the top ten detergents used for membrane protein crystallization.* Crystals, 2017. **7**(7): p. 197.
10. Ma, J., et al., *The effect of residual Triton X-100 on structural stability and infection activity of adenovirus particles.* Molecular Therapy-Methods & Clinical Development, 2020. **19**: p. 35-46.
11. Tanaka, S. and M. Ataka, *Protein crystallization induced by polyethylene glycol: A model study using apoferritin.* The Journal of chemical physics, 2002. **117**(7): p. 3504-3510.
12. Hitscherich, C., et al., *Effects of PEG on detergent micelles: implications for the crystallization of integral membrane proteins.* Acta Crystallographica Section D: Biological Crystallography, 2001. **57**(7): p. 1020-1029.
13. Garavito, R.M. and D. Picot, *The art of crystallizing membrane proteins.* Methods, 1990. **1**(1): p. 57-69.
14. Detitta, G.T. and J.R. Luft, *Rate of water equilibration in vapor-diffusion crystallization: dependence on the residual pressure of air in the vapor space.* Acta Crystallographica Section D: Biological Crystallography, 1995. **51**(5): p. 786-791.
15. García-Ruiz, J.M., F. Otálora, and A. García-Caballero, *The role of mass transport in protein crystallization.* Acta Crystallographica Section F: Structural Biology Communications, 2016. **72**(2): p. 96-104.
16. Berg, W.F., *Crystal growth from solutions.* Proceedings of the Royal Society of London. Series A - Mathematical and Physical Sciences, 1938. **164**(916): p. 79-95.
17. Manzoni, F., et al., *Perdeuteration, crystallization, data collection and comparison of five neutron diffraction data sets of complexes of human galectin-3C.* Acta Crystallographica Section D: Structural Biology, 2016. **72**(11): p. 1194-1202.
18. Liu, X., et al., *The effect of deuteration on protein structure: a high-resolution comparison of hydrogenous and perdeuterated haloalkane dehalogenase.* Acta Crystallographica Section D: Biological Crystallography, 2007. **63**(9): p. 1000-1008.
19. Koruza, K., et al., *Structural comparison of protiated, H/D-exchanged and deuterated human carbonic anhydrase IX.* Acta Crystallogr D Struct Biol, 2019. **75**(Pt 10): p. 895-903.

20. Chayen, N., et al., *Solubility of glucose isomerase in ammonium sulphate solutions.* Journal of Crystal Growth, 1988. **90**(1-3): p. 112-116.
21. Shaw Stewart, P.D., et al., *Random Microseeding: A Theoretical and Practical Exploration of Seed Stability and Seeding Techniques for Successful Protein Crystallization.* Crystal Growth & Design, 2011. **11**(8): p. 3432-3441.
22. Bergfors, T., *Succeeding with seeding: some practical advice*, in *Evolving Methods for Macromolecular Crystallography*. 2007, Springer. p. 1-10.
23. Hjorth-Jensen, S.J., et al., *Prospects for membrane protein crystals in NMX.* Methods in enzymology, 2020. **634**: p. 47-68.
24. Otálora, F., et al., *Counterdiffusion methods applied to protein crystallization.* Progress in biophysics and molecular biology, 2009. **101**(1-3): p. 26-37.
25. Junius, N., et al., *Optimization of crystallization of biological macromolecules using dialysis combined with temperature control.* Journal of Applied Crystallography, 2020. **53**(3).
26. Koruza, K., et al., *Deuteration of human carbonic anhydrase for neutron crystallography: Cell culture media, protein thermostability, and crystallization behavior.* Archives of Biochemistry and Biophysics, 2018.
27. Kresheck, G.C., H. Schneider, and H.A. Scheraga, *The Effect of D2O on the Thermal Stability of Proteins. Thermodynamic Parameters for the Transfer of Model Compounds from H2O to D2O1, 2.* The Journal of physical chemistry, 1965. **69**(9): p. 3132-3144.
28. Fromme, P. and H.T. Witt, *Improved isolation and crystallization of photosystem I for structural analysis.* Biochimica et Biophysica Acta (BBA)-Bioenergetics, 1998. **1365**(1-2): p. 175-184.
29. Lancaster, C.R.D., et al., *Structure of fumarate reductase from Wolinella succinogenes at 2.2 Å resolution.* Nature, 1999. **402**(6760): p. 377-385.
30. Dods, R., et al., *From macrocrystals to microcrystals: a strategy for membrane protein serial crystallography.* Structure, 2017. **25**(9): p. 1461-1468. e2.
31. Kolek, S.A., B. Bräuning, and P.D. Shaw Stewart, *A novel microseeding method for the crystallization of membrane proteins in lipidic cubic phase.* Acta Crystallographica Section F: Structural Biology Communications, 2016. **72**(4): p. 307-312.
32. Moraes, I., et al., *Membrane protein structure determination—the next generation.* Biochimica et Biophysica Acta (BBA)-Biomembranes, 2014. **1838**(1): p. 78-87.
33. Budayova-Spano, M., et al., *A methodology and an instrument for the temperature-controlled optimization of crystal growth.* Acta Crystallographica Section D: Biological Crystallography, 2007. **63**(3): p. 339-347.
34. Candoni, N., et al., *Practical physics behind growing crystals of biological macromolecules.* Protein and peptide letters, 2012. **19**(7): p. 714-724.
Oksanen, E., et al., *Design of a novel Peltier-based cooling device and its use in neutron diffraction data collection of perdeuterated yeast pyrophosphatase.* Journal of Applied Crystallography, 2010. **43**(5): p. 1113-1120.
Wierenga, R., E. Kapetaniou, and R. Venkatesan, *Triosephosphate isomerase: a highly evolved biocatalyst.* Cellular and molecular life sciences, 2010. **67**(23): p. 3961-3982.
2. HELFERT, S., et al., *Roles of triosephosphate isomerase and aerobic metabolism in Trypanosoma brucei.* Biochemical Journal, 2001. **357**(1): p. 117-125.
3. Orosz, F., J. Oláh, and J. Ovádi, *Triosephosphate isomerase deficiency: new insights into an enigmatic disease.* Biochimica et Biophysica Acta (BBA)-Molecular Basis of Disease, 2009. **1792**(12): p. 1168-1174.
4. Orosz, F., J. Olah, and J. Ovadi, *Triosephosphate isomerase deficiency: facts and doubts.* IUBMB life, 2006. **58**(12): p. 703-715.
5. Blacklow, S.C., et al., *Triosephosphate isomerase catalysis is diffusion controlled.* Biochemistry, 1988. **27**(4): p. 1158-1165.

6. Albery, W.J. and J.R. Knowles, *Free-energy profile for the reaction catalyzed by triosephosphate isomerase.* Biochemistry, 1976. **15**(25): p. 5627-5631.
7. Rozovsky, S. and A.E. McDermott, *Substrate product equilibrium on a reversible enzyme, triosephosphate isomerase.* Proceedings of the National Academy of Sciences, 2007. **104**(7): p. 2080-2085.
8. Albery, W.J. and J.R. Knowles, *Evolution of enzyme function and the development of catalytic efficiency.* Biochemistry, 1976. **15**(25): p. 5631-5640.
9. Banner, D., et al., *Structure of chicken muscle triose phosphate isomerase determined crystallographically at 2.5 Å resolution: using amino acid sequence data.* Nature, 1975. **255**(5510): p. 609-614.
10. Nagano, N., E. Gail Hutchinson, and J.M. Thornton, *Barrel structures in proteins: automatic identification and classification including a sequence analysis of TIM barrels.* Protein Science, 1999. **8**(10): p. 2072-2084.
11. Wierenga, R., *The TIM-barrel fold: a versatile framework for efficient enzymes.* FEBS letters, 2001. **492**(3): p. 193-198.
12. Pompliano, D.L., A. Peyman, and J.R. Knowles, *Stabilization of a reaction intermediate as a catalytic device: definition of the functional role of the flexible loop in triosephosphate isomerase.* Biochemistry, 1990. **29**(13): p. 3186-3194.
13. Röthlisberger, D., et al., *Kemp elimination catalysts by computational enzyme design.* Nature, 2008. **453**(7192): p. 190-195.
14. Cleland, W.W., P.A. Frey, and J.A. Gerlt, *The low barrier hydrogen bond in enzymatic catalysis.* Journal of Biological Chemistry, 1998. **273**(40): p. 25529-25532.
15. Jogl, G., et al., *Optimal alignment for enzymatic proton transfer: structure of the Michaelis complex of triosephosphate isomerase at 1.2-Å resolution.* Proceedings of the National Academy of Sciences, 2003. **100**(1): p. 50-55.
16. Alahuhta, M. and R.K. Wierenga, *Atomic resolution crystallography of a complex of triosephosphate isomerase with a reaction-intermediate analog: New insight in the proton transfer reaction mechanism.* Proteins: Structure, Function, and Bioinformatics, 2010. **78**(8): p. 1878-1888.
17. Kursula, I. and R.K. Wierenga, *Crystal structure of triosephosphate isomerase complexed with 2-phosphoglycolate at 0.83-Å resolution.* Journal of Biological Chemistry, 2003. **278**(11): p. 9544-9551.
18. Malabanan, M.M., et al., *Magnitude and origin of the enhanced basicity of the catalytic glutamate of triosephosphate isomerase.* Journal of the American Chemical Society, 2013. **135**(16): p. 5978-5981.
19. Schliebs, W., et al., *Active site properties of monomeric triosephosphate isomerase (monoTIM) as deduced from mutational and structural studies.* Protein science, 1996. **5**(2): p. 229-239.
20. Knowles, J.R., *Enzyme catalysis: not different, just better.* Nature, 1991. **350**(6314): p. 121-124.
21. Blacklow, S.C., K.D. Liu, and J.R. Knowles, *Stepwise improvements in catalytic effectiveness: independence and interdependence in combinations of point mutations of a sluggish triosephosphate isomerase.* Biochemistry, 1991. **30**(34): p. 8470-8476.
22. Samanta, M., et al., *Revisiting the mechanism of the triosephosphate isomerase reaction: the role of the fully conserved glutamic acid 97 residue.* ChemBioChem, 2011. **12**(12): p. 1886-1896.
23. Richard, J.P., *A Paradigm for Enzyme-Catalyzed Proton Transfer at Carbon: Triosephosphate Isomerase.* Biochemistry, 2012. **51**(13): p. 2652-2661.
24. Campbell, J., et al., *LAUEGEN version 6.0 and INTLDM.* Journal of Applied Crystallography, 1998. **31**(3): p. 496-502.

25. Evans, P., *Scaling and assessment of data quality.* Acta Crystallographica Section D: Biological Crystallography, 2006. **62**(1): p. 72-82.
26. Adams, P.D., et al., *The Phenix software for automated determination of macromolecular structures.* Methods, 2011. **55**(1): p. 94-106.
27. Emsley, P. and K. Cowtan, *Coot: model-building tools for molecular graphics.* Acta crystallographica section D: biological crystallography, 2004. **60**(12): p. 2126-2132.
28. Morrow, J.R., T.L. Amyes, and J.P. Richard, *Phosphate binding energy and catalysis by small and large molecules.* Accounts of chemical research, 2008. **41**(4): p. 539-548.
29. Cui, Q. and M. Karplus, *Quantum mechanics/molecular mechanics studies of triosephosphate isomerase-catalyzed reactions: effect of geometry and tunneling on proton-transfer rate constants.* Journal of the American Chemical Society, 2002. **124**(12): p. 3093-3124.
30. Lodi, P.J. and J.R. Knowles, *Neutral imidazole is the electrophile in the reaction catalyzed by triosephosphate isomerase: structural origins and catalytic implications.* Biochemistry, 1991. **30**(28): p. 6948-6956.
31. Lodi, P.J., et al., *Triosephosphate isomerase requires a positively charged active site: the role of lysine-12.* Biochemistry, 1994. **33**(10): p. 2809-2814.
[1] J. C. Kendrew, G. Bodo, H. M. Dintzis, R. Parrish, H. Wyckoff, and D. C. Phillips, "A three-dimensional model of the myoglobin molecule obtained by x-ray analysis," *Nature,* vol. 181, no. 4610, pp. 662-666, 1958.
[2] J. Drenth, *Principles of protein X-ray crystallography*. Springer Science & Business Media, 2007.
[3] T. Huxford, "X-Ray Crystallography," 2013.
[4] D. P. Mitchell and P. N. Powers, "Bragg reflection of slow neutrons," *Physical Review,* vol. 50, no. 5, p. 486, 1936.
[5] P. Preiswerk and H. von Halban, "Preuve experimental de la diffraction des neutrons," *CR Acad. Sci. Paris,* vol. 203, pp. 73-75, 1936.
[6] M. P. Blakeley, S. S. Hasnain, and S. V. Antonyuk, "Sub-atomic resolution X-ray crystallography and neutron crystallography: promise, challenges and potential," *IUCrJ,* vol. 2, no. 4, pp. 464-474, 2015.
[7] M. P. Blakeley, P. Langan, N. Niimura, and A. Podjarny, "Neutron crystallography: opportunities, challenges, and limitations," in *Current Opinion in Structural Biology*, ed, 2008.
[8] E. Oksanen, J. C.-H. Chen, and S. Z. Fisher, "Neutron Crystallography for the Study of Hydrogen Bonds in Macromolecules," *Molecules,* vol. 22, no. 4, p. 596, 2017-04-07 2017, doi: 10.3390/molecules22040596.
[9] E. Oksanen, M. P. Blakeley, M. El-Hajji, U. Ryde, and M. Budayova-Spano, "The neutron structure of urate oxidase resolves a long-standing mechanistic conundrum and reveals unexpected changes in protonation," *PLoS One,* vol. 9, no. 1, p. e86651, 2014.
[10] I. T. Weber *et al.*, "Joint X-ray/Neutron Crystallographic Study of HIV-1 Protease with Clinical Inhibitor Amprenavir: Insights for Drug Design," *Journal of Medicinal Chemistry,* vol. 56, no. 13, pp. 5631-5635, 2013-07-11 2013, doi: 10.1021/jm400684f.
[11] K. Koruza *et al.*, "Structural comparison of protiated, H/D-exchanged and deuterated human carbonic anhydrase IX," *Acta Crystallogr D Struct Biol,* vol. 75, no. Pt 10, pp. 895-903, Oct 1 2019, doi: 10.1107/S2059798319010027.
[12] P. S. Langan, V. G. Vandavasi, B. Sullivan, J. Harp, K. Weiss, and L. Coates, "Crystallization of a potassium ion channel and X-ray and neutron data collection," *Acta Crystallographica Section F Structural Biology Communications,* vol. 75, no. 6, pp. 435-438, 2019-06-01 2019, doi: 10.1107/s2053230x19006630.

[13] R. Ashkar *et al.*, "Neutron scattering in the biological sciences: progress and prospects," *Acta Crystallographica Section D: Structural Biology,* vol. 74, no. 12, pp. 1129-1168, 2018.
[14] V. F. Sears, "Neutron scattering lengths and cross sections," *Neutron News,* 1992, doi: 10.1080/10448639208218770.
[15] T. Gonen *et al.*, "Lipid–protein interactions in double-layered two-dimensional AQP0 crystals," *Nature,* vol. 438, no. 7068, pp. 633-638, 2005.
[16] K. Mitsuoka *et al.*, "The structure of bacteriorhodopsin at 3.0 Å resolution based on electron crystallography: implication of the charge distribution," *Journal of molecular biology,* vol. 286, no. 3, pp. 861-882, 1999.
[17] R. Henderson, J. M. Baldwin, T. A. Ceska, F. Zemlin, E. Beckmann, and K. H. Downing, "Model for the structure of bacteriorhodopsin based on high-resolution electron cryo-microscopy," *Journal of molecular biology,* vol. 213, no. 4, pp. 899-929, 1990.
[18] K. Yonekura, K. Kato, M. Ogasawara, M. Tomita, and C. Toyoshima, "Electron crystallography of ultrathin 3D protein crystals: atomic model with charges," *Proc Natl Acad Sci U S A,* vol. 112, no. 11, pp. 3368-73, Mar 17 2015, doi: 10.1073/pnas.1500724112.
[19] R. M. Glaeser, "Electron crystallography of biological macromolecules," *Annual Review of Physical Chemistry,* vol. 36, no. 1, pp. 243-275, 1985.
[20] D. Shi, B. L. Nannenga, M. G. Iadanza, and T. Gonen, "Three-dimensional electron crystallography of protein microcrystals," *Elife,* vol. 2, p. e01345, Nov 19 2013, doi: 10.7554/eLife.01345.
[21] J. Dubochet and A. McDowall, "Vitrification of pure water for electron microscopy," *Journal of Microscopy,* vol. 124, no. 3, pp. 3-4, 1981.
[22] R. Henderson and P. N. T. Unwin, "Three-dimensional model of purple membrane obtained by electron microscopy," *Nature,* vol. 257, no. 5521, pp. 28-32, 1975.
[23] C. Suloway *et al.*, "Automated molecular microscopy: the new Leginon system," *Journal of structural biology,* vol. 151, no. 1, pp. 41-60, 2005.
[24] M. Liao, E. Cao, D. Julius, and Y. Cheng, "Structure of the TRPV1 ion channel determined by electron cryo-microscopy," *Nature,* vol. 504, no. 7478, pp. 107-112, 2013.
[25] K. Murata *et al.*, "Structural determinants of water permeation through aquaporin-1," *Nature,* vol. 407, no. 6804, pp. 599-605, 2000.
[26] P. Lu *et al.*, "Three-dimensional structure of human γ-secretase," *Nature,* vol. 512, no. 7513, pp. 166-170, 2014.
[27] M. R. Baker, G. Fan, and I. I. Serysheva, "Single-particle cryo-EM of the ryanodine receptor channel in an aqueous environment," *European journal of translational myology,* vol. 25, no. 1, p. 35, 2015.
[28] A. P. Burada, R. Vinnakota, and J. Kumar, "Cryo-EM structures of the ionotropic glutamate receptor GluD1 reveal a non-swapped architecture," *Nature structural & molecular biology,* vol. 27, no. 1, pp. 84-91, 2020.
[29] R. Henderson, "The potential and limitations of neutrons, electrons and X-rays for atomic resolution microscopy of unstained biological molecules," *Q Rev Biophys,* vol. 28, no. 2, pp. 171-93, May 1995, doi: 10.1017/s003358350000305x.
[30] M. Khoshouei, R. Danev, J. M. Plitzko, and W. Baumeister, "Revisiting the structure of hemoglobin and myoglobin with cryo-electron microscopy," *Journal of molecular biology,* vol. 429, no. 17, pp. 2611-2618, 2017.

[31] M. Jaremko *et al.*, "High-Resolution NMR Determination of the Dynamic Structure of Membrane Proteins," *Angew Chem Int Ed Engl,* vol. 55, no. 35, pp. 10518-21, Aug 22 2016, doi: 10.1002/anie.201602639.
[32] S. H. Park *et al.*, "Structure of the chemokine receptor CXCR1 in phospholipid bilayers," *Nature,* vol. 491, no. 7426, pp. 779-783, 2012.
[33] N. J. Traaseth, L. Shi, R. Verardi, D. G. Mullen, G. Barany, and G. Veglia, "Structure and topology of monomeric phospholamban in lipid membranes determined by a hybrid solution and solid-state NMR approach," *Proceedings of the National Academy of Sciences,* vol. 106, no. 25, pp. 10165-10170, 2009.
[34] N. Das, J. Dai, I. Hung, M. Rajagopalan, H.-X. Zhou, and T. A. Cross, "Structure of CrgA, a cell division structural and regulatory protein from Mycobacterium tuberculosis, in lipid bilayers," *Proceedings of the National Academy of Sciences,* vol. 112, no. 2, pp. E119-E126, 2015.
[35] T. Ikeya, D. Ban, D. Lee, Y. Ito, K. Kato, and C. Griesinger, "Solution NMR views of dynamical ordering of biomacromolecules," *Biochimica et Biophysica Acta (BBA) - General Subjects,* vol. 1862, no. 2, pp. 287-306, 2018-02-01 2018, doi: 10.1016/j.bbagen.2017.08.020.
[36] T. Ikeya, P. Güntert, and Y. Ito, "Protein Structure Determination in Living Cells," *International Journal of Molecular Sciences,* vol. 20, no. 10, p. 2442, 2019-05-17 2019, doi: 10.3390/ijms20102442.
[37] V. Kanelis, J. D. Forman-Kay, and L. E. Kay, "Multidimensional NMR Methods for Protein Structure Determination," *IUBMB Life (International Union of Biochemistry and Molecular Biology: Life),* vol. 52, no. 6, pp. 291-302, 2001-12-01 2001, doi: 10.1080/152165401317291147.
[38] B. Jacrot, "The study of biological structures by neutron scattering from solution," *Reports on progress in physics,* vol. 39, no. 10, p. 911, 1976.
[39] A. Mcpherson, "Introduction to protein crystallization," *Methods,* vol. 34, no. 3, pp. 254-265, 2004-11-01 2004, doi: 10.1016/j.ymeth.2004.03.019.
[40] A. McPherson and J. A. Gavira, "Introduction to protein crystallization," *Acta Crystallographica Section F: Structural Biology Communications,* vol. 70, no. 1, pp. 2-20, 2014.
[41] N. Asherie, "Protein crystallization and phase diagrams," *Methods,* vol. 34, no. 3, pp. 266-272, 2004-11-01 2004, doi: 10.1016/j.ymeth.2004.03.028.
[42] N. Chayen, J. Akins, S. Campbell-Smith, and D. Blow, "Solubility of glucose isomerase in ammonium sulphate solutions," *Journal of Crystal Growth,* vol. 90, no. 1-3, pp. 112-116, 1988.
[43] N. Asherie, C. Ginsberg, S. Blass, A. Greenbaum, and S. Knafo, "Solubility of thaumatin," *Crystal Growth and Design,* vol. 8, no. 6, pp. 1815-1817, 2008.
[44] M. L. Pusey and K. Gernert, "A method for rapid liquid-solid phase solubility measurements using the protein lysozyme," *Journal of crystal growth,* vol. 88, no. 3, pp. 419-424, 1988.
[45] J.-F. Gaucher, M. Riès-Kautt, F. Reiss-Husson, and A. Ducruix, "Solubility diagram of the Rhodobacter sphaeroides
reaction center as a function of PEG concentration," *FEBS Letters,* vol. 401, no. 2-3, pp. 113-116, 1997-01-20 1997, doi: 10.1016/s0014-5793(96)01446-9.
[46] M. Ataka, K. Shinzawa-Itoh, and S. Yoshikawa, "Phase diagrams of a crystalline membrane protein, bovine heart cytochromec oxidase, in the salting-in region," *Journal of crystal growth,* vol. 122, no. 1-4, pp. 60-65, 1992.
[47] T. Bergfors, *Protein Crystallization: Techniques, Strategies, and Tips*. International University Line, 1999.

[48] B. Rupp, *Biomolecular crystallography: principles, practice, and application to structural biology*. Garland Science, 2009.
[49] F. Otálora, J. A. Gavira, J. D. Ng, and J. M. García-Ruiz, "Counterdiffusion methods applied to protein crystallization," *Progress in biophysics and molecular biology,* vol. 101, no. 1-3, pp. 26-37, 2009.
[50] J. Garcia-Ruiz, A. Moreno, C. Viedma, and M. Coll, "Crystal quality of lysozyme single crystals grown by the gel acupuncture method," *Materials research bulletin,* vol. 28, no. 6, pp. 541-546, 1993.
[51] S. J. Hjorth-Jensen, E. Oksanen, P. Nissen, and T. L.-M. Sørensen, "Prospects for membrane protein crystals in NMX," *Methods in enzymology,* vol. 634, pp. 47-68, 2020.
[52] N. E. Chayen, "A novel technique to control the rate of vapour diffusion, giving larger protein crystals," *Journal of Applied Crystallography,* vol. 30, no. 2, pp. 198-202, 1997.
[53] M. Caffrey, "Crystallizing membrane proteins for structure determination: use of lipidic mesophases," *Annual review of biophysics,* vol. 38, pp. 29-51, 2009.
[54] C. Ostermeier and H. Michel, "Crystallization of membrane proteins," *Current opinion in structural biology,* vol. 7, no. 5, pp. 697-701, 1997.
[55] G. Katona, U. Andreasson, E. M. Landau, L.-E. Andreasson, and R. Neutze, "Lipidic cubic phase crystal structure of the photosynthetic reaction centre from Rhodobacter sphaeroides at 2.35 Å resolution," *Journal of molecular biology,* vol. 331, no. 3, pp. 681-692, 2003.
[56] V. Cherezov *et al.*, "High-resolution crystal structure of an engineered human β2-adrenergic G protein–coupled receptor," *science,* vol. 318, no. 5854, pp. 1258-1265, 2007.
[57] V.-P. Jaakola *et al.*, "The 2.6 angstrom crystal structure of a human A2A adenosine receptor bound to an antagonist," *Science,* vol. 322, no. 5905, pp. 1211-1217, 2008.
[58] S. Agah and S. Faham, "Crystallization of Membrane Proteins in Bicelles," in *Membrane Protein Structure and Dynamics*: Humana Press, 2012, pp. 3-16.
[59] E. A. Stura and I. A. Wilson, "Applications of the streak seeding technique in protein crystallization," *Journal of crystal growth,* vol. 110, no. 1-2, pp. 270-282, 1991.
[60] T. Bergfors, "Seeds to crystals," *Journal of structural biology,* vol. 142, no. 1, pp. 66-76, 2003.
[61] E. A. Stura and I. A. Wilson, "Analytical and production seeding techniques," *Methods,* vol. 1, no. 1, pp. 38-49, 1990.
[62] V. Kelpšas, B. Lafumat, M. P. Blakeley, N. Coquelle, E. Oksanen, and C. Von Wachenfeldt, "Perdeuteration, large crystal growth and neutron data collection of Leishmania mexicana triose-phosphate isomerase E65Q variant," *Acta Crystallographica Section F: Structural Biology Communications,* vol. 75, no. 4, pp. 260-269, 2019.
[63] F. Fadel, Y. Zhao, A. Cousido-Siah, F. X. Ruiz, A. Mitschler, and A. Podjarny, "X-ray crystal structure of the full length human chitotriosidase (CHIT1) reveals features of its chitin binding domain," *PloS one,* vol. 11, no. 4, p. e0154190, 2016.
[64] E. Oksanen, M. P. Blakeley, F. Bonnete, M. T. Dauvergne, F. Dauvergne, and M. Budayova-Spano, "Large crystal growth by thermal control allows combined X-ray and neutron crystallographic studies to elucidate the protonation states in Aspergillus flavus urate oxidase," *J R Soc Interface,* vol. 6 Suppl 5, pp. S599-610, Oct 6 2009, doi: 10.1098/rsif.2009.0162.focus.
[65] M. Ataka and M. Asai, "Systematic studies on the crystallization of lysozyme: Determination and use of phase diagrams," *Journal of Crystal Growth,* vol. 90, no. 1-3, pp. 86-93, 1988.

[66] V. Mikol and R. Giegé, "Phase diagram of a crystalline protein: Determination of the solubility of concanavalin A by a microquantitation assay," *Journal of crystal growth,* vol. 97, no. 2, pp. 324-332, 1989.
[67] R. M. Garavito and D. Picot, "Crystallization of membrane proteins: a minireview," *Journal of crystal growth,* vol. 110, no. 1-2, pp. 89-95, 1991.
[68] B. Lorber, L. J. DeLucas, and J. B. Bishop, "Changes in the physico-chemical properties of the detergent octyl glucoside during membrane protein crystallization using a salt as the precipitant," *Journal of crystal growth,* vol. 110, no. 1-2, pp. 103-113, 1991.
[69] N. Junius, E. Vahdatahar, E. Oksanen, J.-L. Ferrer, and M. Budayova-Spano, "Optimization of crystallization of biological macromolecules using dialysis combined with temperature control," *Journal of Applied Crystallography,* vol. 53, no. 3, 2020.
[70] M. Budayova-Spano *et al.*, "Production and X-ray crystallographic analysis of fully deuterated human carbonic anhydrase II," *Acta Crystallographica Section F: Structural Biology and Crystallization Communications,* vol. 62, no. 1, pp. 6-9, 2006.
[71] R. Wierenga, E. Kapetaniou, and R. Venkatesan, "Triosephosphate isomerase: a highly evolved biocatalyst," *Cellular and molecular life sciences,* vol. 67, no. 23, pp. 3961-3982, 2010.
[72] S. HELFERT, A. M. Estévez, B. Bakker, P. Michels, and C. Clayton, "Roles of triosephosphate isomerase and aerobic metabolism in Trypanosoma brucei," *Biochemical Journal,* vol. 357, no. 1, pp. 117-125, 2001.
[73] F. Orosz, J. Oláh, and J. Ovádi, "Triosephosphate isomerase deficiency: new insights into an enigmatic disease," *Biochimica et Biophysica Acta (BBA)-Molecular Basis of Disease,* vol. 1792, no. 12, pp. 1168-1174, 2009.
[74] F. Orosz, J. Olah, and J. Ovadi, "Triosephosphate isomerase deficiency: facts and doubts," *IUBMB life,* vol. 58, no. 12, pp. 703-715, 2006.
[75] S. C. Blacklow, R. T. Raines, W. A. Lim, P. D. Zamore, and J. R. Knowles, "Triosephosphate isomerase catalysis is diffusion controlled," *Biochemistry,* vol. 27, no. 4, pp. 1158-1165, 1988.
[76] W. J. Albery and J. R. Knowles, "Free-energy profile for the reaction catalyzed by triosephosphate isomerase," *Biochemistry,* vol. 15, no. 25, pp. 5627-5631, 1976.
[77] S. Rozovsky and A. E. McDermott, "Substrate product equilibrium on a reversible enzyme, triosephosphate isomerase," *Proceedings of the National Academy of Sciences,* vol. 104, no. 7, pp. 2080-2085, 2007.
[78] W. J. Albery and J. R. Knowles, "Evolution of enzyme function and the development of catalytic efficiency," *Biochemistry,* vol. 15, no. 25, pp. 5631-5640, 1976.
[79] D. Banner *et al.*, "Structure of chicken muscle triose phosphate isomerase determined crystallographically at 2.5 Å resolution: using amino acid sequence data," *Nature,* vol. 255, no. 5510, pp. 609-614, 1975.
[80] N. Nagano, E. Gail Hutchinson, and J. M. Thornton, "Barrel structures in proteins: automatic identification and classification including a sequence analysis of TIM barrels," *Protein Science,* vol. 8, no. 10, pp. 2072-2084, 1999.
[81] R. Wierenga, "The TIM-barrel fold: a versatile framework for efficient enzymes," *FEBS letters,* vol. 492, no. 3, pp. 193-198, 2001.
[82] D. L. Pompliano, A. Peyman, and J. R. Knowles, "Stabilization of a reaction intermediate as a catalytic device: definition of the functional role of the flexible loop in triosephosphate isomerase," *Biochemistry,* vol. 29, no. 13, pp. 3186-3194, 1990.
[83] D. Röthlisberger *et al.*, "Kemp elimination catalysts by computational enzyme design," *Nature,* vol. 453, no. 7192, pp. 190-195, 2008.

[84] W. W. Cleland, P. A. Frey, and J. A. Gerlt, "The low barrier hydrogen bond in enzymatic catalysis," *Journal of Biological Chemistry,* vol. 273, no. 40, pp. 25529-25532, 1998.

[85] G. Jogl, S. Rozovsky, A. E. McDermott, and L. Tong, "Optimal alignment for enzymatic proton transfer: structure of the Michaelis complex of triosephosphate isomerase at 1.2-Å resolution," *Proceedings of the National Academy of Sciences,* vol. 100, no. 1, pp. 50-55, 2003.

[86] M. Alahuhta and R. K. Wierenga, "Atomic resolution crystallography of a complex of triosephosphate isomerase with a reaction-intermediate analog: New insight in the proton transfer reaction mechanism," *Proteins: Structure, Function, and Bioinformatics,* vol. 78, no. 8, pp. 1878-1888, 2010-06-01 2010, doi: 10.1002/prot.22701.

[87] I. Kursula and R. K. Wierenga, "Crystal structure of triosephosphate isomerase complexed with 2-phosphoglycolate at 0.83-Å resolution," *Journal of Biological Chemistry,* vol. 278, no. 11, pp. 9544-9551, 2003.

[88] M. M. Malabanan, L. Nitsch-Velasquez, T. L. Amyes, and J. P. Richard, "Magnitude and origin of the enhanced basicity of the catalytic glutamate of triosephosphate isomerase," *Journal of the American Chemical Society,* vol. 135, no. 16, pp. 5978-5981, 2013.

[89] W. Schliebs, N. Thanki, R. Eritja, and R. Wierenga, "Active site properties of monomeric triosephosphate isomerase (monoTIM) as deduced from mutational and structural studies," *Protein science,* vol. 5, no. 2, pp. 229-239, 1996.

[90] J. R. Knowles, "Enzyme catalysis: not different, just better," *Nature,* vol. 350, no. 6314, pp. 121-124, 1991.

[91] S. C. Blacklow, K. D. Liu, and J. R. Knowles, "Stepwise improvements in catalytic effectiveness: independence and interdependence in combinations of point mutations of a sluggish triosephosphate isomerase," *Biochemistry,* vol. 30, no. 34, pp. 8470-8476, 1991.

[92] M. Samanta, M. Murthy, H. Balaram, and P. Balaram, "Revisiting the mechanism of the triosephosphate isomerase reaction: the role of the fully conserved glutamic acid 97 residue," *ChemBioChem,* vol. 12, no. 12, pp. 1886-1896, 2011.

[93] J. P. Richard, "A Paradigm for Enzyme-Catalyzed Proton Transfer at Carbon: Triosephosphate Isomerase," *Biochemistry,* vol. 51, no. 13, pp. 2652-2661, 2012-04-03 2012, doi: 10.1021/bi300195b.

[94] P. B. Moore, "[50] The preparation of deuterated ribosomal materials for neutron scattering," in *Methods in enzymology,* vol. 59: Elsevier, 1979, pp. 639-655.

[95] G. A. Olah, S. E. Rokop, C.-L. A. Wang, S. L. Blechner, and J. Trewhella, "Troponin I encompasses an extended troponin C in the Ca2+-bound complex: a small-angle X-ray and neutron scattering study," *Biochemistry,* vol. 33, no. 27, pp. 8233-8239, 1994.

[96] D. M. LeMaster and F. M. Richards, "Preparative-scale isolation of isotopically labeled amino acids," *Analytical biochemistry,* vol. 122, no. 2, pp. 238-247, 1982.

[97] A. Sosa-Peinado, D. Mustafi, and M. W. Makinen, "Overexpression and biosynthetic deuterium enrichment of TEM-1 β-lactamase for structural characterization by magnetic resonance methods," *Protein expression and purification,* vol. 19, no. 2, pp. 235-245, 2000.

[98] F. Meilleur, M.-T. Dauvergne, I. Schlichting, and D. A. Myles, "Production and X-ray crystallographic analysis of fully deuterated cytochrome P450cam," *Acta Crystallographica Section D: Biological Crystallography,* vol. 61, no. 5, pp. 539-544, 2005.

[99] I. Hazemann *et al.*, "High-resolution neutron protein crystallography with radically small crystal volumes: application of perdeuteration to human aldose reductase," *Acta Crystallographica Section D: Biological Crystallography,* vol. 61, no. 10, pp. 1413-1417, 2005.

[100] Anthony P. Duff*, Karyn L. Wilde*, Agata Rekas*, Vanessa Lake*, Peter J. Holden†, "Robust High-Yield Methodologies for 2H and 2H/15N/13C Labeling
of Proteins for Structural Investigations Using Neutron Scattering and NMR," *Methods in Enzymology,* vol. 565, 2015.

[101] O. Paliy, D. Bloor, D. Brockwell, P. Gilbert, and J. Barber, "Improved methods of cultivation and production of deuteriated proteins from E. coli strains grown on fully deuteriated minimal medium," *Journal of Applied Microbiology,* 2003, doi: 10.1046/j.1365-2672.2003.01866.x.

[102] K. A. Datsenko and B. L. Wanner, "One-step inactivation of chromosomal genes in Escherichia coli K-12 using PCR products," *Proceedings of the National Academy of Sciences,* vol. 97, no. 12, pp. 6640-6645, 2000.

[103] C. A. Schnaitman, "Effect of ethylenediaminetetraacetic acid, Triton X-100, and lysozyme on the morphology and chemical composition of isolated cell walls of Escherichia coli," *Journal of Bacteriology,* vol. 108, no. 1, pp. 553-563, 1971.

[104] F. Baneyx and M. Mujacic, "Recombinant protein folding and misfolding in Escherichia coli," *Nature biotechnology,* vol. 22, no. 11, pp. 1399-1408, 2004.

[105] A. Vera, N. González-Montalbán, A. Arís, and A. Villaverde, "The conformational quality of insoluble recombinant proteins is enhanced at low growth temperatures," *Biotechnology and bioengineering,* vol. 96, no. 6, pp. 1101-1106, 2007.

[106] O. Paliy and T. S. Gunasekera, "Growth of E. coli BL21 in minimal media with different gluconeogenic carbon sources and salt contents," *Applied microbiology and biotechnology,* vol. 73, no. 5, pp. 1169-1172, 2007.

[107] V. Kelpšas and C. v. Wachenfeldt, "Strain improvement of Escherichia coli K-12 for recombinant production of deuterated proteins," *Scientific Reports,* 2019, doi: 10.1038/s41598-019-54196-w.

[108] K. Koruza, B. Lafumat, Végvári, W. Knecht, and S. Z. Fisher, "Deuteration of human carbonic anhydrase for neutron crystallography: Cell culture media, protein thermostability, and crystallization behavior," *Archives of Biochemistry and Biophysics,* 2018, doi: 10.1016/j.abb.2018.03.008.

[109] K. D. Rand, M. Zehl, and T. J. Jørgensen, "Measuring the hydrogen/deuterium exchange of proteins at high spatial resolution by mass spectrometry: overcoming gas-phase hydrogen/deuterium scrambling," *Accounts of chemical research,* vol. 47, no. 10, pp. 3018-3027, 2014.

[110] D. Resetca and D. J. Wilson, "Characterizing rapid, activity-linked conformational transitions in proteins via sub-second hydrogen deuterium exchange mass spectrometry," *FEBS Journal,* vol. 280, no. 22, pp. 5616-5625, 2013-11-01 2013, doi: 10.1111/febs.12332.

[111] H. Naveed, D. Jimenez-Morales, J. Tian, V. Pasupuleti, L. J. Kenney, and J. Liang, "Engineered oligomerization state of OmpF protein through computational design decouples oligomer dissociation from unfolding," *Journal of molecular biology,* vol. 419, no. 1-2, pp. 89-101, 2012.

[112] O. D. Novikova *et al.*, "Peculiarities of thermal denaturation of OmpF porin from Yersinia ruckeri," *Molecular BioSystems,* vol. 13, no. 9, pp. 1854-1862, 2017.

[113] E. Borek and D. Rittenberg, "Anomalous growth of microorganisms produced by changes in isotopes in their environment," *Proceedings of the National Academy of Sciences of the United States of America,* vol. 46, no. 6, p. 777, 1960.

[114] W. Kightlinger, K. Chen, A. Pourmir, D. W. Crunkleton, G. L. Price, and T. W. Johannes, "Production and characterization of algae extract from Chlamydomonas reinhardtii," *Electronic Journal of Biotechnology,* vol. 17, no. 1, pp. 3-3, 2014.
[115] B. Franke *et al.*, "Production of isotope-labeled proteins in insect cells for NMR," *Journal of biomolecular NMR,* vol. 71, no. 3, pp. 173-184, 2018.
[116] F. Löhr, V. Katsemi, J. Hartleib, U. Günther, and H. Rüterjans, "A strategy to obtain backbone resonance assignments of deuterated proteins in the presence of incomplete amide 2 H/1 H back-exchange," *Journal of biomolecular NMR,* vol. 25, no. 4, pp. 291-311, 2003.
[117] Y. Ashani and G. N. Catravas, "Highly reactive impurities in Triton X-100 and Brij 35: partial characterization and removal," *Analytical biochemistry,* vol. 109, no. 1, pp. 55-62, 1980.
[118] M. Turowski *et al.*, "Deuterium isotope effects on hydrophobic interactions: the importance of dispersion interactions in the hydrophobic phase," *Journal of the American Chemical Society,* vol. 125, no. 45, pp. 13836-13849, 2003.
[119] W. B. O'Dell, A. M. Bodenheimer, and F. Meilleur, "Neutron protein crystallography: A complementary tool for locating hydrogens in proteins," *Arch Biochem Biophys,* vol. 602, pp. 48-60, Jul 15 2016, doi: 10.1016/j.abb.2015.11.033.
[120] M. Budayova-Spano, K. Koruza, and Z. Fisher, "Large crystal growth for neutron protein crystallography," *Methods in enzymology,* vol. 634, pp. 21-46, 2020.
[121] E. Yamashita, M. V. Zhalnina, S. D. Zakharov, O. Sharma, and W. A. Cramer, "Crystal structures of the OmpF porin: Function in a colicin translocon," *EMBO Journal,* 2008, doi: 10.1038/emboj.2008.137.
[122] A. Stetsenko and A. Guskov, "An overview of the top ten detergents used for membrane protein crystallization," *Crystals,* vol. 7, no. 7, p. 197, 2017.
[123] J. Ma *et al.*, "The effect of residual Triton X-100 on structural stability and infection activity of adenovirus particles," *Molecular Therapy-Methods & Clinical Development,* vol. 19, pp. 35-46, 2020.
[124] S. Tanaka and M. Ataka, "Protein crystallization induced by polyethylene glycol: A model study using apoferritin," *The Journal of chemical physics,* vol. 117, no. 7, pp. 3504-3510, 2002.
[125] C. Hitscherich, V. Aseyev, J. Wiencek, and P. J. Loll, "Effects of PEG on detergent micelles: implications for the crystallization of integral membrane proteins," *Acta Crystallographica Section D: Biological Crystallography,* vol. 57, no. 7, pp. 1020-1029, 2001.
[126] R. M. Garavito and D. Picot, "The art of crystallizing membrane proteins," *Methods,* vol. 1, no. 1, pp. 57-69, 1990.
[127] G. T. Detitta and J. R. Luft, "Rate of water equilibration in vapor-diffusion crystallization: dependence on the residual pressure of air in the vapor space," *Acta Crystallographica Section D: Biological Crystallography,* vol. 51, no. 5, pp. 786-791, 1995.
[128] J. M. García-Ruiz, F. Otálora, and A. García-Caballero, "The role of mass transport in protein crystallization," *Acta Crystallographica Section F: Structural Biology Communications,* vol. 72, no. 2, pp. 96-104, 2016.
[129] W. F. Berg, "Crystal growth from solutions," *Proceedings of the Royal Society of London. Series A - Mathematical and Physical Sciences,* vol. 164, no. 916, pp. 79-95, 1938-01-07 1938, doi: 10.1098/rspa.1938.0006.
[130] F. Manzoni *et al.*, "Perdeuteration, crystallization, data collection and comparison of five neutron diffraction data sets of complexes of human galectin-3C," *Acta Crystallographica Section D: Structural Biology,* vol. 72, no. 11, pp. 1194-1202, 2016.

[131] X. Liu, B. L. Hanson, P. Langan, and R. E. Viola, "The effect of deuteration on protein structure: a high-resolution comparison of hydrogenous and perdeuterated haloalkane dehalogenase," *Acta Crystallographica Section D: Biological Crystallography,* vol. 63, no. 9, pp. 1000-1008, 2007.
[132] P. D. Shaw Stewart, S. A. Kolek, R. A. Briggs, N. E. Chayen, and P. F. M. Baldock, "Random Microseeding: A Theoretical and Practical Exploration of Seed Stability and Seeding Techniques for Successful Protein Crystallization," *Crystal Growth & Design,* vol. 11, no. 8, pp. 3432-3441, 2011-08-03 2011, doi: 10.1021/cg2001442.
[133] T. Bergfors, "Succeeding with seeding: some practical advice," in *Evolving Methods for Macromolecular Crystallography*: Springer, 2007, pp. 1-10.
[134] G. C. Kresheck, H. Schneider, and H. A. Scheraga, "The Effect of D2O on the Thermal Stability of Proteins. Thermodynamic Parameters for the Transfer of Model Compounds from H2O to D2O1, 2," *The Journal of physical chemistry,* vol. 69, no. 9, pp. 3132-3144, 1965.
[135] P. Fromme and H. T. Witt, "Improved isolation and crystallization of photosystem I for structural analysis," *Biochimica et Biophysica Acta (BBA)-Bioenergetics,* vol. 1365, no. 1-2, pp. 175-184, 1998.
[136] C. R. D. Lancaster, A. Kröger, M. Auer, and H. Michel, "Structure of fumarate reductase from Wolinella succinogenes at 2.2 Å resolution," *Nature,* vol. 402, no. 6760, pp. 377-385, 1999-11-01 1999, doi: 10.1038/46483.
[137] R. Dods *et al.*, "From macrocrystals to microcrystals: a strategy for membrane protein serial crystallography," *Structure,* vol. 25, no. 9, pp. 1461-1468. e2, 2017.
[138] S. A. Kolek, B. Bräuning, and P. D. Shaw Stewart, "A novel microseeding method for the crystallization of membrane proteins in lipidic cubic phase," *Acta Crystallographica Section F: Structural Biology Communications,* vol. 72, no. 4, pp. 307-312, 2016.
[139] I. Moraes, G. Evans, J. Sanchez-Weatherby, S. Newstead, and P. D. S. Stewart, "Membrane protein structure determination—the next generation," *Biochimica et Biophysica Acta (BBA)-Biomembranes,* vol. 1838, no. 1, pp. 78-87, 2014.
[140] M. Budayova-Spano, F. Dauvergne, M. Audiffren, T. Bactivelane, and S. Cusack, "A methodology and an instrument for the temperature-controlled optimization of crystal growth," *Acta Crystallographica Section D: Biological Crystallography,* vol. 63, no. 3, pp. 339-347, 2007.
[141] N. Candoni, R. Grossier, Z. Hammadi, R. Morin, and S. Veesler, "Practical physics behind growing crystals of biological macromolecules," *Protein and peptide letters,* vol. 19, no. 7, pp. 714-724, 2012.
[142] E. Oksanen, F. Dauvergne, A. Goldman, and M. Budayova-Spano, "Design of a novel Peltier-based cooling device and its use in neutron diffraction data collection of perdeuterated yeast pyrophosphatase," *Journal of Applied Crystallography,* vol. 43, no. 5, pp. 1113-1120, 2010.
[143] J. Campbell, Q. Hao, M. Harding, N. Nguti, and C. Wilkinson, "LAUEGEN version 6.0 and INTLDM," *Journal of Applied Crystallography,* vol. 31, no. 3, pp. 496-502, 1998.
[144] P. Evans, "Scaling and assessment of data quality," *Acta Crystallographica Section D: Biological Crystallography,* vol. 62, no. 1, pp. 72-82, 2006.
[145] P. D. Adams *et al.*, "The Phenix software for automated determination of macromolecular structures," *Methods,* vol. 55, no. 1, pp. 94-106, 2011.
[146] P. Emsley and K. Cowtan, "Coot: model-building tools for molecular graphics," *Acta crystallographica section D: biological crystallography,* vol. 60, no. 12, pp. 2126-2132, 2004.

[147] J. R. Morrow, T. L. Amyes, and J. P. Richard, "Phosphate binding energy and catalysis by small and large molecules," *Accounts of chemical research*, vol. 41, no. 4, pp. 539-548, 2008.
[148] Q. Cui and M. Karplus, "Quantum mechanics/molecular mechanics studies of triosephosphate isomerase-catalyzed reactions: effect of geometry and tunneling on proton-transfer rate constants," *Journal of the American Chemical Society*, vol. 124, no. 12, pp. 3093-3124, 2002.
[149] P. J. Lodi and J. R. Knowles, "Neutral imidazole is the electrophile in the reaction catalyzed by triosephosphate isomerase: structural origins and catalytic implications," *Biochemistry*, vol. 30, no. 28, pp. 6948-6956, 1991.
[150] P. J. Lodi, L. C. Chang, J. R. Knowles, and E. A. Komives, "Triosephosphate isomerase requires a positively charged active site: the role of lysine-12," *Biochemistry*, vol. 33, no. 10, pp. 2809-2814, 1994.
[151] E. A. Komives, L. C. Chang, E. Lolis, R. F. Tilton, G. A. Petsko, and J. R. Knowles, "Electrophilic catalysis in triosephosphate isomerase: the role of histidine-95," *Biochemistry*, vol. 30, no. 12, pp. 3011-3019, 1991.
[152] E. A. Ruben *et al.*, "Ground state destabilization from a positioned general base in the ketosteroid isomerase active site," *Biochemistry*, vol. 52, no. 6, pp. 1074-1081, 2013.
[1] J. C. Kendrew, G. Bodo, H. M. Dintzis, R. Parrish, H. Wyckoff, and D. C. Phillips, "A three-dimensional model of the myoglobin molecule obtained by x-ray analysis," *Nature*, vol. 181, no. 4610, pp. 662-666, 1958.
[2] J. Drenth, *Principles of protein X-ray crystallography*. Springer Science & Business Media, 2007.
[3] T. Huxford, "X-Ray Crystallography," 2013.
[4] D. P. Mitchell and P. N. Powers, "Bragg reflection of slow neutrons," *Physical Review*, vol. 50, no. 5, p. 486, 1936.
[5] P. Preiswerk and H. von Halban, "Preuve experimental de la diffraction des neutrons," *CR Acad. Sci. Paris*, vol. 203, pp. 73-75, 1936.
[6] M. P. Blakeley, S. S. Hasnain, and S. V. Antonyuk, "Sub-atomic resolution X-ray crystallography and neutron crystallography: promise, challenges and potential," *IUCrJ*, vol. 2, no. 4, pp. 464-474, 2015.
[7] M. P. Blakeley, P. Langan, N. Niimura, and A. Podjarny, "Neutron crystallography: opportunities, challenges, and limitations," in *Current Opinion in Structural Biology*, ed, 2008.
[8] E. Oksanen, J. C.-H. Chen, and S. Z. Fisher, "Neutron Crystallography for the Study of Hydrogen Bonds in Macromolecules," *Molecules*, vol. 22, no. 4, p. 596, 2017-04-07 2017, doi: 10.3390/molecules22040596.
[9] E. Oksanen, M. P. Blakeley, M. El-Hajji, U. Ryde, and M. Budayova-Spano, "The neutron structure of urate oxidase resolves a long-standing mechanistic conundrum and reveals unexpected changes in protonation," *PLoS One*, vol. 9, no. 1, p. e86651, 2014.
[10] I. T. Weber *et al.*, "Joint X-ray/Neutron Crystallographic Study of HIV-1 Protease with Clinical Inhibitor Amprenavir: Insights for Drug Design," *Journal of Medicinal Chemistry*, vol. 56, no. 13, pp. 5631-5635, 2013-07-11 2013, doi: 10.1021/jm400684f.
[11] K. Koruza *et al.*, "Structural comparison of protiated, H/D-exchanged and deuterated human carbonic anhydrase IX," *Acta Crystallogr D Struct Biol*, vol. 75, no. Pt 10, pp. 895-903, Oct 1 2019, doi: 10.1107/S2059798319010027.
[12] P. S. Langan, V. G. Vandavasi, B. Sullivan, J. Harp, K. Weiss, and L. Coates, "Crystallization of a potassium ion channel and X-ray and neutron data collection," *Acta Crystallographica Section F Structural Biology Communications*, vol. 75, no. 6, pp. 435-438, 2019-06-01 2019, doi: 10.1107/s2053230x19006630.

[13] R. Ashkar *et al.*, "Neutron scattering in the biological sciences: progress and prospects," *Acta Crystallographica Section D: Structural Biology*, vol. 74, no. 12, pp. 1129-1168, 2018.
[14] V. F. Sears, "Neutron scattering lengths and cross sections," *Neutron News*, 1992, doi: 10.1080/10448639208218770.
[15] T. Renner, *Quantities, units and symbols in physical chemistry*. Royal Society of Chemistry, 2007.
[16] E. Borek and D. Rittenberg, "Anomalous growth of microorganisms produced by changes in isotopes in their environment," *Proceedings of the National Academy of Sciences of the United States of America*, vol. 46, no. 6, p. 777, 1960.
[17] B. Kollars and R. Geraets, "Effects of Deuterium on Chlamydomonas reinhardtii," *The Journal of Undergraduate Research*, vol. 6, no. 1, p. 12, 2008.
[18] P. R. Gross and W. Spindel, "Mitotic arrest by deuterium oxide," *Science*, vol. 131, no. 3392, pp. 37-39, 1960.
[19] K. Unno, T. Kishido, M. Morioka, S. Okada, and N. Oku, "Increased expression of Hsp70 for resistance to deuterium oxide in a yeast mutant cell line," *Biological and Pharmaceutical Bulletin*, vol. 26, no. 6, pp. 799-802, 2003.
[20] M. U. Caglar *et al.*, "The E. coli molecular phenotype under different growth conditions," *Scientific reports*, vol. 7, no. 1, pp. 1-15, 2017.
[21] V. Kelpšas and C. von Wachenfeldt, "Strain improvement of Escherichia coli K-12 for recombinant production of deuterated proteins," *Scientific reports*, vol. 9, no. 1, pp. 1-9, 2019.
[22] G. Walsh and R. Jefferis, "Post-translational modifications in the context of therapeutic proteins," *Nature biotechnology*, vol. 24, no. 10, pp. 1241-1252, 2006.
[23] V. Kelpšas and C. v. Wachenfeldt, "Strain improvement of Escherichia coli K-12 for recombinant production of deuterated proteins," *Scientific Reports*, 2019, doi: 10.1038/s41598-019-54196-w.
[24] O. Paliy, D. Bloor, D. Brockwell, P. Gilbert, and J. Barber, "Improved methods of cultivation and production of deuteriated proteins from E. coli strains grown on fully deuteriated minimal medium," *Journal of Applied Microbiology*, 2003, doi: 10.1046/j.1365-2672.2003.01866.x.
[25] M. Haertlein, M. Moulin, J. M. Devos, V. Laux, O. Dunne, and V. T. Forsyth, "Biomolecular deuteration for neutron structural biology and dynamics," *Methods in enzymology*, vol. 566, pp. 113-157, 2016.
[26] T. Hiromoto *et al.*, "Neutron structure of the T26H mutant of T4 phage lysozyme provides insight into the catalytic activity of the mutant enzyme and how it differs from that of wild type," *Protein Science*, vol. 26, no. 10, pp. 1953-1963, 2017.
[27] R. Wierenga, E. Kapetaniou, and R. Venkatesan, "Triosephosphate isomerase: a highly evolved biocatalyst," *Cellular and molecular life sciences*, vol. 67, no. 23, pp. 3961-3982, 2010.
[28] S. HELFERT, A. M. Estévez, B. Bakker, P. Michels, and C. Clayton, "Roles of triosephosphate isomerase and aerobic metabolism in Trypanosoma brucei," *Biochemical Journal*, vol. 357, no. 1, pp. 117-125, 2001.
[29] F. Orosz, J. Oláh, and J. Ovádi, "Triosephosphate isomerase deficiency: new insights into an enigmatic disease," *Biochimica et Biophysica Acta (BBA)-Molecular Basis of Disease*, vol. 1792, no. 12, pp. 1168-1174, 2009.
[30] F. Orosz, J. Olah, and J. Ovadi, "Triosephosphate isomerase deficiency: facts and doubts," *IUBMB life*, vol. 58, no. 12, pp. 703-715, 2006.

[31] S. C. Blacklow, R. T. Raines, W. A. Lim, P. D. Zamore, and J. R. Knowles, "Triosephosphate isomerase catalysis is diffusion controlled," *Biochemistry,* vol. 27, no. 4, pp. 1158-1165, 1988.
[32] W. J. Albery and J. R. Knowles, "Free-energy profile for the reaction catalyzed by triosephosphate isomerase," *Biochemistry,* vol. 15, no. 25, pp. 5627-5631, 1976.
[33] S. Rozovsky and A. E. McDermott, "Substrate product equilibrium on a reversible enzyme, triosephosphate isomerase," *Proceedings of the National Academy of Sciences,* vol. 104, no. 7, pp. 2080-2085, 2007.
[34] W. J. Albery and J. R. Knowles, "Evolution of enzyme function and the development of catalytic efficiency," *Biochemistry,* vol. 15, no. 25, pp. 5631-5640, 1976.
[35] D. Banner *et al.*, "Structure of chicken muscle triose phosphate isomerase determined crystallographically at 2.5 Å resolution: using amino acid sequence data," *Nature,* vol. 255, no. 5510, pp. 609-614, 1975.
[36] N. Nagano, E. Gail Hutchinson, and J. M. Thornton, "Barrel structures in proteins: automatic identification and classification including a sequence analysis of TIM barrels," *Protein Science,* vol. 8, no. 10, pp. 2072-2084, 1999.
[37] R. Wierenga, "The TIM-barrel fold: a versatile framework for efficient enzymes," *FEBS letters,* vol. 492, no. 3, pp. 193-198, 2001.
[38] D. L. Pompliano, A. Peyman, and J. R. Knowles, "Stabilization of a reaction intermediate as a catalytic device: definition of the functional role of the flexible loop in triosephosphate isomerase," *Biochemistry,* vol. 29, no. 13, pp. 3186-3194, 1990.
[39] D. Röthlisberger *et al.*, "Kemp elimination catalysts by computational enzyme design," *Nature,* vol. 453, no. 7192, pp. 190-195, 2008.
[40] W. W. Cleland, P. A. Frey, and J. A. Gerlt, "The low barrier hydrogen bond in enzymatic catalysis," *Journal of Biological Chemistry,* vol. 273, no. 40, pp. 25529-25532, 1998.
[41] G. Jogl, S. Rozovsky, A. E. McDermott, and L. Tong, "Optimal alignment for enzymatic proton transfer: structure of the Michaelis complex of triosephosphate isomerase at 1.2-Å resolution," *Proceedings of the National Academy of Sciences,* vol. 100, no. 1, pp. 50-55, 2003.
[42] M. Alahuhta and R. K. Wierenga, "Atomic resolution crystallography of a complex of triosephosphate isomerase with a reaction-intermediate analog: New insight in the proton transfer reaction mechanism," *Proteins: Structure, Function, and Bioinformatics,* vol. 78, no. 8, pp. 1878-1888, 2010-06-01 2010, doi: 10.1002/prot.22701.
[43] I. Kursula and R. K. Wierenga, "Crystal structure of triosephosphate isomerase complexed with 2-phosphoglycolate at 0.83-Å resolution," *Journal of Biological Chemistry,* vol. 278, no. 11, pp. 9544-9551, 2003.
[44] M. M. Malabanan, L. Nitsch-Velasquez, T. L. Amyes, and J. P. Richard, "Magnitude and origin of the enhanced basicity of the catalytic glutamate of triosephosphate isomerase," *Journal of the American Chemical Society,* vol. 135, no. 16, pp. 5978-5981, 2013.
[45] W. Schliebs, N. Thanki, R. Eritja, and R. Wierenga, "Active site properties of monomeric triosephosphate isomerase (monoTIM) as deduced from mutational and structural studies," *Protein science,* vol. 5, no. 2, pp. 229-239, 1996.
[46] J. R. Knowles, "Enzyme catalysis: not different, just better," *Nature,* vol. 350, no. 6314, pp. 121-124, 1991.
[47] S. C. Blacklow, K. D. Liu, and J. R. Knowles, "Stepwise improvements in catalytic effectiveness: independence and interdependence in combinations of point mutations

of a sluggish triosephosphate isomerase," *Biochemistry,* vol. 30, no. 34, pp. 8470-8476, 1991.

[48] M. Samanta, M. Murthy, H. Balaram, and P. Balaram, "Revisiting the mechanism of the triosephosphate isomerase reaction: the role of the fully conserved glutamic acid 97 residue," *ChemBioChem,* vol. 12, no. 12, pp. 1886-1896, 2011.

[49] J. P. Richard, "A Paradigm for Enzyme-Catalyzed Proton Transfer at Carbon: Triosephosphate Isomerase," *Biochemistry,* vol. 51, no. 13, pp. 2652-2661, 2012-04-03 2012, doi: 10.1021/bi300195b.

[50] R. M. Garavito and J. P. Rosenbusch, "Three-dimensional crystals of an integral membrane protein: an initial x-ray analysis.," *Journal of Cell Biology,* vol. 86, no. 1, pp. 327-329, 1980-07-01 1980, doi: 10.1083/jcb.86.1.327.

[51] S. W. Cowan *et al.*, "Crystal structures explain functional properties of two E. coli porins," *Nature,* vol. 358, no. 6389, pp. 727-733, 1992-08-01 1992, doi: 10.1038/358727a0.

[52] E. Yamashita, M. V. Zhalnina, S. D. Zakharov, O. Sharma, and W. A. Cramer, "Crystal structures of the OmpF porin: Function in a colicin translocon," *EMBO Journal,* 2008, doi: 10.1038/emboj.2008.137.

[53] W. Im and B. t. Roux, "Ions and counterions in a biological channel: a molecular dynamics simulation of OmpF porin from Escherichia coli in an explicit membrane with 1 M KCl aqueous salt solution," *Journal of molecular biology,* vol. 319, no. 5, pp. 1177-1197, 2002.

[54] P. S. Phale *et al.*, "Stability of trimeric OmpF porin: the contributions of the latching loop L2," *Biochemistry,* vol. 37, no. 45, pp. 15663-70, Nov 10 1998, doi: 10.1021/bi981215c.

[55] B. K. Ziervogel and B. Roux, "The binding of antibiotics in OmpF porin," *Structure,* vol. 21, no. 1, pp. 76-87, 2013.

[56] J. Bredin *et al.*, "Alteration of pore properties of Escherichia coli OmpF induced by mutation of key residues in anti-loop 3 region," *Biochemical Journal,* vol. 363, no. 3, pp. 521-528, 2002.

[57] S. Varma, S.-W. Chiu, and E. Jakobsson, "The influence of amino acid protonation states on molecular dynamics simulations of the bacterial porin OmpF," *Biophysical journal,* vol. 90, no. 1, pp. 112-123, 2006.

[58] N. Liu and A. H. Delcour, "The spontaneous gating activity of OmpC porin is affected by mutations of a putative hydrogen bond network or of a salt bridge between the L3 loop and the barrel," *Protein engineering,* vol. 11, no. 9, pp. 797-802, 1998.

[59] A. Mcpherson, "Introduction to protein crystallization," *Methods,* vol. 34, no. 3, pp. 254-265, 2004-11-01 2004, doi: 10.1016/j.ymeth.2004.03.019.

[60] A. McPherson and J. A. Gavira, "Introduction to protein crystallization," *Acta Crystallographica Section F: Structural Biology Communications,* vol. 70, no. 1, pp. 2-20, 2014.

[61] N. Asherie, "Protein crystallization and phase diagrams," *Methods,* vol. 34, no. 3, pp. 266-272, 2004-11-01 2004, doi: 10.1016/j.ymeth.2004.03.028.

[62] N. Chayen, J. Akins, S. Campbell-Smith, and D. Blow, "Solubility of glucose isomerase in ammonium sulphate solutions," *Journal of Crystal Growth,* vol. 90, no. 1-3, pp. 112-116, 1988.

[63] N. Asherie, C. Ginsberg, S. Blass, A. Greenbaum, and S. Knafo, "Solubility of thaumatin," *Crystal Growth and Design,* vol. 8, no. 6, pp. 1815-1817, 2008.

[64] M. L. Pusey and K. Gernert, "A method for rapid liquid-solid phase solubility measurements using the protein lysozyme," *Journal of crystal growth,* vol. 88, no. 3, pp. 419-424, 1988.

[65] M. Budayova-Spano, F. Dauvergne, M. Audiffren, T. Bactivelane, and S. Cusack, "A methodology and an instrument for the temperature-controlled optimization of crystal growth," *Acta Crystallographica Section D: Biological Crystallography,* vol. 63, no. 3, pp. 339-347, 2007.

[66] J.-F. Gaucher, M. Riès-Kautt, F. Reiss-Husson, and A. Ducruix, "Solubility diagram of the Rhodobacter sphaeroides
reaction center as a function of PEG concentration," *FEBS Letters,* vol. 401, no. 2-3, pp. 113-116, 1997-01-20 1997, doi: 10.1016/s0014-5793(96)01446-9.

[67] M. Ataka, K. Shinzawa-Itoh, and S. Yoshikawa, "Phase diagrams of a crystalline membrane protein, bovine heart cytochromec oxidase, in the salting-in region," *Journal of crystal growth,* vol. 122, no. 1-4, pp. 60-65, 1992.

[68] T. Bergfors, *Protein Crystallization: Techniques, Strategies, and Tips*. International University Line, 1999.

[69] B. Rupp, *Biomolecular crystallography: principles, practice, and application to structural biology*. Garland Science, 2009.

[70] F. Otálora, J. A. Gavira, J. D. Ng, and J. M. García-Ruiz, "Counterdiffusion methods applied to protein crystallization," *Progress in biophysics and molecular biology,* vol. 101, no. 1-3, pp. 26-37, 2009.

[71] J. Garcia-Ruiz, A. Moreno, C. Viedma, and M. Coll, "Crystal quality of lysozyme single crystals grown by the gel acupuncture method," *Materials research bulletin,* vol. 28, no. 6, pp. 541-546, 1993.

[72] S. J. Hjorth-Jensen, E. Oksanen, P. Nissen, and T. L.-M. Sørensen, "Prospects for membrane protein crystals in NMX," *Methods in enzymology,* vol. 634, pp. 47-68, 2020.

[73] N. E. Chayen, "A novel technique to control the rate of vapour diffusion, giving larger protein crystals," *Journal of Applied Crystallography,* vol. 30, no. 2, pp. 198-202, 1997.

[74] E. A. Stura and I. A. Wilson, "Applications of the streak seeding technique in protein crystallization," *Journal of crystal growth,* vol. 110, no. 1-2, pp. 270-282, 1991.

[75] T. Bergfors, "Seeds to crystals," *Journal of structural biology,* vol. 142, no. 1, pp. 66-76, 2003.

[76] E. A. Stura and I. A. Wilson, "Analytical and production seeding techniques," *Methods,* vol. 1, no. 1, pp. 38-49, 1990.

[77] V. Kelpšas, B. Lafumat, M. P. Blakeley, N. Coquelle, E. Oksanen, and C. Von Wachenfeldt, "Perdeuteration, large crystal growth and neutron data collection of Leishmania mexicana triose-phosphate isomerase E65Q variant," *Acta Crystallographica Section F: Structural Biology Communications,* vol. 75, no. 4, pp. 260-269, 2019.

[78] F. Fadel, Y. Zhao, A. Cousido-Siah, F. X. Ruiz, A. Mitschler, and A. Podjarny, "X-ray crystal structure of the full length human chitotriosidase (CHIT1) reveals features of its chitin binding domain," *PloS one,* vol. 11, no. 4, p. e0154190, 2016.

[79] E. Oksanen, M. P. Blakeley, F. Bonnete, M. T. Dauvergne, F. Dauvergne, and M. Budayova-Spano, "Large crystal growth by thermal control allows combined X-ray and neutron crystallographic studies to elucidate the protonation states in Aspergillus flavus urate oxidase," *J R Soc Interface,* vol. 6 Suppl 5, pp. S599-610, Oct 6 2009, doi: 10.1098/rsif.2009.0162.focus.

[80] M. Ataka and M. Asai, "Systematic studies on the crystallization of lysozyme: Determination and use of phase diagrams," *Journal of Crystal Growth,* vol. 90, no. 1-3, pp. 86-93, 1988.

[81] V. Mikol and R. Giegé, "Phase diagram of a crystalline protein: Determination of the solubility of concanavalin A by a microquantitation assay," *Journal of crystal growth,* vol. 97, no. 2, pp. 324-332, 1989.
[82] R. M. Garavito and D. Picot, "Crystallization of membrane proteins: a minireview," *Journal of crystal growth,* vol. 110, no. 1-2, pp. 89-95, 1991.
[83] B. Lorber, L. J. DeLucas, and J. B. Bishop, "Changes in the physico-chemical properties of the detergent octyl glucoside during membrane protein crystallization using a salt as the precipitant," *Journal of crystal growth,* vol. 110, no. 1-2, pp. 103-113, 1991.
[84] N. Junius, E. Vahdatahar, E. Oksanen, J.-L. Ferrer, and M. Budayova-Spano, "Optimization of crystallization of biological macromolecules using dialysis combined with temperature control," *Journal of Applied Crystallography,* vol. 53, no. 3, 2020.
[85] M. Budayova-Spano *et al.*, "Production and X-ray crystallographic analysis of fully deuterated human carbonic anhydrase II," *Acta Crystallographica Section F: Structural Biology and Crystallization Communications,* vol. 62, no. 1, pp. 6-9, 2006.
[86] M. Caffrey, "Crystallizing membrane proteins for structure determination: use of lipidic mesophases," *Annual review of biophysics,* vol. 38, pp. 29-51, 2009.
[87] C. Ostermeier and H. Michel, "Crystallization of membrane proteins," *Current opinion in structural biology,* vol. 7, no. 5, pp. 697-701, 1997.
[88] G. Katona, U. Andreasson, E. M. Landau, L.-E. Andreasson, and R. Neutze, "Lipidic cubic phase crystal structure of the photosynthetic reaction centre from Rhodobacter sphaeroides at 2.35 Å resolution," *Journal of molecular biology,* vol. 331, no. 3, pp. 681-692, 2003.
[89] V. Cherezov *et al.*, "High-resolution crystal structure of an engineered human β2-adrenergic G protein–coupled receptor," *science,* vol. 318, no. 5854, pp. 1258-1265, 2007.
[90] V.-P. Jaakola *et al.*, "The 2.6 angstrom crystal structure of a human A2A adenosine receptor bound to an antagonist," *Science,* vol. 322, no. 5905, pp. 1211-1217, 2008.
[91] S. Agah and S. Faham, "Crystallization of Membrane Proteins in Bicelles," in *Membrane Protein Structure and Dynamics*: Humana Press, 2012, pp. 3-16.
[92] P. B. Moore, "[50] The preparation of deuterated ribosomal materials for neutron scattering," in *Methods in enzymology,* vol. 59: Elsevier, 1979, pp. 639-655.
[93] G. A. Olah, S. E. Rokop, C.-L. A. Wang, S. L. Blechner, and J. Trewhella, "Troponin I encompasses an extended troponin C in the Ca2+-bound complex: a small-angle X-ray and neutron scattering study," *Biochemistry,* vol. 33, no. 27, pp. 8233-8239, 1994.
[94] D. M. LeMaster and F. M. Richards, "Preparative-scale isolation of isotopically labeled amino acids," *Analytical biochemistry,* vol. 122, no. 2, pp. 238-247, 1982.
[95] A. Sosa-Peinado, D. Mustafi, and M. W. Makinen, "Overexpression and biosynthetic deuterium enrichment of TEM-1 β-lactamase for structural characterization by magnetic resonance methods," *Protein expression and purification,* vol. 19, no. 2, pp. 235-245, 2000.
[96] F. Meilleur, M.-T. Dauvergne, I. Schlichting, and D. A. Myles, "Production and X-ray crystallographic analysis of fully deuterated cytochrome P450cam," *Acta Crystallographica Section D: Biological Crystallography,* vol. 61, no. 5, pp. 539-544, 2005.
[97] I. Hazemann *et al.*, "High-resolution neutron protein crystallography with radically small crystal volumes: application of perdeuteration to human aldose reductase," *Acta Crystallographica Section D: Biological Crystallography,* vol. 61, no. 10, pp. 1413-1417, 2005.

[98] Anthony P. Duff*, Karyn L. Wilde*, Agata Rekas*, Vanessa Lake*, Peter J. Holden†, "Robust High-Yield Methodologies for 2H and 2H/15N/13C Labeling
of Proteins for Structural Investigations Using Neutron Scattering and NMR," *Methods in Enzymology,* vol. 565, 2015.
[99] K. A. Datsenko and B. L. Wanner, "One-step inactivation of chromosomal genes in Escherichia coli K-12 using PCR products," *Proceedings of the National Academy of Sciences,* vol. 97, no. 12, pp. 6640-6645, 2000.
[100] C. A. Schnaitman, "Effect of ethylenediaminetetraacetic acid, Triton X-100, and lysozyme on the morphology and chemical composition of isolated cell walls of Escherichia coli," *Journal of Bacteriology,* vol. 108, no. 1, pp. 553-563, 1971.
[101] F. Baneyx and M. Mujacic, "Recombinant protein folding and misfolding in Escherichia coli," *Nature biotechnology,* vol. 22, no. 11, pp. 1399-1408, 2004.
[102] A. Vera, N. González-Montalbán, A. Arís, and A. Villaverde, "The conformational quality of insoluble recombinant proteins is enhanced at low growth temperatures," *Biotechnology and bioengineering,* vol. 96, no. 6, pp. 1101-1106, 2007.
[103] O. Paliy and T. S. Gunasekera, "Growth of E. coli BL21 in minimal media with different gluconeogenic carbon sources and salt contents," *Applied microbiology and biotechnology,* vol. 73, no. 5, pp. 1169-1172, 2007.
[104] K. Koruza, B. Lafumat, Végvári, W. Knecht, and S. Z. Fisher, "Deuteration of human carbonic anhydrase for neutron crystallography: Cell culture media, protein thermostability, and crystallization behavior," *Archives of Biochemistry and Biophysics,* 2018, doi: 10.1016/j.abb.2018.03.008.
[105] K. D. Rand, M. Zehl, and T. J. Jørgensen, "Measuring the hydrogen/deuterium exchange of proteins at high spatial resolution by mass spectrometry: overcoming gas-phase hydrogen/deuterium scrambling," *Accounts of chemical research,* vol. 47, no. 10, pp. 3018-3027, 2014.
[106] D. Resetca and D. J. Wilson, "Characterizing rapid, activity-linked conformational transitions in proteins via sub-second hydrogen deuterium exchange mass spectrometry," *FEBS Journal,* vol. 280, no. 22, pp. 5616-5625, 2013-11-01 2013, doi: 10.1111/febs.12332.
[107] H. Naveed, D. Jimenez-Morales, J. Tian, V. Pasupuleti, L. J. Kenney, and J. Liang, "Engineered oligomerization state of OmpF protein through computational design decouples oligomer dissociation from unfolding," *Journal of molecular biology,* vol. 419, no. 1-2, pp. 89-101, 2012.
[108] O. D. Novikova *et al.,* "Peculiarities of thermal denaturation of OmpF porin from Yersinia ruckeri," *Molecular BioSystems,* vol. 13, no. 9, pp. 1854-1862, 2017.
[109] W. Kightlinger, K. Chen, A. Pourmir, D. W. Crunkleton, G. L. Price, and T. W. Johannes, "Production and characterization of algae extract from Chlamydomonas reinhardtii," *Electronic Journal of Biotechnology,* vol. 17, no. 1, pp. 3-3, 2014.
[110] B. Franke *et al.,* "Production of isotope-labeled proteins in insect cells for NMR," *Journal of biomolecular NMR,* vol. 71, no. 3, pp. 173-184, 2018.
[111] F. Löhr, V. Katsemi, J. Hartleib, U. Günther, and H. Rüterjans, "A strategy to obtain backbone resonance assignments of deuterated proteins in the presence of incomplete amide 2 H/1 H back-exchange," *Journal of biomolecular NMR,* vol. 25, no. 4, pp. 291-311, 2003.
[112] Y. Ashani and G. N. Catravas, "Highly reactive impurities in Triton X-100 and Brij 35: partial characterization and removal," *Analytical biochemistry,* vol. 109, no. 1, pp. 55-62, 1980.

[113] M. Turowski *et al.*, "Deuterium isotope effects on hydrophobic interactions: the importance of dispersion interactions in the hydrophobic phase," *Journal of the American Chemical Society*, vol. 125, no. 45, pp. 13836-13849, 2003.
[114] W. B. O'Dell, A. M. Bodenheimer, and F. Meilleur, "Neutron protein crystallography: A complementary tool for locating hydrogens in proteins," *Arch Biochem Biophys*, vol. 602, pp. 48-60, Jul 15 2016, doi: 10.1016/j.abb.2015.11.033.
[115] M. Budayova-Spano, K. Koruza, and Z. Fisher, "Large crystal growth for neutron protein crystallography," *Methods in enzymology*, vol. 634, pp. 21-46, 2020.
[116] A. Stetsenko and A. Guskov, "An overview of the top ten detergents used for membrane protein crystallization," *Crystals*, vol. 7, no. 7, p. 197, 2017.
[117] J. Ma *et al.*, "The effect of residual Triton X-100 on structural stability and infection activity of adenovirus particles," *Molecular Therapy-Methods & Clinical Development*, vol. 19, pp. 35-46, 2020.
[118] S. Tanaka and M. Ataka, "Protein crystallization induced by polyethylene glycol: A model study using apoferritin," *The Journal of chemical physics*, vol. 117, no. 7, pp. 3504-3510, 2002.
[119] C. Hitscherich, V. Aseyev, J. Wiencek, and P. J. Loll, "Effects of PEG on detergent micelles: implications for the crystallization of integral membrane proteins," *Acta Crystallographica Section D: Biological Crystallography*, vol. 57, no. 7, pp. 1020-1029, 2001.
[120] R. M. Garavito and D. Picot, "The art of crystallizing membrane proteins," *Methods*, vol. 1, no. 1, pp. 57-69, 1990.
[121] G. T. Detitta and J. R. Luft, "Rate of water equilibration in vapor-diffusion crystallization: dependence on the residual pressure of air in the vapor space," *Acta Crystallographica Section D: Biological Crystallography*, vol. 51, no. 5, pp. 786-791, 1995.
[122] J. M. García-Ruiz, F. Otálora, and A. García-Caballero, "The role of mass transport in protein crystallization," *Acta Crystallographica Section F: Structural Biology Communications*, vol. 72, no. 2, pp. 96-104, 2016.
[123] W. F. Berg, "Crystal growth from solutions," *Proceedings of the Royal Society of London. Series A - Mathematical and Physical Sciences*, vol. 164, no. 916, pp. 79-95, 1938-01-07 1938, doi: 10.1098/rspa.1938.0006.
[124] F. Manzoni *et al.*, "Perdeuteration, crystallization, data collection and comparison of five neutron diffraction data sets of complexes of human galectin-3C," *Acta Crystallographica Section D: Structural Biology*, vol. 72, no. 11, pp. 1194-1202, 2016.
[125] X. Liu, B. L. Hanson, P. Langan, and R. E. Viola, "The effect of deuteration on protein structure: a high-resolution comparison of hydrogenous and perdeuterated haloalkane dehalogenase," *Acta Crystallographica Section D: Biological Crystallography*, vol. 63, no. 9, pp. 1000-1008, 2007.
[126] P. D. Shaw Stewart, S. A. Kolek, R. A. Briggs, N. E. Chayen, and P. F. M. Baldock, "Random Microseeding: A Theoretical and Practical Exploration of Seed Stability and Seeding Techniques for Successful Protein Crystallization," *Crystal Growth & Design*, vol. 11, no. 8, pp. 3432-3441, 2011-08-03 2011, doi: 10.1021/cg2001442.
[127] T. Bergfors, "Succeeding with seeding: some practical advice," in *Evolving Methods for Macromolecular Crystallography*: Springer, 2007, pp. 1-10.
[128] G. C. Kresheck, H. Schneider, and H. A. Scheraga, "The Effect of D2O on the Thermal Stability of Proteins. Thermodynamic Parameters for the Transfer of Model Compounds from H2O to D2O1, 2," *The Journal of physical chemistry*, vol. 69, no. 9, pp. 3132-3144, 1965.

[129] P. Fromme and H. T. Witt, "Improved isolation and crystallization of photosystem I for structural analysis," *Biochimica et Biophysica Acta (BBA)-Bioenergetics,* vol. 1365, no. 1-2, pp. 175-184, 1998.
[130] C. R. D. Lancaster, A. Kröger, M. Auer, and H. Michel, "Structure of fumarate reductase from Wolinella succinogenes at 2.2 Å resolution," *Nature,* vol. 402, no. 6760, pp. 377-385, 1999-11-01 1999, doi: 10.1038/46483.
[131] R. Dods *et al.*, "From macrocrystals to microcrystals: a strategy for membrane protein serial crystallography," *Structure,* vol. 25, no. 9, pp. 1461-1468. e2, 2017.
[132] S. A. Kolek, B. Bräuning, and P. D. Shaw Stewart, "A novel microseeding method for the crystallization of membrane proteins in lipidic cubic phase," *Acta Crystallographica Section F: Structural Biology Communications,* vol. 72, no. 4, pp. 307-312, 2016.
[133] I. Moraes, G. Evans, J. Sanchez-Weatherby, S. Newstead, and P. D. S. Stewart, "Membrane protein structure determination—the next generation," *Biochimica et Biophysica Acta (BBA)-Biomembranes,* vol. 1838, no. 1, pp. 78-87, 2014.
[134] N. Candoni, R. Grossier, Z. Hammadi, R. Morin, and S. Veesler, "Practical physics behind growing crystals of biological macromolecules," *Protein and peptide letters,* vol. 19, no. 7, pp. 714-724, 2012.
[135] J. Campbell, Q. Hao, M. Harding, N. Nguti, and C. Wilkinson, "LAUEGEN version 6.0 and INTLDM," *Journal of Applied Crystallography,* vol. 31, no. 3, pp. 496-502, 1998.
[136] P. Evans, "Scaling and assessment of data quality," *Acta Crystallographica Section D: Biological Crystallography,* vol. 62, no. 1, pp. 72-82, 2006.
[137] P. D. Adams *et al.*, "The Phenix software for automated determination of macromolecular structures," *Methods,* vol. 55, no. 1, pp. 94-106, 2011.
[138] P. Emsley and K. Cowtan, "Coot: model-building tools for molecular graphics," *Acta crystallographica section D: biological crystallography,* vol. 60, no. 12, pp. 2126-2132, 2004.
[139] E. Oksanen, F. Dauvergne, A. Goldman, and M. Budayova-Spano, "Design of a novel Peltier-based cooling device and its use in neutron diffraction data collection of perdeuterated yeast pyrophosphatase," *Journal of Applied Crystallography,* vol. 43, no. 5, pp. 1113-1120, 2010.
[140] J. R. Morrow, T. L. Amyes, and J. P. Richard, "Phosphate binding energy and catalysis by small and large molecules," *Accounts of chemical research,* vol. 41, no. 4, pp. 539-548, 2008.
[141] Q. Cui and M. Karplus, "Quantum mechanics/molecular mechanics studies of triosephosphate isomerase-catalyzed reactions: effect of geometry and tunneling on proton-transfer rate constants," *Journal of the American Chemical Society,* vol. 124, no. 12, pp. 3093-3124, 2002.
[142] P. J. Lodi and J. R. Knowles, "Neutral imidazole is the electrophile in the reaction catalyzed by triosephosphate isomerase: structural origins and catalytic implications," *Biochemistry,* vol. 30, no. 28, pp. 6948-6956, 1991.
[143] P. J. Lodi, L. C. Chang, J. R. Knowles, and E. A. Komives, "Triosephosphate isomerase requires a positively charged active site: the role of lysine-12," *Biochemistry,* vol. 33, no. 10, pp. 2809-2814, 1994.
[144] E. A. Komives, L. C. Chang, E. Lolis, R. F. Tilton, G. A. Petsko, and J. R. Knowles, "Electrophilic catalysis in triosephosphate isomerase: the role of histidine-95," *Biochemistry,* vol. 30, no. 12, pp. 3011-3019, 1991.
[145] E. A. Ruben *et al.*, "Ground state destabilization from a positioned general base in the ketosteroid isomerase active site," *Biochemistry,* vol. 52, no. 6, pp. 1074-1081, 2013.

[1] C. I. Branden and J. Tooze, *Introduction to protein structure*. Garland Science, 2012.
[2] T. E. Creighton, *Proteins: structures and molecular properties*. Macmillan, 1993.
[3] A. S. Cole and J. E. Eastoe, *Biochemistry and oral biology*. Butterworth-Heinemann, 2014.
[4] G. C. Terstappen and A. Reggiani, "In silico research in drug discovery," *Trends in pharmacological sciences,* vol. 22, no. 1, pp. 23-26, 2001.
[5] S. H. White and W. C. Wimley, "Membrane protein folding and stability: physical principles," *Annual review of biophysics and biomolecular structure,* vol. 28, no. 1, pp. 319-365, 1999.
[6] A. Sadaf, K. H. Cho, B. Byrne, and P. S. Chae, "Amphipathic agents for membrane protein study," *Methods in enzymology,* vol. 557, pp. 57-94, 2015.
[7] J. C. Kendrew, G. Bodo, H. M. Dintzis, R. Parrish, H. Wyckoff, and D. C. Phillips, "A three-dimensional model of the myoglobin molecule obtained by x-ray analysis," *Nature,* vol. 181, no. 4610, pp. 662-666, 1958.
[8] J. Drenth, *Principles of protein X-ray crystallography*. Springer Science & Business Media, 2007.
[9] T. Huxford, "X-Ray Crystallography," 2013.
[10] D. P. Mitchell and P. N. Powers, "Bragg reflection of slow neutrons," *Physical Review,* vol. 50, no. 5, p. 486, 1936.
[11] P. Preiswerk and H. von Halban, "Preuve experimental de la diffraction des neutrons," *CR Acad. Sci. Paris,* vol. 203, pp. 73-75, 1936.
[12] M. P. Blakeley, S. S. Hasnain, and S. V. Antonyuk, "Sub-atomic resolution X-ray crystallography and neutron crystallography: promise, challenges and potential," *IUCrJ,* vol. 2, no. 4, pp. 464-474, 2015.
[13] M. P. Blakeley, P. Langan, N. Niimura, and A. Podjarny, "Neutron crystallography: opportunities, challenges, and limitations," in *Current Opinion in Structural Biology*, ed, 2008.
[14] E. Oksanen, J. C.-H. Chen, and S. Z. Fisher, "Neutron Crystallography for the Study of Hydrogen Bonds in Macromolecules," *Molecules,* vol. 22, no. 4, p. 596, 2017-04-07 2017, doi: 10.3390/molecules22040596.
[15] E. Oksanen, M. P. Blakeley, M. El-Hajji, U. Ryde, and M. Budayova-Spano, "The neutron structure of urate oxidase resolves a long-standing mechanistic conundrum and reveals unexpected changes in protonation," *PLoS One,* vol. 9, no. 1, p. e86651, 2014.
[16] I. T. Weber *et al.*, "Joint X-ray/Neutron Crystallographic Study of HIV-1 Protease with Clinical Inhibitor Amprenavir: Insights for Drug Design," *Journal of Medicinal Chemistry,* vol. 56, no. 13, pp. 5631-5635, 2013-07-11 2013, doi: 10.1021/jm400684f.
[17] K. Koruza *et al.*, "Structural comparison of protiated, H/D-exchanged and deuterated human carbonic anhydrase IX," *Acta Crystallogr D Struct Biol,* vol. 75, no. Pt 10, pp. 895-903, Oct 1 2019, doi: 10.1107/S2059798319010027.
[18] P. S. Langan, V. G. Vandavasi, B. Sullivan, J. Harp, K. Weiss, and L. Coates, "Crystallization of a potassium ion channel and X-ray and neutron data collection," *Acta Crystallographica Section F Structural Biology Communications,* vol. 75, no. 6, pp. 435-438, 2019-06-01 2019, doi: 10.1107/s2053230x19006630.
[19] R. Ashkar *et al.*, "Neutron scattering in the biological sciences: progress and prospects," *Acta Crystallographica Section D: Structural Biology,* vol. 74, no. 12, pp. 1129-1168, 2018.
[20] V. F. Sears, "Neutron scattering lengths and cross sections," *Neutron News,* 1992, doi: 10.1080/10448639208218770.

[21] T. Renner, *Quantities, units and symbols in physical chemistry*. Royal Society of Chemistry, 2007.
[22] E. Borek and D. Rittenberg, "Anomalous growth of microorganisms produced by changes in isotopes in their environment," *Proceedings of the National Academy of Sciences of the United States of America,* vol. 46, no. 6, p. 777, 1960.
[23] B. Kollars and R. Geraets, "Effects of Deuterium on Chlamydomonas reinhardtii," *The Journal of Undergraduate Research,* vol. 6, no. 1, p. 12, 2008.
[24] P. R. Gross and W. Spindel, "Mitotic arrest by deuterium oxide," *Science,* vol. 131, no. 3392, pp. 37-39, 1960.
[25] K. Unno, T. Kishido, M. Morioka, S. Okada, and N. Oku, "Increased expression of Hsp70 for resistance to deuterium oxide in a yeast mutant cell line," *Biological and Pharmaceutical Bulletin,* vol. 26, no. 6, pp. 799-802, 2003.
[26] M. U. Caglar *et al.*, "The E. coli molecular phenotype under different growth conditions," *Scientific reports,* vol. 7, no. 1, pp. 1-15, 2017.
[27] V. Kelpšas and C. von Wachenfeldt, "Strain improvement of Escherichia coli K-12 for recombinant production of deuterated proteins," *Scientific reports,* vol. 9, no. 1, pp. 1-9, 2019.
[28] G. Walsh and R. Jefferis, "Post-translational modifications in the context of therapeutic proteins," *Nature biotechnology,* vol. 24, no. 10, pp. 1241-1252, 2006.
[29] V. Kelpšas and C. v. Wachenfeldt, "Strain improvement of Escherichia coli K-12 for recombinant production of deuterated proteins," *Scientific Reports,* 2019, doi: 10.1038/s41598-019-54196-w.
[30] O. Paliy, D. Bloor, D. Brockwell, P. Gilbert, and J. Barber, "Improved methods of cultivation and production of deuteriated proteins from E. coli strains grown on fully deuteriated minimal medium," *Journal of Applied Microbiology,* 2003, doi: 10.1046/j.1365-2672.2003.01866.x.
[31] M. Haertlein, M. Moulin, J. M. Devos, V. Laux, O. Dunne, and V. T. Forsyth, "Biomolecular deuteration for neutron structural biology and dynamics," *Methods in enzymology,* vol. 566, pp. 113-157, 2016.
[32] T. Hiromoto *et al.*, "Neutron structure of the T26H mutant of T4 phage lysozyme provides insight into the catalytic activity of the mutant enzyme and how it differs from that of wild type," *Protein Science,* vol. 26, no. 10, pp. 1953-1963, 2017.
[33] R. Wierenga, E. Kapetaniou, and R. Venkatesan, "Triosephosphate isomerase: a highly evolved biocatalyst," *Cellular and molecular life sciences,* vol. 67, no. 23, pp. 3961-3982, 2010.
[34] S. HELFERT, A. M. Estévez, B. Bakker, P. Michels, and C. Clayton, "Roles of triosephosphate isomerase and aerobic metabolism in Trypanosoma brucei," *Biochemical Journal,* vol. 357, no. 1, pp. 117-125, 2001.
[35] F. Orosz, J. Oláh, and J. Ovádi, "Triosephosphate isomerase deficiency: new insights into an enigmatic disease," *Biochimica et Biophysica Acta (BBA)-Molecular Basis of Disease,* vol. 1792, no. 12, pp. 1168-1174, 2009.
[36] F. Orosz, J. Olah, and J. Ovadi, "Triosephosphate isomerase deficiency: facts and doubts," *IUBMB life,* vol. 58, no. 12, pp. 703-715, 2006.
[37] S. C. Blacklow, R. T. Raines, W. A. Lim, P. D. Zamore, and J. R. Knowles, "Triosephosphate isomerase catalysis is diffusion controlled," *Biochemistry,* vol. 27, no. 4, pp. 1158-1165, 1988.
[38] W. J. Albery and J. R. Knowles, "Free-energy profile for the reaction catalyzed by triosephosphate isomerase," *Biochemistry,* vol. 15, no. 25, pp. 5627-5631, 1976.

[39] S. Rozovsky and A. E. McDermott, "Substrate product equilibrium on a reversible enzyme, triosephosphate isomerase," *Proceedings of the National Academy of Sciences,* vol. 104, no. 7, pp. 2080-2085, 2007.
[40] W. J. Albery and J. R. Knowles, "Evolution of enzyme function and the development of catalytic efficiency," *Biochemistry,* vol. 15, no. 25, pp. 5631-5640, 1976.
[41] D. Banner *et al.*, "Structure of chicken muscle triose phosphate isomerase determined crystallographically at 2.5 Å resolution: using amino acid sequence data," *Nature,* vol. 255, no. 5510, pp. 609-614, 1975.
[42] N. Nagano, E. Gail Hutchinson, and J. M. Thornton, "Barrel structures in proteins: automatic identification and classification including a sequence analysis of TIM barrels," *Protein Science,* vol. 8, no. 10, pp. 2072-2084, 1999.
[43] R. Wierenga, "The TIM-barrel fold: a versatile framework for efficient enzymes," *FEBS letters,* vol. 492, no. 3, pp. 193-198, 2001.
[44] D. L. Pompliano, A. Peyman, and J. R. Knowles, "Stabilization of a reaction intermediate as a catalytic device: definition of the functional role of the flexible loop in triosephosphate isomerase," *Biochemistry,* vol. 29, no. 13, pp. 3186-3194, 1990.
[45] D. Röthlisberger *et al.*, "Kemp elimination catalysts by computational enzyme design," *Nature,* vol. 453, no. 7192, pp. 190-195, 2008.
[46] W. W. Cleland, P. A. Frey, and J. A. Gerlt, "The low barrier hydrogen bond in enzymatic catalysis," *Journal of Biological Chemistry,* vol. 273, no. 40, pp. 25529-25532, 1998.
[47] G. Jogl, S. Rozovsky, A. E. McDermott, and L. Tong, "Optimal alignment for enzymatic proton transfer: structure of the Michaelis complex of triosephosphate isomerase at 1.2-Å resolution," *Proceedings of the National Academy of Sciences,* vol. 100, no. 1, pp. 50-55, 2003.
[48] M. Alahuhta and R. K. Wierenga, "Atomic resolution crystallography of a complex of triosephosphate isomerase with a reaction-intermediate analog: New insight in the proton transfer reaction mechanism," *Proteins: Structure, Function, and Bioinformatics,* vol. 78, no. 8, pp. 1878-1888, 2010-06-01 2010, doi: 10.1002/prot.22701.
[49] I. Kursula and R. K. Wierenga, "Crystal structure of triosephosphate isomerase complexed with 2-phosphoglycolate at 0.83-Å resolution," *Journal of Biological Chemistry,* vol. 278, no. 11, pp. 9544-9551, 2003.
[50] M. M. Malabanan, L. Nitsch-Velasquez, T. L. Amyes, and J. P. Richard, "Magnitude and origin of the enhanced basicity of the catalytic glutamate of triosephosphate isomerase," *Journal of the American Chemical Society,* vol. 135, no. 16, pp. 5978-5981, 2013.
[51] W. Schliebs, N. Thanki, R. Eritja, and R. Wierenga, "Active site properties of monomeric triosephosphate isomerase (monoTIM) as deduced from mutational and structural studies," *Protein science,* vol. 5, no. 2, pp. 229-239, 1996.
[52] J. R. Knowles, "Enzyme catalysis: not different, just better," *Nature,* vol. 350, no. 6314, pp. 121-124, 1991.
[53] S. C. Blacklow, K. D. Liu, and J. R. Knowles, "Stepwise improvements in catalytic effectiveness: independence and interdependence in combinations of point mutations of a sluggish triosephosphate isomerase," *Biochemistry,* vol. 30, no. 34, pp. 8470-8476, 1991.
[54] M. Samanta, M. Murthy, H. Balaram, and P. Balaram, "Revisiting the mechanism of the triosephosphate isomerase reaction: the role of the fully conserved glutamic acid 97 residue," *ChemBioChem,* vol. 12, no. 12, pp. 1886-1896, 2011.

[55] J. P. Richard, "A Paradigm for Enzyme-Catalyzed Proton Transfer at Carbon: Triosephosphate Isomerase," *Biochemistry,* vol. 51, no. 13, pp. 2652-2661, 2012-04-03 2012, doi: 10.1021/bi300195b.
[56] R. M. Garavito and J. P. Rosenbusch, "Three-dimensional crystals of an integral membrane protein: an initial x-ray analysis.," *Journal of Cell Biology,* vol. 86, no. 1, pp. 327-329, 1980-07-01 1980, doi: 10.1083/jcb.86.1.327.
[57] S. W. Cowan *et al.*, "Crystal structures explain functional properties of two E. coli porins," *Nature,* vol. 358, no. 6389, pp. 727-733, 1992-08-01 1992, doi: 10.1038/358727a0.
[58] E. Yamashita, M. V. Zhalnina, S. D. Zakharov, O. Sharma, and W. A. Cramer, "Crystal structures of the OmpF porin: Function in a colicin translocon," *EMBO Journal,* 2008, doi: 10.1038/emboj.2008.137.
[59] W. Im and B. t. Roux, "Ions and counterions in a biological channel: a molecular dynamics simulation of OmpF porin from Escherichia coli in an explicit membrane with 1 M KCl aqueous salt solution," *Journal of molecular biology,* vol. 319, no. 5, pp. 1177-1197, 2002.
[60] P. S. Phale *et al.*, "Stability of trimeric OmpF porin: the contributions of the latching loop L2," *Biochemistry,* vol. 37, no. 45, pp. 15663-70, Nov 10 1998, doi: 10.1021/bi981215c.
[61] B. K. Ziervogel and B. Roux, "The binding of antibiotics in OmpF porin," *Structure,* vol. 21, no. 1, pp. 76-87, 2013.
[62] J. Bredin *et al.*, "Alteration of pore properties of Escherichia coli OmpF induced by mutation of key residues in anti-loop 3 region," *Biochemical Journal,* vol. 363, no. 3, pp. 521-528, 2002.
[63] S. Varma, S.-W. Chiu, and E. Jakobsson, "The influence of amino acid protonation states on molecular dynamics simulations of the bacterial porin OmpF," *Biophysical journal,* vol. 90, no. 1, pp. 112-123, 2006.
[64] N. Liu and A. H. Delcour, "The spontaneous gating activity of OmpC porin is affected by mutations of a putative hydrogen bond network or of a salt bridge between the L3 loop and the barrel," *Protein engineering,* vol. 11, no. 9, pp. 797-802, 1998.
[65] A. Mcpherson, "Introduction to protein crystallization," *Methods,* vol. 34, no. 3, pp. 254-265, 2004-11-01 2004, doi: 10.1016/j.ymeth.2004.03.019.
[66] A. McPherson and J. A. Gavira, "Introduction to protein crystallization," *Acta Crystallographica Section F: Structural Biology Communications,* vol. 70, no. 1, pp. 2-20, 2014.
[67] N. Asherie, "Protein crystallization and phase diagrams," *Methods,* vol. 34, no. 3, pp. 266-272, 2004-11-01 2004, doi: 10.1016/j.ymeth.2004.03.028.
[68] N. Chayen, J. Akins, S. Campbell-Smith, and D. Blow, "Solubility of glucose isomerase in ammonium sulphate solutions," *Journal of Crystal Growth,* vol. 90, no. 1-3, pp. 112-116, 1988.
[69] N. Asherie, C. Ginsberg, S. Blass, A. Greenbaum, and S. Knafo, "Solubility of thaumatin," *Crystal Growth and Design,* vol. 8, no. 6, pp. 1815-1817, 2008.
[70] M. L. Pusey and K. Gernert, "A method for rapid liquid-solid phase solubility measurements using the protein lysozyme," *Journal of crystal growth,* vol. 88, no. 3, pp. 419-424, 1988.
[71] M. Budayova-Spano, F. Dauvergne, M. Audiffren, T. Bactivelane, and S. Cusack, "A methodology and an instrument for the temperature-controlled optimization of crystal growth," *Acta Crystallographica Section D: Biological Crystallography,* vol. 63, no. 3, pp. 339-347, 2007.

[72] J.-F. Gaucher, M. Riès-Kautt, F. Reiss-Husson, and A. Ducruix, "Solubility diagram of the Rhodobacter sphaeroides
reaction center as a function of PEG concentration," *FEBS Letters,* vol. 401, no. 2-3, pp. 113-116, 1997-01-20 1997, doi: 10.1016/s0014-5793(96)01446-9.
[73] M. Ataka, K. Shinzawa-Itoh, and S. Yoshikawa, "Phase diagrams of a crystalline membrane protein, bovine heart cytochromec oxidase, in the salting-in region," *Journal of crystal growth,* vol. 122, no. 1-4, pp. 60-65, 1992.
[74] T. Bergfors, *Protein Crystallization: Techniques, Strategies, and Tips*. International University Line, 1999.
[75] B. Rupp, *Biomolecular crystallography: principles, practice, and application to structural biology*. Garland Science, 2009.
[76] F. Otálora, J. A. Gavira, J. D. Ng, and J. M. García-Ruiz, "Counterdiffusion methods applied to protein crystallization," *Progress in biophysics and molecular biology,* vol. 101, no. 1-3, pp. 26-37, 2009.
[77] J. Garcia-Ruiz, A. Moreno, C. Viedma, and M. Coll, "Crystal quality of lysozyme single crystals grown by the gel acupuncture method," *Materials research bulletin,* vol. 28, no. 6, pp. 541-546, 1993.
[78] S. J. Hjorth-Jensen, E. Oksanen, P. Nissen, and T. L.-M. Sørensen, "Prospects for membrane protein crystals in NMX," *Methods in enzymology,* vol. 634, pp. 47-68, 2020.
[79] N. E. Chayen, "A novel technique to control the rate of vapour diffusion, giving larger protein crystals," *Journal of Applied Crystallography,* vol. 30, no. 2, pp. 198-202, 1997.
[80] E. A. Stura and I. A. Wilson, "Applications of the streak seeding technique in protein crystallization," *Journal of crystal growth,* vol. 110, no. 1-2, pp. 270-282, 1991.
[81] T. Bergfors, "Seeds to crystals," *Journal of structural biology,* vol. 142, no. 1, pp. 66-76, 2003.
[82] E. A. Stura and I. A. Wilson, "Analytical and production seeding techniques," *Methods,* vol. 1, no. 1, pp. 38-49, 1990.
[83] V. Kelpšas, B. Lafumat, M. P. Blakeley, N. Coquelle, E. Oksanen, and C. Von Wachenfeldt, "Perdeuteration, large crystal growth and neutron data collection of Leishmania mexicana triose-phosphate isomerase E65Q variant," *Acta Crystallographica Section F: Structural Biology Communications,* vol. 75, no. 4, pp. 260-269, 2019.
[84] F. Fadel, Y. Zhao, A. Cousido-Siah, F. X. Ruiz, A. Mitschler, and A. Podjarny, "X-ray crystal structure of the full length human chitotriosidase (CHIT1) reveals features of its chitin binding domain," *PloS one,* vol. 11, no. 4, p. e0154190, 2016.
[85] E. Oksanen, M. P. Blakeley, F. Bonnete, M. T. Dauvergne, F. Dauvergne, and M. Budayova-Spano, "Large crystal growth by thermal control allows combined X-ray and neutron crystallographic studies to elucidate the protonation states in Aspergillus flavus urate oxidase," *J R Soc Interface,* vol. 6 Suppl 5, pp. S599-610, Oct 6 2009, doi: 10.1098/rsif.2009.0162.focus.
[86] M. Ataka and M. Asai, "Systematic studies on the crystallization of lysozyme: Determination and use of phase diagrams," *Journal of Crystal Growth,* vol. 90, no. 1-3, pp. 86-93, 1988.
[87] V. Mikol and R. Giegé, "Phase diagram of a crystalline protein: Determination of the solubility of concanavalin A by a microquantitation assay," *Journal of crystal growth,* vol. 97, no. 2, pp. 324-332, 1989.
[88] R. M. Garavito and D. Picot, "Crystallization of membrane proteins: a minireview," *Journal of crystal growth,* vol. 110, no. 1-2, pp. 89-95, 1991.

[89] B. Lorber, L. J. DeLucas, and J. B. Bishop, "Changes in the physico-chemical properties of the detergent octyl glucoside during membrane protein crystallization using a salt as the precipitant," *Journal of crystal growth,* vol. 110, no. 1-2, pp. 103-113, 1991.
[90] N. Junius, E. Vahdatahar, E. Oksanen, J.-L. Ferrer, and M. Budayova-Spano, "Optimization of crystallization of biological macromolecules using dialysis combined with temperature control," *Journal of Applied Crystallography,* vol. 53, no. 3, 2020.
[91] M. Budayova-Spano *et al.*, "Production and X-ray crystallographic analysis of fully deuterated human carbonic anhydrase II," *Acta Crystallographica Section F: Structural Biology and Crystallization Communications,* vol. 62, no. 1, pp. 6-9, 2006.
[92] M. Caffrey, "Crystallizing membrane proteins for structure determination: use of lipidic mesophases," *Annual review of biophysics,* vol. 38, pp. 29-51, 2009.
[93] C. Ostermeier and H. Michel, "Crystallization of membrane proteins," *Current opinion in structural biology,* vol. 7, no. 5, pp. 697-701, 1997.
[94] G. Katona, U. Andreasson, E. M. Landau, L.-E. Andreasson, and R. Neutze, "Lipidic cubic phase crystal structure of the photosynthetic reaction centre from Rhodobacter sphaeroides at 2.35 Å resolution," *Journal of molecular biology,* vol. 331, no. 3, pp. 681-692, 2003.
[95] V. Cherezov *et al.*, "High-resolution crystal structure of an engineered human β2-adrenergic G protein–coupled receptor," *science,* vol. 318, no. 5854, pp. 1258-1265, 2007.
[96] V.-P. Jaakola *et al.*, "The 2.6 angstrom crystal structure of a human A2A adenosine receptor bound to an antagonist," *Science,* vol. 322, no. 5905, pp. 1211-1217, 2008.
[97] S. Agah and S. Faham, "Crystallization of Membrane Proteins in Bicelles," in *Membrane Protein Structure and Dynamics*: Humana Press, 2012, pp. 3-16.
[98] P. B. Moore, "[50] The preparation of deuterated ribosomal materials for neutron scattering," in *Methods in enzymology,* vol. 59: Elsevier, 1979, pp. 639-655.
[99] G. A. Olah, S. E. Rokop, C.-L. A. Wang, S. L. Blechner, and J. Trewhella, "Troponin I encompasses an extended troponin C in the Ca2+-bound complex: a small-angle X-ray and neutron scattering study," *Biochemistry,* vol. 33, no. 27, pp. 8233-8239, 1994.
[100] D. M. LeMaster and F. M. Richards, "Preparative-scale isolation of isotopically labeled amino acids," *Analytical biochemistry,* vol. 122, no. 2, pp. 238-247, 1982.
[101] A. Sosa-Peinado, D. Mustafi, and M. W. Makinen, "Overexpression and biosynthetic deuterium enrichment of TEM-1 β-lactamase for structural characterization by magnetic resonance methods," *Protein expression and purification,* vol. 19, no. 2, pp. 235-245, 2000.
[102] F. Meilleur, M.-T. Dauvergne, I. Schlichting, and D. A. Myles, "Production and X-ray crystallographic analysis of fully deuterated cytochrome P450cam," *Acta Crystallographica Section D: Biological Crystallography,* vol. 61, no. 5, pp. 539-544, 2005.
[103] I. Hazemann *et al.*, "High-resolution neutron protein crystallography with radically small crystal volumes: application of perdeuteration to human aldose reductase," *Acta Crystallographica Section D: Biological Crystallography,* vol. 61, no. 10, pp. 1413-1417, 2005.
[104] Anthony P. Duff*, Karyn L. Wilde*, Agata Rekas*, Vanessa Lake*, Peter J. Holden†, "Robust High-Yield Methodologies for 2H and 2H/15N/13C Labeling
of Proteins for Structural Investigations Using Neutron Scattering and NMR," *Methods in Enzymology,* vol. 565, 2015.

[105] K. A. Datsenko and B. L. Wanner, "One-step inactivation of chromosomal genes in Escherichia coli K-12 using PCR products," *Proceedings of the National Academy of Sciences,* vol. 97, no. 12, pp. 6640-6645, 2000.
[106] C. A. Schnaitman, "Effect of ethylenediaminetetraacetic acid, Triton X-100, and lysozyme on the morphology and chemical composition of isolated cell walls of Escherichia coli," *Journal of Bacteriology,* vol. 108, no. 1, pp. 553-563, 1971.
[107] F. Baneyx and M. Mujacic, "Recombinant protein folding and misfolding in Escherichia coli," *Nature biotechnology,* vol. 22, no. 11, pp. 1399-1408, 2004.
[108] A. Vera, N. González-Montalbán, A. Arís, and A. Villaverde, "The conformational quality of insoluble recombinant proteins is enhanced at low growth temperatures," *Biotechnology and bioengineering,* vol. 96, no. 6, pp. 1101-1106, 2007.
[109] O. Paliy and T. S. Gunasekera, "Growth of E. coli BL21 in minimal media with different gluconeogenic carbon sources and salt contents," *Applied microbiology and biotechnology,* vol. 73, no. 5, pp. 1169-1172, 2007.
[110] K. Koruza, B. Lafumat, Végvári, W. Knecht, and S. Z. Fisher, "Deuteration of human carbonic anhydrase for neutron crystallography: Cell culture media, protein thermostability, and crystallization behavior," *Archives of Biochemistry and Biophysics,* 2018, doi: 10.1016/j.abb.2018.03.008.
[111] K. D. Rand, M. Zehl, and T. J. Jørgensen, "Measuring the hydrogen/deuterium exchange of proteins at high spatial resolution by mass spectrometry: overcoming gas-phase hydrogen/deuterium scrambling," *Accounts of chemical research,* vol. 47, no. 10, pp. 3018-3027, 2014.
[112] D. Resetca and D. J. Wilson, "Characterizing rapid, activity-linked conformational transitions in proteins via sub-second hydrogen deuterium exchange mass spectrometry," *FEBS Journal,* vol. 280, no. 22, pp. 5616-5625, 2013-11-01 2013, doi: 10.1111/febs.12332.
[113] H. Naveed, D. Jimenez-Morales, J. Tian, V. Pasupuleti, L. J. Kenney, and J. Liang, "Engineered oligomerization state of OmpF protein through computational design decouples oligomer dissociation from unfolding," *Journal of molecular biology,* vol. 419, no. 1-2, pp. 89-101, 2012.
[114] O. D. Novikova *et al.*, "Peculiarities of thermal denaturation of OmpF porin from Yersinia ruckeri," *Molecular BioSystems,* vol. 13, no. 9, pp. 1854-1862, 2017.
[115] W. Kightlinger, K. Chen, A. Pourmir, D. W. Crunkleton, G. L. Price, and T. W. Johannes, "Production and characterization of algae extract from Chlamydomonas reinhardtii," *Electronic Journal of Biotechnology,* vol. 17, no. 1, pp. 3-3, 2014.
[116] B. Franke *et al.*, "Production of isotope-labeled proteins in insect cells for NMR," *Journal of biomolecular NMR,* vol. 71, no. 3, pp. 173-184, 2018.
[117] F. Löhr, V. Katsemi, J. Hartleib, U. Günther, and H. Rüterjans, "A strategy to obtain backbone resonance assignments of deuterated proteins in the presence of incomplete amide 2 H/1 H back-exchange," *Journal of biomolecular NMR,* vol. 25, no. 4, pp. 291-311, 2003.
[118] Y. Ashani and G. N. Catravas, "Highly reactive impurities in Triton X-100 and Brij 35: partial characterization and removal," *Analytical biochemistry,* vol. 109, no. 1, pp. 55-62, 1980.
[119] M. Turowski *et al.*, "Deuterium isotope effects on hydrophobic interactions: the importance of dispersion interactions in the hydrophobic phase," *Journal of the American Chemical Society,* vol. 125, no. 45, pp. 13836-13849, 2003.
[120] W. B. O'Dell, A. M. Bodenheimer, and F. Meilleur, "Neutron protein crystallography: A complementary tool for locating hydrogens in proteins," *Arch Biochem Biophys,* vol. 602, pp. 48-60, Jul 15 2016, doi: 10.1016/j.abb.2015.11.033.

[121] M. Budayova-Spano, K. Koruza, and Z. Fisher, "Large crystal growth for neutron protein crystallography," *Methods in enzymology,* vol. 634, pp. 21-46, 2020.
[122] A. Stetsenko and A. Guskov, "An overview of the top ten detergents used for membrane protein crystallization," *Crystals,* vol. 7, no. 7, p. 197, 2017.
[123] J. Ma *et al.,* "The effect of residual Triton X-100 on structural stability and infection activity of adenovirus particles," *Molecular Therapy-Methods & Clinical Development,* vol. 19, pp. 35-46, 2020.
[124] S. Tanaka and M. Ataka, "Protein crystallization induced by polyethylene glycol: A model study using apoferritin," *The Journal of chemical physics,* vol. 117, no. 7, pp. 3504-3510, 2002.
[125] C. Hitscherich, V. Aseyev, J. Wiencek, and P. J. Loll, "Effects of PEG on detergent micelles: implications for the crystallization of integral membrane proteins," *Acta Crystallographica Section D: Biological Crystallography,* vol. 57, no. 7, pp. 1020-1029, 2001.
[126] R. M. Garavito and D. Picot, "The art of crystallizing membrane proteins," *Methods,* vol. 1, no. 1, pp. 57-69, 1990.
[127] G. T. Detitta and J. R. Luft, "Rate of water equilibration in vapor-diffusion crystallization: dependence on the residual pressure of air in the vapor space," *Acta Crystallographica Section D: Biological Crystallography,* vol. 51, no. 5, pp. 786-791, 1995.
[128] J. M. García-Ruiz, F. Otálora, and A. García-Caballero, "The role of mass transport in protein crystallization," *Acta Crystallographica Section F: Structural Biology Communications,* vol. 72, no. 2, pp. 96-104, 2016.
[129] W. F. Berg, "Crystal growth from solutions," *Proceedings of the Royal Society of London. Series A - Mathematical and Physical Sciences,* vol. 164, no. 916, pp. 79-95, 1938-01-07 1938, doi: 10.1098/rspa.1938.0006.
[130] F. Manzoni *et al.,* "Perdeuteration, crystallization, data collection and comparison of five neutron diffraction data sets of complexes of human galectin-3C," *Acta Crystallographica Section D: Structural Biology,* vol. 72, no. 11, pp. 1194-1202, 2016.
[131] X. Liu, B. L. Hanson, P. Langan, and R. E. Viola, "The effect of deuteration on protein structure: a high-resolution comparison of hydrogenous and perdeuterated haloalkane dehalogenase," *Acta Crystallographica Section D: Biological Crystallography,* vol. 63, no. 9, pp. 1000-1008, 2007.
[132] P. D. Shaw Stewart, S. A. Kolek, R. A. Briggs, N. E. Chayen, and P. F. M. Baldock, "Random Microseeding: A Theoretical and Practical Exploration of Seed Stability and Seeding Techniques for Successful Protein Crystallization," *Crystal Growth & Design,* vol. 11, no. 8, pp. 3432-3441, 2011-08-03 2011, doi: 10.1021/cg2001442.
[133] T. Bergfors, "Succeeding with seeding: some practical advice," in *Evolving Methods for Macromolecular Crystallography*: Springer, 2007, pp. 1-10.
[134] G. C. Kresheck, H. Schneider, and H. A. Scheraga, "The Effect of D2O on the Thermal Stability of Proteins. Thermodynamic Parameters for the Transfer of Model Compounds from H2O to D2O1, 2," *The Journal of physical chemistry,* vol. 69, no. 9, pp. 3132-3144, 1965.
[135] P. Fromme and H. T. Witt, "Improved isolation and crystallization of photosystem I for structural analysis," *Biochimica et Biophysica Acta (BBA)-Bioenergetics,* vol. 1365, no. 1-2, pp. 175-184, 1998.
[136] C. R. D. Lancaster, A. Kröger, M. Auer, and H. Michel, "Structure of fumarate reductase from Wolinella succinogenes at 2.2 Å resolution," *Nature,* vol. 402, no. 6760, pp. 377-385, 1999-11-01 1999, doi: 10.1038/46483.

[137] R. Dods *et al.*, "From macrocrystals to microcrystals: a strategy for membrane protein serial crystallography," *Structure,* vol. 25, no. 9, pp. 1461-1468. e2, 2017.
[138] S. A. Kolek, B. Bräuning, and P. D. Shaw Stewart, "A novel microseeding method for the crystallization of membrane proteins in lipidic cubic phase," *Acta Crystallographica Section F: Structural Biology Communications,* vol. 72, no. 4, pp. 307-312, 2016.
[139] I. Moraes, G. Evans, J. Sanchez-Weatherby, S. Newstead, and P. D. S. Stewart, "Membrane protein structure determination—the next generation," *Biochimica et Biophysica Acta (BBA)-Biomembranes,* vol. 1838, no. 1, pp. 78-87, 2014.
[140] N. Candoni, R. Grossier, Z. Hammadi, R. Morin, and S. Veesler, "Practical physics behind growing crystals of biological macromolecules," *Protein and peptide letters,* vol. 19, no. 7, pp. 714-724, 2012.
[141] J. Campbell, Q. Hao, M. Harding, N. Nguti, and C. Wilkinson, "LAUEGEN version 6.0 and INTLDM," *Journal of Applied Crystallography,* vol. 31, no. 3, pp. 496-502, 1998.
[142] P. Evans, "Scaling and assessment of data quality," *Acta Crystallographica Section D: Biological Crystallography,* vol. 62, no. 1, pp. 72-82, 2006.
[143] P. D. Adams *et al.*, "The Phenix software for automated determination of macromolecular structures," *Methods,* vol. 55, no. 1, pp. 94-106, 2011.
[144] P. Emsley and K. Cowtan, "Coot: model-building tools for molecular graphics," *Acta crystallographica section D: biological crystallography,* vol. 60, no. 12, pp. 2126-2132, 2004.
[145] E. Oksanen, F. Dauvergne, A. Goldman, and M. Budayova-Spano, "Design of a novel Peltier-based cooling device and its use in neutron diffraction data collection of perdeuterated yeast pyrophosphatase," *Journal of Applied Crystallography,* vol. 43, no. 5, pp. 1113-1120, 2010.
[146] J. R. Morrow, T. L. Amyes, and J. P. Richard, "Phosphate binding energy and catalysis by small and large molecules," *Accounts of chemical research,* vol. 41, no. 4, pp. 539-548, 2008.
[147] Q. Cui and M. Karplus, "Quantum mechanics/molecular mechanics studies of triosephosphate isomerase-catalyzed reactions: effect of geometry and tunneling on proton-transfer rate constants," *Journal of the American Chemical Society,* vol. 124, no. 12, pp. 3093-3124, 2002.
[148] P. J. Lodi and J. R. Knowles, "Neutral imidazole is the electrophile in the reaction catalyzed by triosephosphate isomerase: structural origins and catalytic implications," *Biochemistry,* vol. 30, no. 28, pp. 6948-6956, 1991.
[149] P. J. Lodi, L. C. Chang, J. R. Knowles, and E. A. Komives, "Triosephosphate isomerase requires a positively charged active site: the role of lysine-12," *Biochemistry,* vol. 33, no. 10, pp. 2809-2814, 1994.
[150] E. A. Komives, L. C. Chang, E. Lolis, R. F. Tilton, G. A. Petsko, and J. R. Knowles, "Electrophilic catalysis in triosephosphate isomerase: the role of histidine-95," *Biochemistry,* vol. 30, no. 12, pp. 3011-3019, 1991.
[151] E. A. Ruben *et al.*, "Ground state destabilization from a positioned general base in the ketosteroid isomerase active site," *Biochemistry,* vol. 52, no. 6, pp. 1074-1081, 2013.
[1] C. I. Branden and J. Tooze, *Introduction to protein structure*. Garland Science, 2012.
[2] T. E. Creighton, *Proteins: structures and molecular properties*. Macmillan, 1993.
[3] A. S. Cole and J. E. Eastoe, *Biochemistry and oral biology*. Butterworth-Heinemann, 2014.
[4] G. C. Terstappen and A. Reggiani, "In silico research in drug discovery," *Trends in pharmacological sciences,* vol. 22, no. 1, pp. 23-26, 2001.

[5] S. H. White and W. C. Wimley, "Membrane protein folding and stability: physical principles," *Annual review of biophysics and biomolecular structure,* vol. 28, no. 1, pp. 319-365, 1999.
[6] A. Sadaf, K. H. Cho, B. Byrne, and P. S. Chae, "Amphipathic agents for membrane protein study," *Methods in enzymology,* vol. 557, pp. 57-94, 2015.